THE LOW TEMPERATURE COOPERATIVE BEHAVIOR OF THE RARE EARTH SALTS GdC13 AND PrC13

Thesis for the Degree of Ph.D. MICHIGAN STATE UNIVERSITY JAN PAUL HESSLER 1971





This is to certify that the

thesis entitled

The Low Temperature Cooperative
Behavior of the Rare Earth
Salts GdCl₃ and PrCl₃
presented by

Jan Paul Hessler

has been accepted towards fulfillment of the requirements for

Ph.D. degree in Physics

Major professor

Date 9 June, 1971

O-7639

ABSTRACT

THE LOW TEMPERATURE COOPERATIVE BEHAVIOR OF THE RARE EARTH SALTS GdCl, and PrCl,

By

Jan Paul Hessler

We have studied the three-dimensional ordered phases of $GdCl_3$ and $PrCl_3$ with Cl nuclear magnetic resonance in the temperature range 0.3 K to the transition temperature. The resonance transition frequencies were measured with a simple pulsed N.M.R. spectrometer to an accuracy of \pm 1 kHz. Simple 3 He and 4 He systems were used to obtain the necessary low temperatures. The absolute temperature was measured to an accuracy of \pm 2 mK.

GdCl $_3$ is an ionic ferromagnet with a Curie temperature of 2.2 K. In the ordered state the internal field at the chlorine site is along the principal X-axis of the electrostatic field gradient tensor. The method of energy moments is used to determine the asymmetry parameter, $\eta = 0.4265 \pm 0.0001$. The nuclear quadrupole interaction Hamiltonian is diagonalized and a chi squared analysis is used to determine the internal fields at the chlorine site, B(T). Both 35 Cl and 37 Cl transition frequencies are observed and used in the analysis.

In the critical region, $T/T_c > 0.91$, the internal field follows the relationship $B(T) = A(T_c - T)^{\beta}$ where

Jan Paul Hessler

A = (4368.4 ± 31.1) gauss/K^{\beta}, T_C = (2.214 ± 0.0016) K, and β = 0.3904 ± 0.006 . Below 1.0 K the internal field follows B(T) = B_O - $(A_1T^{3/2} + A_2T^{5/2})\exp(-\theta/T)$ where B_O = (4950.8 ± 2.9) gauss, A₁ = (963.1 ± 68.3) gauss/K^{3/2}, A₂ = $-(90.7 \pm 41.6)$ gauss/K^{5/2}, and θ = (0.430 ± 0.037) K.

The measured temperature dependence of the internal field below 0.6 K is compared with the spin wave predictions based on the exchange parameters measured by pair spectra. There is a definite discrepancy. By comparing the internal field measurements to the bulk measurements of magnetization, we have calibrated the internal field in terms of the magnetization. This indicates an anomalously large zero-point magnetization defect. The magnetization measurements are also compared to the molecular field and Green function predictions. A possible mechanism and experiments to test the mechanism are put forth to explain the large zero-point magnetization defect.

The low temperature phase of $PrCl_3$, $T_{critical} = 0.4$ K, was studied to determine the nature and symmetry of the ordered state. In the paramagnetic region the asymmetry parameter was determined by applying an external field along the principal X-axis of the electric field gradient tensor and using the method of energy moments. η was found to be 0.4937 \pm 0.0001. In the ordered state, the local magnetic and electric field gradients were measured at the Cl site by applying an external field perpendicular to the high

Jan Paul Hessler symmetry axis, C_3 , and studying the symmetry and behavior of the rotational spectrum.

The splitting of the pure quadrupole resonance line at 0.4 K is attributed to an effective crystallographic transition. The application of a 10 Kgauss field appears to have no effect on the zero field splitting and on the transition temperature. The crystal space group is lowered from $P6_3/m$ to $P\overline{6}$ or P3. An interpretation of the observed asymmetric line shape in the ordered state is presented which implies that the three-fold symmetry is slightly distorted.

THE LOW TEMPERATURE COOPERATIVE BEHAVIOR OF THE RARE EARTH SALTS GdCl_3 AND PrCl_3

by

Jan Paul Hessler

A THESIS

Submitted to

Michigan State University
in partial fulfillment of the requirements

for the degree of

DOCTOR OF PHILOSOPHY

Department of Physics

1971

67/85/

DEDICATION

To my parents, Ada and Harold Hessler, who taught me to never allow an educational institute to interfere with my education, and to Nancy, who lives so successfully in our ménage à trois: me, her, and physics, I dedicate this thesis.

ACKNOWLEDGEMENTS

My sincere thanks goes to Prof. Edward H. Carlson who suggested the topic for this thesis and gave me the freedom to pursue it on my own. For their many hours of conversation and stimulation I wish to thank Robert D. Spence and Thomas A. Kaplan. The numerous authors that have communicated their work prior to publication were a great help.

A special thanks to David H. Current for his help in designing the apparatus and performing the experiments as well as being a patient listener for many of my wild and untested ideas.

TABLE OF CONTENTS

		Page
LIST OF	TABLES	νi
LIST OF	FIGURES	vii
Chapter		
I.	INTRODUCTION	1
II.	EXPERIMENTAL TECHNIQUE	9
	A. Crystal Preparation	9
	B. Crystal Structure	9
	C. N.M.R. Measurements	10
	D. Temperature, Calibration and Measurement	12
III.	GdCl ₃ THEORY AND BACKGROUND	17
	A. Gd ³⁺ Ion Properties	17
	B. GdCl ₃ Bulk Properties	18
	C. Pair Spectra of Gd ³⁺	18
	D. Relation of Pair Exchange Constants to Bulk Properties .	19
	E. Magnetization Calculations	20
IV.	Cl N.M.R. IN GdCl ₃ : RESULTS AND	
	DISCUSSION	32
	A. N.M.R. Hamiltonian	32
	B. Determine η by the Method of Moments	35
	C. Determine the Magnitude of the Internal Field	39
	D. Comparison of Temperature Dependence to Theory	42

																		Page	:
	E.	Cor	lC]	Lus	sic	n	•	•	•	•	•	•	•	•	•	•	•	61	
v.	Pro	213	Τŀ	IEC	RY	C P	NE	E	BAC	CKC	RC	UC	ND	•	•	•	•	63	
	A.	Pr	3+	Ic	n	Pr	op	er	ti	les	3	•	•	•	•	•	•	63	
	в.	Pr	3+	an	nd	Pa	ir	F	Res	or	nar	nce	9	•	•	•	•	64	
	c.	Bul	Lk	Pr	op	eı	ti	.es	3	•	•	•	•	•	•	•	•	67	
VI.	Cl	N.M	1.1	₹.	RE	ESU	IJ	'S	FC	R	Pı	cC!	L ₃	•	•	•	•	69	
	A.	Par	ar	nag	jn e	eti	.c	Ph	as	se	•	•	•	•	•	•	•	69	
	В.	Low	, 1	l'en	ıρε	era	ıtu	re	e E	Pha	se	≥,	T	<	0.	. 4	K	72	
	c.	Cor	ic]	lus	sic	ns	5	•	•	•	•	•		•	•	•	•	82	
REFERENC	CES	•	•	•	•	•	•	•	•	•	•	•		•	•	•	•	83	
APPENDIX	K A	•		•	•	•	•	•	•	•	•	•	•	•	•	•	•	87	
APPENDIX	КВ	•	•	•	•	•	•	•	•	•	•	•	•	•	•	•	•	93	
APPENDIX	C C															_		109	

LIST OF TABLES

Table		Page
3.1	Exchange Constants for $GdC1_3$	19
4.1	Low Temperature Analysis	55
5.1	Spin-Spin Interaction Parameters for Pr ³⁺ Axial Pairs	66
6.1	Analysis of Possible Space Groups for $PrCl_3$	78
A.1	Susceptibility Coil Calibration Data	88
A.2	Coefficients for ${}^3\mathrm{He}$ Solitron Ge Resistor	89
A.3	Raw Data for Ge Resistor Calibration	90
A.4	R vs. T Calibration Data and Deviation	91
B.1	C1 Transition Frequencies in GdC1 ₃	94
B.2	Results of χ^2 Analysis for B(T)	105
B.3	Comparison of B(T) with Analytic Expression for $T \sim T_c$	107
B.4	Comparison of B(T) with Analytic Expression for $T < 1.0 \text{ K} \dots \dots \dots \dots$	108
C.1	C1 Transition Frequencies in PrC1,	110

LIST OF FIGURES

Figur	P P	age
1.1	Pr ³⁺ ion Energy Levels in LaCl ₃	3
2.1	Structure of the Rare Earth Trichlorides La to Gd	11
2.2	Low Temperature Section of ³ He Cryostat	14
4.1	³⁵ Cl Transition Frequencies in GdCl ₃	34
4.2	Energy Levels for a Spin 3/2 Nucleus in a Crystal	38
4.3	Internal Field at Chlorine Site vs. Temperature for GdCl ₃	43
4.4	Comparison of N.M.R. and Isentropic Magnetization Data	46
4.5	Comparison of N.M.R. and Magnetization Data	47
4.6	$lnB(T)$ vs. $ln(T_c - T)$ for $T/T_c > 0.91$	50
4.7	Internal Field vs. T ^{3/2} for T < 1.2 K	54
4.8	Comparison of Low Temperature Data with Spin Wave Theory	56
4.9	Reduced Magnetization vs. Reduced Temperature .	60
5.1	Zero Field Splitting of Pure Quadrupole Line, PrCl ₃	68
6.1	Transition Frequencies vs. Field	70
6.2	Rotation Diagram, H L C , High Temperature Phase	71
6.3	Rotation Diagram, H L C 3, Low Temperature Phase	73
6.4	Transition Frequencies vs. Field, Low Temperature Phase	74
6.5	High Field Behavior of Transition Frequencies, Low Temperature Phase	76

Figure	e	P	age
6.6	Second Derivative of Absorption Curve, PrCl ₃	•	79
6.7	Calculated Second Derivative of Absorption Curve		81

I. INTRODUCTION

Magnetism is a cooperative phenomenon. This fact makes its study both interesting and challenging. Most attempts to describe the cooperative behavior in ionic compounds have assumed that we may use the concept of localized moments and the description of these local moments as a starting point. We then assume that a satisfactory approach to the understanding of magnetic phenomena will follow from:

1) a knowledge of the localized magnetic ions, 2) a knowledge of the interactions between the localized ions, and
3) an accurate treatment of the statistical mechanics for the implications of the above two models for the behavior of the system.

Parts one and two of this approach have motivated the idea of a spin Hamiltonian. The spin Hamiltonian is simply a mathematical model which is sufficiently general to account for all the experimental information observed in one and two. It is in this sense that the spin Hamiltonian is phenomenological. For a discussion of the derivation of spin Hamiltonians see Stevens (1963). Of paramount importance is the assertion that the spin Hamiltonian describing the interaction between two isolated spins plus the principles of statistical mechanics is sufficient to deduce the cooperative many body behavior of magnetism.

A knowledge of the low lying states of the magnetic ion is obtained by studying the configuration terms of the

free ion by optical methods (Judd, 1963). Paramagnetic resonance is then used to study the effect of the crystalline environment on the low lying levels (Hutchings, 1964). Figure 1.1 is a schematic representation of the Pr^{3+} ion in the C_{3h} symmetry of $PrCl_3$ (Judd, 1957).

The interaction between the spins may also be studied by paramagnetic resonance, and generally may be described by a spin Hamiltonian of the form

$$H_{12} = \vec{s}_1 \cdot \vec{j}_{12} \cdot \vec{s}_2 + j(\vec{s}_1 \cdot \vec{s}_2)^2$$
 (1.1)

For a rather complete discussion of exchange see Anderson (1963a, 1963b) and Wolf (1971). This form of the interaction has proved very useful, especially for the transition metal ions. However, in the rare earths the 4f electrons are shielded by the 5s² and 5p⁶ shells, resulting in a significantly smaller exchange interaction due to the decreased overlap. Because of this reduction, competing effects from the crystal fields and the spin-orbit coupling contribution to the magnetic moment must also be considered. This complicates the form of the exchange interaction and allows other interactions to act as coupling mechanisms.

The best known coupling mechanism is the dipole-dipole coupling, and it is the only one encountered classically. From magnetostatics the magnetic dipole energy is given by

$$E = (\vec{M}_1 \cdot \vec{M}_2 - 3(\vec{M}_1 \cdot \hat{r}_1) (\vec{M}_2 \cdot \hat{r}_2)) / |\vec{r}_1 - \vec{r}_2|^3$$
 (1.2)

where \vec{M}_1 and \vec{M}_2 are magnetic moments located at \vec{r}_1 and \vec{r}_2 respectively. For the special case of S state ions with

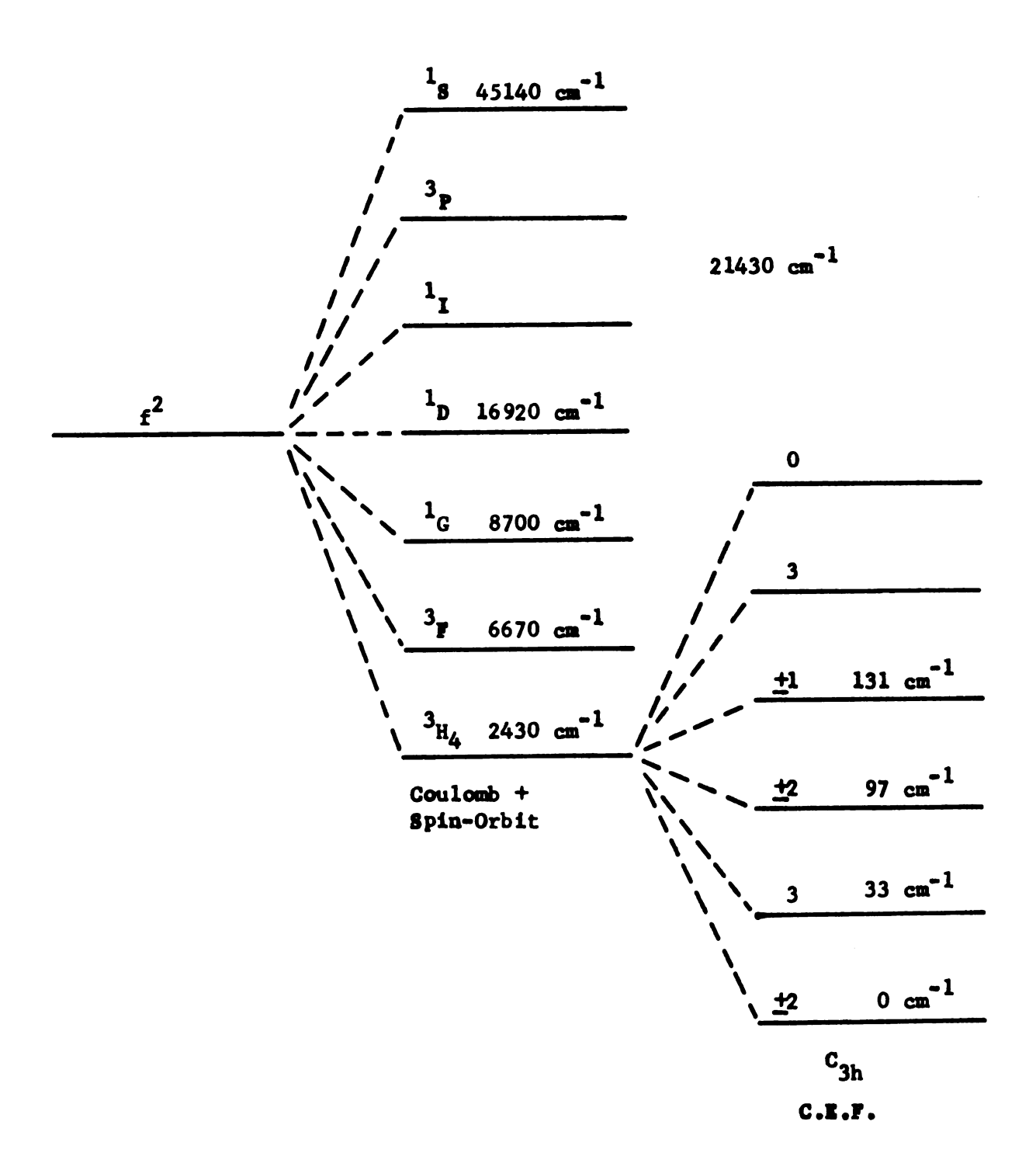


Figure 1.1 Pr3+ ion Energy Levels in LaCl3.

 $(\vec{r}_1 - \vec{r}_2)$ the axis of quantization, the spin Hamiltonian simplifies to

$$H_{12} = g^2 \mu_B^2 (\vec{s}_1 \cdot \vec{s}_2 - 3s_1^z s_2^z) / r_{12}^3.$$
 (1.3)

The well known exchange interaction was introduced by Heisenberg (1926) and by Dirac (1929). Exchange effects are a direct consequence of the Pauli principle. Dirac showed that for the particular case of n electrons confined to specific orthogonal orbits, the splitting of the energy levels is the same as though we forgot about permutation degeneracy and used the potential

$$v_{ex} = -\sum_{i>j} (1/2 + 2\vec{s}_{i} \cdot \vec{s}_{j}) J_{ij}$$
 where

 $J_{ij} = \int dr_1 dr_2 \psi_i^{\dagger}(r_1) \psi_j^{\dagger}(r_2) \frac{e^2}{|\vec{r}_1 - \vec{r}_2|} \psi_i(r_2) \psi_j(r_1) , (1.5)$ and ψ_i and ψ_j are the orbital wave functions for the states i and j respectively. Extensions of this idea have led to equation (1.1).

A third type of coupling is due to the aspherical charge distribution found in non S state ions. The moments may be coupled via electric multipole moment interactions. An example of this is the electric quadrupole-quadrupole interaction observed in CeCl₃ (Birgeneau, Hutchings, and Rogers, 1968).

A fourth coupling mechanism is virtual phonon exchange. This interaction is similar to the above and may be viewed in two ways. For non S state ions, the electrostatic interactions in the form of the crystal field

and the interacting multipoles may be induced or modified by the phonons. In the case of the S state ions the exchange and dipole-dipole interaction coefficients J_{ij} and α_{ij} , where $\alpha_{ij} = 1/r_{ij}^3$, are strong functions of distance and can couple to the phonons. Although this is generally considered a weak interaction, it is very important in the case of non-Kramers orbital degeneracy. This mechanism has been used to account for the antiferromagnetism in UO₂ (Allen, 1968).

An approach to studying magnetic systems is now straightforward. From symmetry and other considerations, we deduce the form and number of allowed interactions necessary to construct an interaction Hamiltonian for the system. We then experimentally determine the magnitude and behavior of the interaction coefficients in the Hamiltonian. With this information we apply the laws of statistical mechanics to deduce the cooperative behavior of the system. This behavior is measured, and we compare our results to the theoretical prediction. If the effective Hamiltonian is correct and the statistical mechanics has been applied properly, we should expect agreement. Often this is not the case. We are then left with three alternatives: 1) the effective Hamiltonian is not accurate enough and we must include additional information, 2) the statistical mechanical treatment was inadequate and needs improvement, or 3) the assumption that we can describe the

cooperative phenomena in terms of simple two-spin interactions is not valid.

In this work we study the cooperative behavior of two rare earth salts, GdCl₃ and PrCl₃. We use the chlorine nuclear magnetic resonance as a microscopic probe. This will give us information about the magnetic field and the electric field gradient at the chlorine site.

In chapter II we discuss the crystal preparation and structure, along with the N.M.R. measuring apparatus and the low temperature apparatus. In chapter III we present the single ion optical and paramagnetic resonance results for the Gd³⁺ ion. The pair spectra in LaCl₃ and EuCl₃ along with the high temperature magnetic specific heat results are discussed to arrive at an effective two-spin interaction Hamiltonian. With these parameters we use the cluster expansion technique to derive the molecular field approximation and the two-spin correction term. We discuss the problems involved in evaluating the two-spin correction term, and two approximate solutions. The Green function formalism and the spin wave approximation are also briefly discussed.

In chapter IV we set up the nuclear quadrupole interaction Hamiltonian and apply symmetry arguments to simplify
the analysis of the observed spectrum. The method of
energy moments is used to determine the asymmetry parameter,
and an exact diagonalization is used with a chi squared

analysis to determine the magnitude of the internal field as a function of the observed transition frequencies.

Analytic expressions are found which describe the temperature dependence of the internal field in the critical region and in the spin wave region. The low temperature measurements, T < 0.6 K, are compared to numerical calculations of the temperature dependence of the magnetization based on a spin wave calculation and the measured exchange parameters. Here there is a discrepancy which requires further investigation.

The internal field measurements are also compared to saturation magnetization measurements to calibrate the internal field results in terms of saturation magnetization results. With this we detect an anomalously large zero-point magnetization defect. A possible mechanism to explain this defect is presented along with some experiments which should help our understanding of the low temperature behavior. We also compare our measurements to the molecular field and Green function calculations. Agreement with the molecular field calculation is relatively poor, and the Green function calculation is qualitatively correct.

In chapter V we present the optical and paramagnetic resonance results for a single \Pr^{3+} ion in LaCl_3 . The axial pair spectra measurements are also reported, but no conclusive statement can be made about the interaction mechanism responsible for the three-dimensional ordering at 0.4 K.

In chapter VI we study the low temperature phase of PrCl, by applying an external magnetic field in the plane perpendicular to the symmetry axis, C3. The symmetry of the rotation spectrum, and the behavior extrapolated to zero applied field indicate that the phase transition at 0.4 K is effectively a crystallographic phase transition. Studies in an applied field up to 10 Kgauss indicate that a magnetic field has no effect on the zero field splitting of the pure quadrupole resonance line nor on the transition temperature. Symmetry arguments are used to show that the effective crystallographic space group is either $P\overline{6}$ or P3. An analysis of the observed asymmetric line in the ordered state is presented which indicates that the 3-fold symmetry is also slightly distorted, although this is not verified by an analysis of our rotation spectrum. The fact that PrCl, has a non-Kramers orbitally degenerate ground state leads us to suspect that the ordering mechanism is dominated by the lattice vibrations. We review the literature for evidence to this effect.

II. EXPERIMENTAL TECHNIQUE

A. Crystal Preparation

The anhydrous rare earth trichloride from Lindsay was slowly melted under vacuum in a vertical quartz tube. The polycrystalline sample was then transferred to a horizontal distillation apparatus and distilled in vacuum into a 17 mm diameter quartz tube. After distillation the tube was sealed under vacuum, detached, and placed in a gradient furnace. The lower tip of the tube was placed in the gradient and observed until a single seed crystal was produced. The tube was then slowly lowered through the gradient, producing a clear single crystal.

Because the crystals are very hydroscopic, once they were removed from the tube they were stored in mineral oil when not in use and liberally coated with Apeizon N grease during use. No analysis of the stoichiometry or impurity content was attempted.

The crystals are uniaxial with the axis easily recognized by observation of the striations that appear on the cleavage planes which are parallel to the axis. The crystals were cleaved, cut on a diamond saw, and ground with a grinding wheel to a convenient size and shape.

B. Crystal Structure

Zachariasen (1948) has determined the structure for the rare earth trichloride series lanthanum to gadolinium and found it to be hexagonal with space group P63/m. There

are two molecules per unit cell. The locations of the rare earth ions are determined by symmetry as being $\pm (\frac{1}{3}, \frac{2}{3}, \frac{1}{4})$ while the physically inequivalent chlorines are at $\pm (u, v, 1/4)$, $(\overline{v}, u-v, 1/4)$, $(v-u, \overline{u}, 1/4)$. Morosin (1968) has recently determined the parameters u and v and the cell dimensions for several of the anhydrous rare earth trichlorides. Figure 2.1 shows the crystal structure. The point symmetry for the rare earth ions is C_{3h} . All the rare earths and chlorines lie in the mirror plane.

C. N.M.R. Measurements

All transition frequency measurements were made using a simple pulsed N.M.R. spectrometer developed by S. Parks (1967). This spectrometer compares the applied rf signal from a cw oscillator to the induced rf signal from the spin system. The induced rf frequency is measured by displaying the beat pattern between the two frequencies on an oscilloscope and noting the frequency of the cw oscillator at the zero beat. For accurate measurements five independent readings were taken for each frequency. standard deviation of these readings was generally less than To minimize sample heating at low temperatures a minimum amount of power was applied to the rf pulse by varying the voltage on the transmitter stage of the spectrometer. To assure thermal equilibrium, the line with the largest dv/dT was measured at 10 to 20 minute intervals while the temperature of the bath was maintained constant

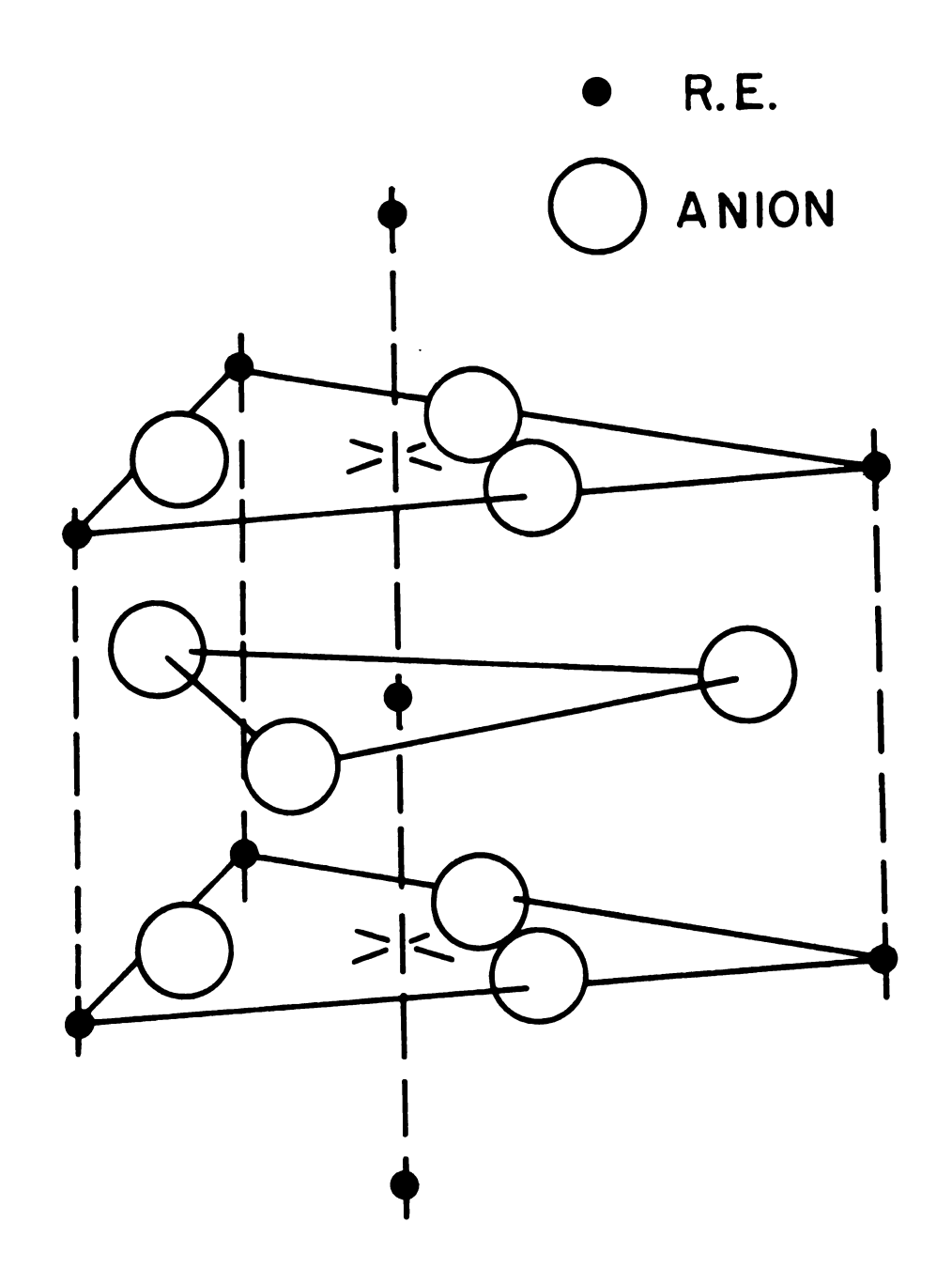


Figure 2.1 Structure of the Rare-Earth Trichlorides La to Gd.

to within 1/4 mK. When two consecutive measurements of frequency agreed to within 1/2 kHz the sample was assumed to be in thermal equilibrium with the bath.

D. Temperature, Calibration and Measurement

All of the interesting phase transitions in the rare earth trichlorides occur below 4 K. This necessitates the use of liquid ⁴He and ³He as refrigerants. Experimental techniques in this temperature range have been discussed by White (1968).

For our experiments in the temperature range of 1.2 K to 4.2 K the sample was immersed directly in the ⁴He bath. A 200 ohm Manganin resistor was used as a heater for fine control of the temperature below the lambda point and as a stirrer above the lambda point. The ⁴He vapor pressure (Brichwedde, 1970) was used as an absolute measure of temperature throughout the entire temperature range. Above a vapor pressure of 100 Torr a standard U-tube mercury manometer was used to determine the vapor pressure. Below 100 Torr an MKS capacitance manometer operated in the digital mode was used. This has a day-to-day reproducibility of 0.02 Torr + 0.05% of the pressure reading. Above 1.3 K this accuracy is well within the accuracy of the 1958 ⁴He Scale of Temperatures.

Below the lambda point the temperature was regulated by monitoring the vapor pressure and keeping it constant to within 0.002 Torr. This corresponds to a temperature fluctuation of 0.45 mK at 1.2 K. The measured vapor pressure and temperature were strongly coupled as indicated by the fact that the resistance of a 33 ohm Ohmite carbon resistor located at the sample site tracked the vapor pressure with no visible lag in time.

For the temperature range of 0.3 to 1.2 K a conventional ³He single shot cryostat was used. The design follows closely that of Walton (1966). Figure 2.2 shows the low temperature section of the cryostat.

Above 0.6 K the ³He vapor pressure was used to determine the temperature (Sherman, Sydoriak, and Roberts, 1962). To measure the vapor pressure a 1/4" o.d. stainless tube was inserted inside the pumping line from the 1.2 K radiation trap to approximately 1 cm above the surface of the liquid. The tube was then increased to 3/8" o.d. and went independently to an MKS capacitance manometer at room temperature. The day-to-day reproducibility when operated in the digital mode is 0.006 Torr + 0.05% of the pressure reading. achieve a desired temperature, the vapor pressure was calculated and the appropriate corrections for the manometer were employed. The digital dials were then set and the temperature was obtained by monitoring the pumping speed of the 3He gas with a series of valves. A pressure fluctuation corresponding to a temperature fluctuation of 0.1 mK was calculated for each temperature and the pressure maintained constant within these limits.

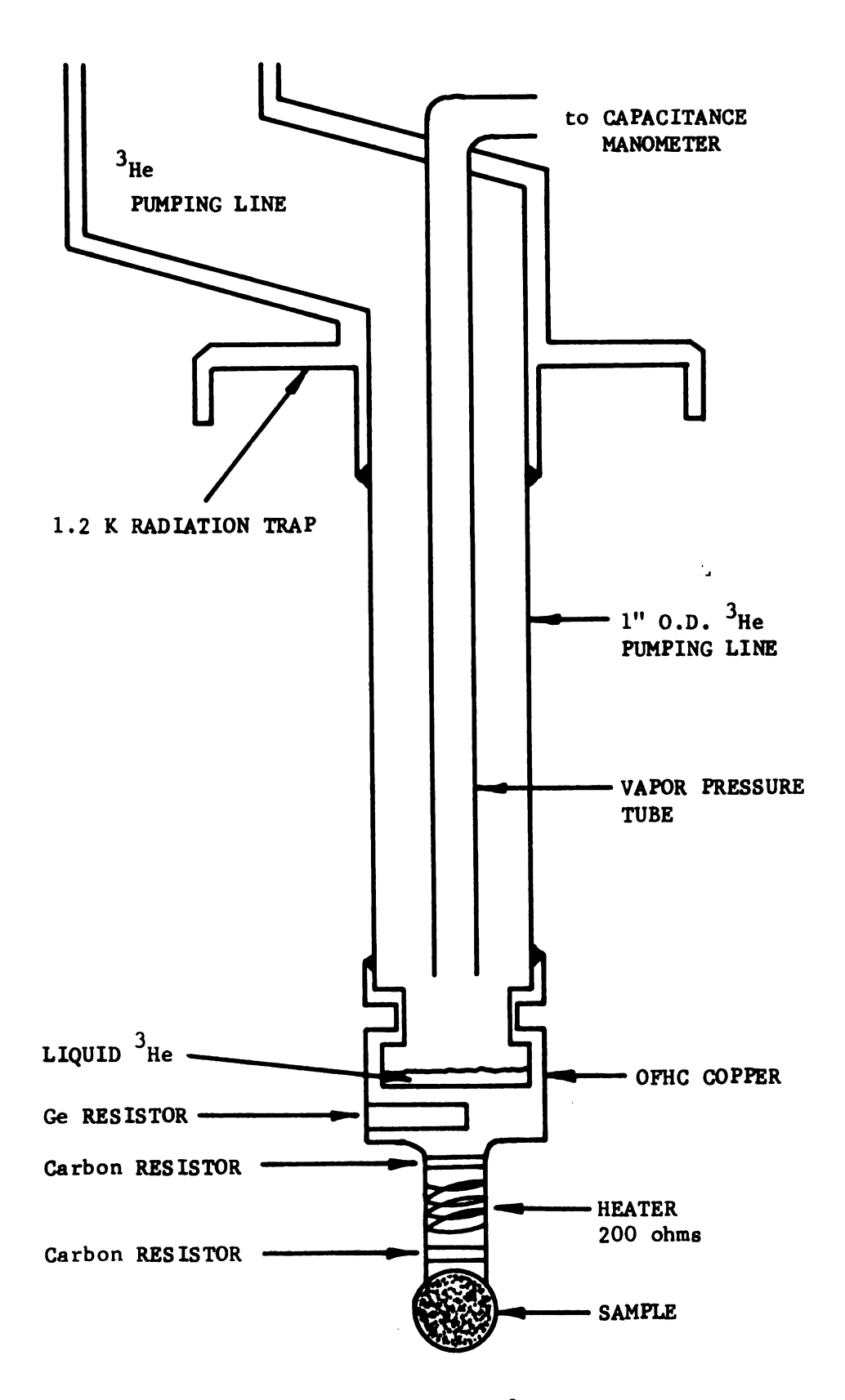


Figure 2.2 Low Temperature Section of ³He Cryostat.

Below 0.6 K the thermomolecular correction becomes significant, even for our large tube (Freddi and Modena, 1968). Also dP/dT becomes small enough that pressure monitoring and measurement are not sensitive enough to keep temperature fluctuations on the order of 0.1 mK. Therefore, below 0.6 K, we used a germanium resistor for temperature measurement and a carbon resistor for temperature fluctuation monitoring.

Both resistances are measured independently by two Wheatstone bridges using a PAR lock-in detector as a source and as a null detector. A Triad G-10 "Geoformer" was used to isolate the unbalanced signal from the preamp and the PAR detector. To eliminate the effect of lead resistance for the germanium resistor a three lead Wheatstone system was used with an arm ratio of 1:1. With this method the lead resistance of 200 ohms at room temperature was effectively nulled to within 2 ohms.

To calibrate the germanium resistor at low temperatures the magnetic temperature, T*, of ferric ammonium alum was used as a standard. The mutual inductance technique (Abel, Anderson, and Wheatley, 1964) was used to determine the susceptibility. The coils were calibrated using the vapor pressure of ³He as the temperature standard between 0.6 K and 1.2 K. The relationship between T* and T for T > 0.2 K is

(2.1)

$$T^* - T = 0.00548/T$$

to within 0.1 mK (Sydoriak and Roberts, 1957).

The resistance vs. temperature data for the germanium resistor was then fitted to the equation

 $\ln(R) = a_0 + a_1 \ln(T) + a_2/T$ (2.2) from 0.3 K to 1.2 K. Four different sets of the coefficients a_0 , a_1 and a_2 were necessary to fit the data to within 1 mK. At 0.7 K the resistance is 2239 ohms with a dR/dT of -8.1 ohms/mK. Our Wheatstone bridge has a sensitivity of approximately 1 ohm with a power level of 10^{-9} Watts, thus we are able to detect temperature fluctuations on the order of 0.2 mK at 0.7 K. The actual calibration data and analysis are discussed in Appendix A.

III. GdCl, THEORY AND BACKGROUND

GdCl₃ belongs to the small set of compounds which are both insulating and ferromagnetic; this is the primary reason for studying it so extensively. From the experimental point of view it belongs to a rather large series of isomorphic compounds which are easy to grow. This allows the experimentalist the opportunity to study the Gd³⁺ ion with many experimental techniques.

A. Gd³⁺ Ion Properties

The ground level of Gd^{3+} is $^8\mathrm{S}_{7/2}$ with the only structure of the order of 0.1 cm $^{-1}$ (Piksis, Dieke, and Crosswhite, 1967). The first excited level of Gd^{3+} in LaCl $_3$ is $^6\mathrm{P}_{7/2}$ at 32100 cm $^{-1}$. The Gd^{3+} ions show the least coupling with the crystal lattice of all the rare earth ions. Superimposed crystal vibrations are generally not observed in any lattice and the lines are reasonably sharp even at room temperature.

Hutchinson Jr., Judd, and Pope (1957) and Hutchinson Jr. and Wong (1958) have measured the paramagnetic resonance absorption of Gd³⁺ in LaCl₃ and CeCl₃. They find a spin Hamiltonian of the form

$$H = \mu_{B} \stackrel{?}{H} \cdot \stackrel{?}{g} \cdot \stackrel{?}{S} = g_{\parallel} \quad \mu_{B} H^{Z} S^{Z} + g_{\perp} \quad \mu_{B} (H^{X} S^{X} + H^{Y} S^{Y}) \quad (3.1)$$
where $g_{\parallel} = g_{\perp} = 1.991 \pm 0.001$.

B. GdCl₃ Bulk Properties

Wolf, Leask, Mangum, and Wyatt (1961) have measured the susceptibility and magnetization of single crystals of GdCl₃ and find that the substance orders ferromagnetically at 2.2 K. The specific heat (Wyatt, 1963) has a lambdalike anomaly at 2.2 K, further substantiating the onset of long range order.

C. Pair Spectra of Gd³⁺

Birgeneau, Hutchings, and Wolf (1967) and Hutchings, Birgeneau, and Wolf (1968) have measured the pair spectra of Gd³⁺ pairs in LaCl₃ and EuCl₃. They find the pair spectra are adequately described by a Hamiltonian of the form

$$H(i,j) = -g\mu_{B}H(S_{i}^{z} + S_{j}^{z}) - J_{ij}\dot{S}_{i}\dot{S}_{j} + \alpha_{ij}(\dot{S}_{i}\dot{S}_{j} - 3S_{i}^{z}S_{j}^{z}) + H_{CEF}(i) + H_{CEF}(j).$$
(3.2)

The axis of the pairs is the z-axis of quantization. J_{ij} is the isotropic exchange interaction and $\alpha_{ij} = g^2 \mu_B^2 / r_{ij}^3$. H_{CEF} is the single ion crystal field Hamiltonian. Because the lattice parameters of LaCl₃ and GdCl₃ differ significantly, the variations of J_{ij} and α_{ij} with respect to temperature were studied in the LaCl₃ case. From this the dependence of J_{ij} on \dot{r}_{ij} was inferred, and extrapolations to the GdCl₃ lattice constants were made. The values of J_{ij} for each case are shown in Table 3.1. It is interesting to note that the nearest-neighbor exchange is antiferromagnetic and weak while the next-nearest-neighbor exchange

is ferromagnetic and approximately four times larger than the nearest-neighbor exchange. There is no definitive explanation for this at the present time.

D. Relation of Pair Exchange Constants to Bulk Properties

There is no a priori reason why the exchange constants measured by pair spectra in a diamagnetic host should determine the magnetic behavior of the bulk system. In spite of this there is relatively good agreement between the bulk properties and the pair exchange constants.

Marquard (1967) has developed a diagramatic technique for calculating the high-temperature expansion coefficients for magnetic systems with arbitrary symmetric tensor interactions between all pairs of spins. He has calculated the first three coefficients for the specific case of GdCl₃. Clover and Wolf (1968) have performed high frequency susceptibility experiments to determine the magnetic specific heat at 20.4 K and 77 K. Their results for the exchange constants along with the pair results are shown in Table 3.1.

Table 3.1 Exchange Constants for GdCl₃

	Specific Heat	LaCl ₃ a	EuCl ₃
J _{nn} (K)	-0.078 ± 0.004	-0.033 ± 0.004	-0.073 ± 0.004
J _{nnn} (K)	0.096 ± 0.004	0.105 ± 0.004	0.091 ± 0.004

aExtrapolated to GdCl₃ lattice parameters

The relatively good agreement between the specific heat results and the pair results for EuCl₃ is encouraging. The discrepancy in the LaCl₃ measurements is not understood, although the extrapolation procedure may not be correct.

E. Magnetization Calculations

Now that we have a relatively good idea of the parameters that go into a phenomenological Hamiltonian for the spin systems we can use these parameters to predict the behavior of the system. There are basically three approaches used in calculating magnetization vs. temperature: the cluster series approximation, the double-time temperature-dependent Green function formalism, and the spin wave approximation.

1) Cluster Expansion (Molecular Field Approximation)

The oldest approximation method of treating the

Hamiltonian of a magnetic system is the molecular field

approximation. This has also had much success in predicting the overall qualitative features of a magnetic system such as: the lambda-like discontinuity in the specific heat, the dependence of magnetization on temperature, the magnetic susceptibility, and the existence of a critical point.

The basic assumption in the molecular field approximation replaces all spin-spin interactions with a spin-effective field interaction. This assumption therefore

eliminates any spin-spin correlation effects. An extension of the "effective field" concept to include correlation effects was first used by Mayer and Mayer (1940) in treating the problem of the non-ideal gas. This technique, commonly called the cluster expansion, was used by Streib, Callen, and Horwitz (1963) to derive a similar series for the Heisenberg ferromagnet. This series has the molecular field approximation as the leading term. We shall treat our Hamiltonian with this technique, thereby reproducing the standard molecular field results and showing how higher order spin-spin correlations may be included, and the difficulties involved.

Extending the pair Hamiltonian to a sum over all pairs we have the Hamiltonian for the system:

$$H = -g\mu_{B} \prod_{i=1}^{N} s_{i}^{z} - \sum_{(i,j)} J_{ij}^{z} \cdot \dot{s}_{j} + (g\mu_{B})^{2} \sum_{(i,j)} \frac{1}{r_{ij}^{3}} \{ \dot{s}_{i} \cdot \dot{s}_{j} - \frac{3(\dot{s}_{i} \cdot \dot{r}_{ij})(\dot{s}_{j} \cdot \dot{r}_{ij})}{r_{ij}^{2}} \}.$$
(3.3)

The first term is the Zeeman energy of the N gadolinium ions, the second is the isotropic exchange interaction, and the third is the dipole-dipole interaction. We assume that the external field, H, is applied along the z-axis. \vec{s}_i is the standard spin operator for the ith ion. Because the ground level is $^8S_{7/2}$, S=7/2 in this case. J_{ij} is the isotropic exchange interaction between the ith and jth ions and \vec{r}_{ij} is the vector between the ith and jth ions.

The summation (i,j) extends over all pairs of ions in the lattice, each pair being counted once.

First we transform the spin operators to the raising and lowering operators, $S_i^{\pm} = S_i^{x} \pm i S_i^{y}$. The Hamiltonian is then

$$H = -g\mu_{B}H \sum_{i=1}^{N} s_{i}^{z} - \sum_{(i,j)} \{A_{ij}s_{i}^{z}s_{j}^{z} + \frac{1}{2}B_{ij}(s_{i}^{+}s_{j}^{-} + s_{i}^{-}s_{j}^{+})$$

$$- [c_{ij}^{+1} (s_{i}^{z}s_{j}^{-} + s_{j}^{z}s_{i}^{-}) + c_{ij}^{-1} (s_{i}^{z}s_{j}^{+} + s_{i}^{+}s_{j}^{z})]$$

$$- [b_{ij}^{+2} s_{i}^{-}s_{j}^{-} + b_{ij}^{+2} s_{i}^{+}s_{j}^{+}]\}$$

$$(3.4)$$

where the coefficients are given by

$$A_{ij} = \alpha_{ij} + J_{ij}, \qquad (3.5a)$$

$$B_{ij} = J_{ij} - \alpha_{ij}/2,$$
 (3.5b)

$$\alpha_{ij} = (g\mu_B)^2 (3\cos^2\theta_{ij} - 1)/r_{ij}^3,$$
 (3.5c)

$$C_{ij}^{\pm i} = \frac{3}{2} (g\mu_B)^2 \frac{1}{r_{ij}^3} \cos\theta_{ij} \sin\theta_{ij} e^{\pm i\phi} ij , \qquad (3.5d)$$

and

$$D_{ij}^{\pm 2} = \frac{3}{4} (g\mu_B)^2 \frac{1}{r_{ij}^3} \sin^2 \theta_{ij} e^{\pm i2\phi} ij$$
 (3.5e)

 $\mathbf{r}_{\mathbf{i}\mathbf{j}},~\theta_{\mathbf{i}\mathbf{j}},~\text{and}~\phi_{\mathbf{i}\mathbf{j}}$ are the standard spherical coordinates.

From the symmetry for a pair we have $\phi_{ij} = \phi_{ji} + \pi$ and $\theta_{ji} = \pi - \theta_{ij}$. This gives $\alpha_{ij} = \alpha_{ji}$ which leads to $A_{ij} = A_{ji}$ and $B_{ij} = B_{ji}$. We also have $C_{ij}^{\pm 1} = -C_{ji}^{\mp 1}$ and $D_{ij}^{\pm 2} = D_{ji}^{\mp 2}$. Because the Gd ions lie on a mirror plane, for every ion above the plane at θ_{ij} there exists an ion below the plane with $\theta_{ij} = \pi - \theta_{ij}$, and with $\phi_{ij} = \phi_{ij}$.

Therefore we have

$$\sum_{(ij)} c_{ij}^{\pm 1} = \sum_{i jj} (c_{ij}^{\pm 1} + c_{ij}^{\pm 1}) = \sum_{ij} (c_{ij}^{\pm 1} - c_{ij}^{\pm 1}) = 0.$$
(3.6)

All the ions on the mirror plane have $C_{ij}^{\pm 1} = 0$. Therefore our Hamiltonian reduces to

$$H = g\mu_{B}H \sum_{i=1}^{N} S_{i}^{z} - \sum_{(ij)} \{A_{ij}S_{i}^{z}S_{j}^{z} + \frac{1}{2} B_{ij}(S_{i}^{+}S_{j}^{-} + S_{i}^{-}S_{j}^{+})\}$$
$$- \sum_{(ij)} \{D_{ij}^{+2} S_{i}^{-}S_{j}^{-} + D_{ij}^{-2} S_{i}^{+}S_{j}^{+}\}.$$
(3.7)

We now divide the Hamiltonian into a perturbed and unperturbed part by introducing an expansion parameter σ_i ,

$$\sigma_{\mathbf{i}} = \overline{S} - S_{\mathbf{i}}^{\mathbf{Z}} . \tag{3.8}$$

The parameter \overline{S} will be chosen to minimize the free energy. This will somehow imbody the behavior of the ions outside the cluster. The actual physical interpretation of \overline{S} must wait until after the analysis is complete. Our Hamiltonian now becomes

$$H = E_0 + L \sum_{i=1}^{N} \sigma_i + H_1 = H_0 + H_1$$
 (3.9)

where

$$E_{o} = -g\mu_{B}HN\overline{S} - NA_{o}\overline{S}^{2}, \qquad (3.10a)$$

$$L = g\mu_B H + 2A_O \overline{S}, \qquad (3.10b)$$

$$A_0 = \sum_{j=1}^{N-1} A_{ij}$$
, (3.10c)

and

$$H_{1} = -\sum_{(ij)} \{A_{ij}\sigma_{i}\sigma_{j} + \frac{1}{2}B_{ij}(s_{i}^{+}s_{j}^{-} + s_{i}^{-}s_{j}^{+}) + D_{ij}^{+2}s_{i}^{-}s_{j}^{-} + D_{ij}^{-2}s_{i}^{+}s_{j}^{+}\}.$$
(3.10d)

The total free energy, F, is given by

$$-\beta F = \ln Tr \exp[-\beta (H_0 + H_1)]$$
 (3.11)

where $\beta = 1/kT$. The unperturbed free energy, F_0 , is given by

$$-\beta F_{\Omega} = \ln \operatorname{Tr} \exp \left[-\beta H_{\Omega}\right]. \tag{3.12}$$

We may introduce a correction to the unperturbed free energy, F', by

$$-\beta F' = -\beta F + \beta F_{O}. \qquad (3.13)$$

To derive the molecular field approximation we simply assume $-\beta F' = 0$. Corrections to the molecular field approximation are obtained by expanding $-\beta F'$ in a cluster series.

Before we carry out the cluster expansion, we will complete the derivation of the molecular field approximation. The unperturbed free energy is given by

$$-\beta F_{O} = -\beta N A_{O} \overline{S}^{2} + N \ln \Phi_{i}$$
 (3.14)

where

$$\Phi_{i} = \text{Tr exp}[\beta LS_{i}^{z}]. \qquad (3.15)$$

We calculate \overline{S} by minimizing F_{o} with respect to \overline{S} .

Therefore

$$\overline{S} = \frac{\partial}{\partial (\beta L)} \ln \operatorname{Tr} \exp[\beta L S_{i}^{z}]$$
 (3.16)

$$\overline{S} = S B_{S}(S\beta L)$$
 (3.17)

where $B_{S}(x)$ is the Brillouin function defined by

$$B_S(x) = \frac{1}{2S} \{ (2S+1) \coth(\frac{2S+1}{2S}) x - \coth(\frac{x}{2S}) \}.$$
 (3.18)

To evaluate the magnetization we have

$$M = -\frac{\partial F_{O}}{\partial H} = \frac{N}{\beta} \frac{\partial}{\partial H} \ln \operatorname{Tr} \exp[\beta LS_{i}^{z}]$$
 (3.19)

or

$$M = Ng\mu_{B} \frac{\partial}{\partial (\beta L)} \ln Tr \exp[\beta LS_{i}^{z}], \qquad (3.20)$$

but from equation (3.16) we have

$$M = Ng\mu_{B}\overline{S} . (3.21)$$

Therefore we identify \overline{S} with $\langle S^Z \rangle$ and have the standard molecular field results.

In comparing our results with the standard molecular field equations, (Smart, 1966), we must remember that our effective exchange interaction, A_{Ω} , is given by

$$A_{O} = \sum_{j} J_{ij} + \alpha_{ij}$$

$$= J_{O} + (g\mu_{B})^{2} \sum_{j} \frac{1}{r_{ij}^{3}} (3 \cos^{2}\theta_{ij} - 1)$$
(3.22)

where

$$J_0 = z_1 J_{nn} + z_2 J_{nnn}$$
 (3.23)

 \mathbf{z}_1 is the number of nearest-neighbors and \mathbf{z}_2 the number of next-nearest neighbors.

Returning to the correction term in the free energy, $-\beta F'$, we see

$$-\beta F' = \ln \operatorname{Tr} \exp[-\beta (H_O + H_1)]$$

$$- \ln \operatorname{Tr} \exp[-\beta H_O]. \qquad (3.24)$$

This is expanded in a cluster series of the form

$$-\beta F' = \ln \operatorname{Tr} \rho_{O} \exp \left[\sum_{\alpha} Q_{\alpha}\right]$$
 (3.25)

where

$$\rho_{\Omega} = \exp[-\beta H_{\Omega}]/\text{Tr } \exp[-\beta H_{\Omega}]$$
 (3.26)

and the index α numbers the pairs (i,j) or "links" in the crystal. The expansion may then be written

$$-\beta F' = \sum_{\alpha} [-\beta F_{\alpha}] \qquad (3.27)$$

where $\{\alpha\}$ denotes each topologically distinct cluster. The correction term can be computed to any desired order, and the parameter \overline{S} is then chosen to minimize the total free energy. A criticism of this approach has been raised by Morita and Tanaka (1966). They point out that the condition of minimizing the free energy with respect to \overline{S} is not justified from the basic principles of statistical mechanics. Using a variational technique, they show that this approach is valid for the pair approximation. We can therefore extend our expansion up to the two-spin approximation.

A problem occurs when carrying the expansion to two spins due to the fact that $H_{\rm O}$ and $H_{\rm I}$ do not commute. However, this can be overcome by applying the theorem

$$e^{\beta A} e^{-\beta (A+B)} = P \exp \left[-\int_{0}^{\beta} B_{\lambda} d\lambda\right]$$
 (3.28)

where P is the Dyson ordering operator, and where

$$B_{\lambda} \equiv e^{\lambda A} B e^{-\lambda A} . \qquad (3.29)$$

We have derived the two-spin correction term and find

$$-\beta F'_{(2)} = \sum_{(i,j)} \ln \text{Tr } \exp[-\beta Q_{ij}] + \text{single ion terms}$$
(3.30)

where

$$Q_{ij} = -\Omega_{ij}(\overline{S}) (S_{i}^{z} + S_{j}^{z}) - A_{ij}S_{i}^{z}S_{j}^{z}$$

$$- \frac{1}{2} B_{ij}(S_{i}^{+}S_{j}^{-} + S_{i}^{-}S_{j}^{+})$$

$$- D_{ij}^{+2} S_{i}^{-}S_{j}^{-} - D_{ij}^{-2} S_{i}^{+}S_{j}^{+}, \qquad (3.31)$$

and

$$\Omega_{ij}(\overline{S}) \equiv g\mu_B H + 2(A_0 - \frac{1}{2}A_{ij})\overline{S}. \qquad (3.32)$$

Because of the dependence of Q_{ij} on \vec{r}_{ij} and \vec{s} , and the necessity to carry out the summation over many ions to adequately include the effect of the dipole-dipole term, this calculation is untractable.

Although Gd^{3+} has a spin of 7/2, thereby making Q_{ij} a 64 x 64 matrix, the calculation difficulties are evident in the case of S = 1/2. We use as a basis set the states $|S_1, S_2, S_1^2, S_2^2\rangle$ where we adopt the convention

$$|S_1, S_2, +1/2, +1/2\rangle \equiv |++\rangle$$
 (3.33)

and

$$|s_1, s_2, +1/2, -1/2\rangle \equiv |+-\rangle$$
 (3.34)

 $Q_{i,j}$ then has the form

$$|++\rangle \qquad |--\rangle \qquad |-+\rangle \qquad |+-\rangle$$

$$|++\rangle \qquad \left[\begin{array}{ccccc} \Omega_{\mathbf{i}\mathbf{j}}(\mathbf{S}) - \frac{1}{4} \, \mathbf{A}_{\mathbf{i}\mathbf{j}} & -\mathbf{D}_{\mathbf{i}\mathbf{j}}^{-2} & 0 & 0 \\ -\mathbf{D}_{\mathbf{i}\mathbf{j}}^{+2} & \Omega_{\mathbf{i}\mathbf{j}}(\mathbf{S}) - \frac{1}{4} \, \mathbf{A}_{\mathbf{i}\mathbf{j}} & 0 & 0 \\ -\mathbf{D}_{\mathbf{i}\mathbf{j}}^{+2} & \Omega_{\mathbf{i}\mathbf{j}}(\mathbf{S}) - \frac{1}{4} \, \mathbf{A}_{\mathbf{i}\mathbf{j}} & 0 & 0 \\ -\mathbf{D}_{\mathbf{i}\mathbf{j}}^{+2} & \Omega_{\mathbf{i}\mathbf{j}}(\mathbf{S}) - \frac{1}{4} \, \mathbf{A}_{\mathbf{i}\mathbf{j}} & 0 & 0 \\ -\mathbf{D}_{\mathbf{i}\mathbf{j}}^{+2} & \Omega_{\mathbf{i}\mathbf{j}}(\mathbf{S}) - \frac{1}{4} \, \mathbf{A}_{\mathbf{i}\mathbf{j}} & 0 & 0 \\ -\mathbf{D}_{\mathbf{i}\mathbf{j}}^{+2} & \Omega_{\mathbf{i}\mathbf{j}}(\mathbf{S}) - \frac{1}{4} \, \mathbf{A}_{\mathbf{i}\mathbf{j}} & 0 & 0 \\ -\mathbf{D}_{\mathbf{i}\mathbf{j}}^{+2} & \Omega_{\mathbf{i}\mathbf{j}}(\mathbf{S}) - \frac{1}{4} \, \mathbf{A}_{\mathbf{i}\mathbf{j}} & 0 & 0 \\ -\mathbf{D}_{\mathbf{i}\mathbf{j}}^{+2} & \Omega_{\mathbf{i}\mathbf{j}}(\mathbf{S}) - \frac{1}{4} \, \mathbf{A}_{\mathbf{i}\mathbf{j}} & 0 & 0 \\ -\mathbf{D}_{\mathbf{i}\mathbf{j}}^{+2} & \Omega_{\mathbf{i}\mathbf{j}}(\mathbf{S}) - \frac{1}{4} \, \mathbf{A}_{\mathbf{i}\mathbf{j}} & 0 & 0 \\ -\mathbf{D}_{\mathbf{i}\mathbf{j}}^{+2} & \Omega_{\mathbf{i}\mathbf{j}}(\mathbf{S}) - \frac{1}{4} \, \mathbf{A}_{\mathbf{i}\mathbf{j}} & 0 & 0 \\ -\mathbf{D}_{\mathbf{i}\mathbf{j}}^{+2} & \Omega_{\mathbf{i}\mathbf{j}}(\mathbf{S}) - \frac{1}{4} \, \mathbf{A}_{\mathbf{i}\mathbf{j}} & 0 & 0 \\ -\mathbf{D}_{\mathbf{i}\mathbf{j}}^{+2} & \Omega_{\mathbf{i}\mathbf{j}}(\mathbf{S}) - \frac{1}{4} \, \mathbf{A}_{\mathbf{i}\mathbf{j}} & 0 & 0 \\ -\mathbf{D}_{\mathbf{i}\mathbf{j}}^{+2} & \Omega_{\mathbf{i}\mathbf{j}}(\mathbf{S}) - \frac{1}{4} \, \mathbf{A}_{\mathbf{i}\mathbf{j}} & 0 & 0 \\ -\mathbf{D}_{\mathbf{i}\mathbf{j}}^{+2} & \Omega_{\mathbf{i}\mathbf{j}}(\mathbf{S}) - \frac{1}{4} \, \mathbf{A}_{\mathbf{i}\mathbf{j}} & 0 & 0 \\ -\mathbf{D}_{\mathbf{i}\mathbf{j}}^{+2} & \Omega_{\mathbf{i}\mathbf{j}}(\mathbf{S}) - \frac{1}{4} \, \mathbf{A}_{\mathbf{i}\mathbf{j}} & 0 & 0 \\ -\mathbf{D}_{\mathbf{i}\mathbf{j}}^{+2} & \Omega_{\mathbf{i}\mathbf{j}}(\mathbf{S}) - \frac{1}{4} \, \mathbf{A}_{\mathbf{i}\mathbf{j}} & 0 & 0 \\ -\mathbf{D}_{\mathbf{i}\mathbf{j}}^{+2} & \Omega_{\mathbf{i}\mathbf{j}}(\mathbf{S}) - \frac{1}{4} \, \mathbf{A}_{\mathbf{i}\mathbf{j}} & 0 & 0 \\ -\mathbf{D}_{\mathbf{i}\mathbf{j}}^{+2} & \Omega_{\mathbf{i}\mathbf{j}}(\mathbf{S}) - \frac{1}{4} \, \mathbf{A}_{\mathbf{i}\mathbf{j}} & 0 & 0 \\ -\mathbf{D}_{\mathbf{i}\mathbf{j}}^{+2} & \Omega_{\mathbf{i}\mathbf{j}\mathbf{j}^{+2} & \Omega_{\mathbf{i}\mathbf{j}\mathbf{j}^{+2} & \Omega_{\mathbf{i}\mathbf{j}}(\mathbf{S}) - \frac{1}{4} \, \mathbf{A}_{\mathbf{i}\mathbf{j}} & 0 \\ -\mathbf{D}_{\mathbf{i}\mathbf{j}}^{+2} & \Omega_{\mathbf{i}\mathbf{j}\mathbf{j}^{+2} & \Omega_{\mathbf{i}\mathbf{j}\mathbf{j}^{+2} & \Omega_{\mathbf{i}\mathbf{j}\mathbf{j}^{+2} & \Omega_{\mathbf{j}\mathbf{j}^{+2}} \\ -\mathbf{D}_{\mathbf{i}\mathbf{j}\mathbf{j}}^{+2} & \Omega_{\mathbf{i}\mathbf{j}\mathbf{j}^{+2} & \Omega_{\mathbf{j}\mathbf{j}\mathbf{j}^{+2} & \Omega_{\mathbf{j}\mathbf{j}^{+2} & \Omega_{\mathbf{j}\mathbf{j}\mathbf{j}^{+2} & \Omega_{\mathbf{j}\mathbf{j}\mathbf{j}^{+2} & \Omega_{\mathbf$$

The coefficients A_{ij} , B_{ij} , and D_{ij} are all of the same order of magnitude, therefore we cannot neglect the off-diagonal terms nor can we apply perturbation theory. All coefficients depend on r_{ij} , θ_{ij} and ϕ_{ij} , the spherical coordinates of the (i,j) pair, and Ω_{ij} also depends on \overline{S} . Therefore we must diagonalize Q_{ij} for each pair in the crystal and for each \overline{S} .

We have carried out calculations in a very crude approximation by neglecting the off-diagonal terms and only considering the nearest-neighbor and next-nearest-neighbor interactions. These calculations predict a transition temperature slightly lower than the observed value, and a temperature dependence of the magnetization which is qualitatively correct. However, the crudity of this approximation renders it invalid, and indicates that the agreement is simply fortuitous.

An improved approximation would be to correctly treat

the operator Q_{ij} for the nearest-neighbor and next-nearest-neighbor pairs and include the effect of the other pairs only in A_o. Although this is an improvement in terms of an accurate treatment of the neighboring spins in the two-spin approximation, the two-spin cluster, even when treated correctly for all spins, does not satisfactorily treat the cooperative phenomena. This is especially true because of the antiferromagnetic nearest-neighbor interaction present in GdCl₃. For this reason this calculation was not pursued further.

2) Green Function

A relatively recent approximation technique employs the double-time temperature-dependent Green function (Zubarev, 1960). The retarded double-time temperaturedependent Green function is defined as

$$<> = -i\theta(t-t')<[A(t), B(t')]>$$
 (3.36)

where $\theta(t-t')$ is the unit step function. <> denotes the ensemble average and <<>> denotes the Green function.

A(t) and B(t') are quantum mechanical operators. The equation of motion for the Green function is

$$i \frac{d}{dt} << A(t), B(t')>> = \delta(t-t')<[A(t), B(t')]>$$

$$+ << [A(t), H]; B(t')>> . (3.37)$$

Taking the Fourier transform over the time variable into the energy variable gives

$$\omega <>_{\omega} = \frac{1}{2\pi} <[A,B]> + <<[A,H];B>>_{\omega}$$
 (3.38)

where h = 1.

Once the operators A and B have been chosen for the problem, the solution of the Green function $<<A;B>>_{\omega}$ is nontrivial since it is given in terms of a higher order Green function $<<[A_1,H];B>>_{\omega}$ which is also unknown. The general technique is to approximate the higher order Green function in terms of the lower order Green function. This is called decoupling the equation of motion.

In magnetic systems the operators A and B are generally S_i^{\pm} and S_j^{\mp} . The higher order Green functions are generally of the form

$$\langle\langle S_{\ell}^{\mathbf{z}} S_{\mathbf{j}}^{\pm}; S_{\mathbf{r}}^{\mathbf{z}} \rangle\rangle_{\omega}$$
 (3.39)

The random phase approximation decouples this by assuming

$$\langle\langle s_{\ell}^{\mathbf{z}} s_{\mathbf{j}}^{\pm}; s_{\mathbf{r}}^{\mathbf{T}} \rangle\rangle_{\omega} |_{\ell \neq \mathbf{j}} \langle s_{\mathbf{z}}^{\mathbf{z}} \rangle\langle\langle s_{\mathbf{j}}^{\pm}; s_{\mathbf{r}}^{\mathbf{T}} \rangle\rangle_{\omega}.$$
 (3.40a)

With this assumption we are now in a position to solve for

$$<< s_{j}^{\pm}; s_{r}^{\mp}>>_{\omega}$$
 (3.40b)

Becker and Plischke (1970) have used the Hamiltonian (3.7) in the Green function formalism and solved the problem using the random phase approximation. We will compare our results to their calculation.

Spin Wave Calculation

Unlike the cluster expansion and Green function approaches which apply to all temperatures, the spin wave

approach applies to a restricted temperature range. In the spin wave approximation we have sacrificed the large temperature range for an exact quantum mechanical treatment. The linear spin wave theory was first considered by Bloch (1930, 1932), and later by Holstein and Primakoff (1940). The spin operators in the Hamiltonian are replaced by creation and annihilation operators, a[†] and a respectively, by the substitution

$$s^+ + (2s)^{1/2}a$$
 (3.41a)

$$s^- \to (2s)^{1/2} a^{\dagger}$$
 (3.41b)

$$S^{Z} \rightarrow S - a^{\dagger}a \tag{3.41c}$$

Only terms quadratic in the creation and annihilation operators are retained. As long as the higher order terms are not significant, i.e. as long as multiple scattering processes are not important, the spin wave approximation is valid.

Marquard and Stinchcombe (1967) have treated the Hamiltonian in the spin wave approximation by generalizing the interaction between the spin operators to include any symmetric interaction. They have also treated the dipoledipole interaction exactly by using the Ewald technique to evaluate the \vec{k} -dependent dipole sums.

IV. Cl N.M.R. IN GdCl3: RESULTS AND DISCUSSION

A. N.M.R. Hamiltonian

When a nucleus of spin $I \geq 1$ is located in a lattice, the Hamiltonian describing the interactions between the nucleus and the local environments at the nuclear site due to the lattice may be written as

$$H = -\stackrel{\rightarrow}{\mu} \stackrel{\bullet}{\cdot} \stackrel{\rightarrow}{B} - \frac{1}{2} \stackrel{\rightarrow}{Q} : \stackrel{\rightarrow}{\vee} \stackrel{\rightarrow}{E} . \tag{4.1}$$

The first term is the Zeeman interaction between the nuclear dipole moments, $\vec{\mu}$, and the internal field \vec{B} . The second term is the quadrupole interaction between the nuclear quadrupole moment tensor, \vec{Q} , and the crystalline electric field gradient (E.F.G.) tensor, $\vec{\nabla}\vec{E}$. We use the XYZ coordinate system which diagonalizes the field gradient tensor, $-(\vec{\nabla}\vec{E})_{ij} = V_{ij}\delta_{ij}$, as our reference frame. The Zeeman interaction is then written

$$H_{M} = - \Omega h \vec{1} \cdot \vec{B}$$

$$= - \Omega h [I_{2}B_{2} + \frac{1}{2} (I^{+}B^{-} + I^{-}B^{+})] \qquad (4.2)$$

where

$$\Omega = \gamma B_{\Omega} , \qquad (4.3)$$

 γ is the nuclear gyromagnetic ratio.

The quadrupole interaction may be written

$$H_{O} = 6A[3I_{z}^{2} - I^{2} + \eta(I_{x}^{2} + I_{y}^{2})]/h^{2}$$
 (4.4)

where

$$A = e^2 QV_{ZZ}/4I(2I+1) = e^2 Qq/4I(2I+1)$$
 (4.5)

and $\boldsymbol{\eta}$ is the field gradient asymmetry parameter,

$$\eta = (V_{xx} - V_{yy})/V_{zz}$$
 (4.6)

with the standard convention $|V_{xx}| \le |V_{yy}| \le |V_{zz}|$.

The matrix elements of the Hamiltonian are given by

$$< m \mid H_{M} \mid m> = - \Omega m \cos \theta,$$
 (4.7a)

$$\langle m | H_M | m+1 \rangle = -\frac{\Omega}{2} \sqrt{(I-m)(I+m+1)} \sin \theta e^{i\phi}$$
, (4.7b)

$$\langle m | H_O | m \rangle = A[3m^2 - I(I+1)],$$
 (4.7c)

and

$$< m \mid H_Q \mid m+2> = < m-2 \mid H_Q \mid m> =$$

$$\sqrt{(I+m)(I-m+1)(I+m-1)(I-m+2)} \frac{A}{2} \eta$$
. (4.7d)

The angles θ and ϕ are the polar and aximuthal angles respectively of \hat{B} in the XYZ principal axis system.

From the analysis of a nuclear resonance spectrum we may determine: 1) the magnitude of the electric field gradient, q, 2) the asymmetry parameter, η , and 3) the direction and magnitude of an internal field \vec{B} . All of these parameters are determined at the nuclear site only.

Figure 4.1 shows the 35 Cl N.M.R. transition frequencies in $GdCl_3$ as a function of temperature below the transition temperature of approximately 2.2 K. The facts that we see only three transition frequencies in the ordered state and that the chlorines lie on a mirror plane indicate that the internal field at the Cl site must be along C_3 . Also, because of the mirror plane one of the principal axes of the E.F.G. must be parallel to C_3 . In

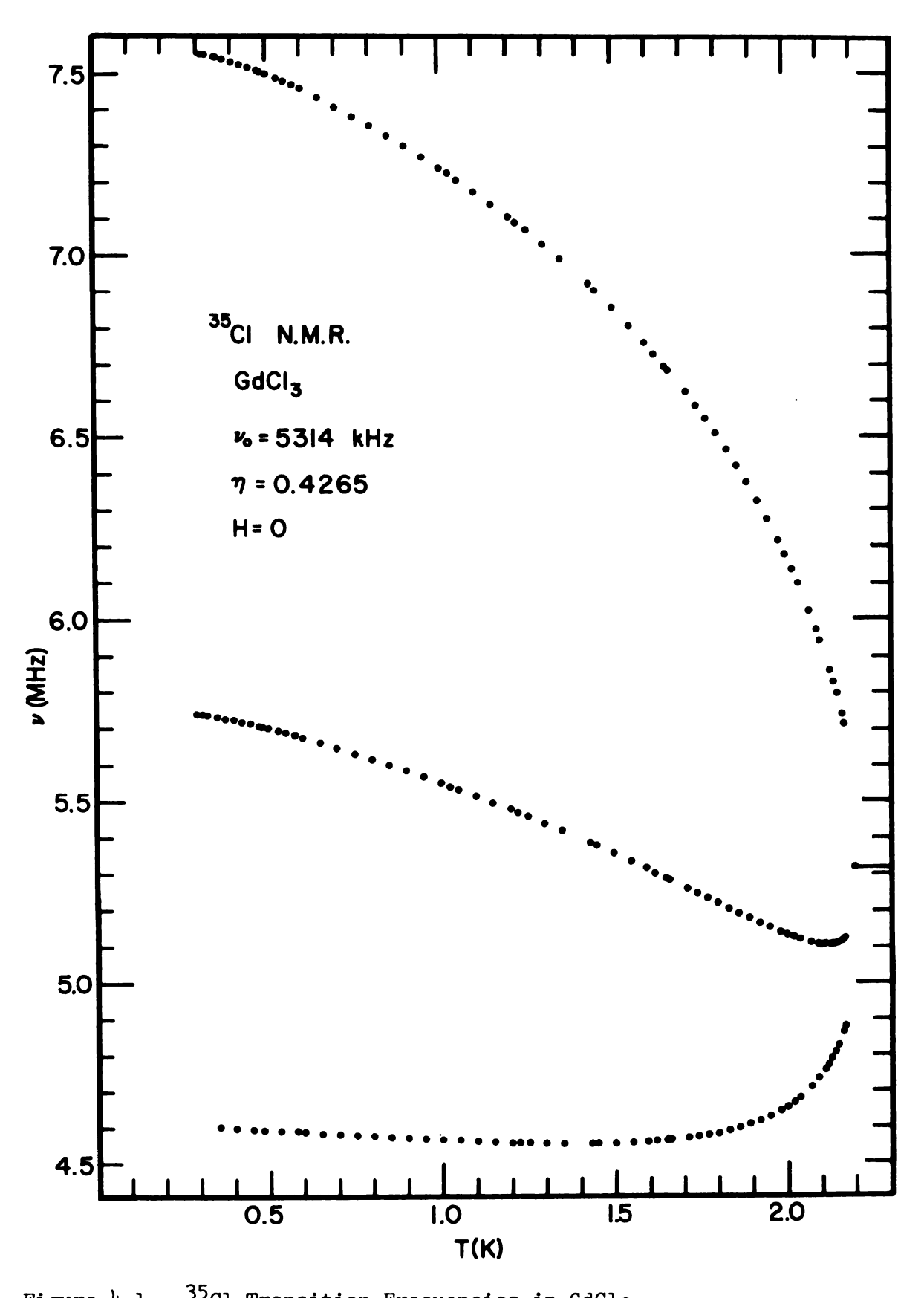


Figure 4.1. 35Cl Transition Frequencies in GdCl₃

all the rare earth trichlorides lanthanum to gadolinium we find this to be the X-axis.

We now use the fact that the X-axis of the E.F.G. and the internal magnetic field coincide to simplify our analysis of the N.M.R. spectrum.

B. Determine η by the Method of Moments

The asymmetry parameter is easily determined by the method of energy moments (Brown and Parker, 1955). They let the (2I + 1) eigenvalues of the Hamiltonian be equal to λ_n , $n = 1, 2, \ldots$ (2I + 1). The moments of energy are defined as

$$S_1 = \sum_{n} \lambda_n , \qquad (4.8a)$$

$$S_2 = \sum_{n} \lambda_n^2 , \qquad (4.8b)$$

and

$$S_3 = \sum_{n} \lambda_n^3 , \qquad (4.8c)$$

The first moment is equal to zero since the representation is traceless. The second and third moments, S_2 and S_3 , can be regarded as experimentally determined quantities if we can construct the energy level diagram from the observed transition frequencies. This is possible if each of the (2I+1) levels is implicated in at least one observed transition. Brown and Parker show that it follows without approximation that

$$S_2 = P_2 C_3^2 \left(1 + \frac{1}{3} \eta^2\right) + P_1 v^2$$
 (4.9a)

and

$$S_3 = P_3 C_3^2 (1 - \eta^2) + 3P_2 C_3 v^2 x$$

$$(3 \cos^2 \theta - 1 + \eta \cos 2\phi \sin^2 \theta). \tag{4.9b}$$

 C_3 is the pure quadrupole frequency interval with η = 0,

$$C_3 = 3 e^2 Qg/2I(2I-1)h = 6A,$$
 (4.10)

 ν is the Larmor frequency of $\vec{\mu}$ in the field \vec{B} ,

$$v = \mu B/Ih. \tag{4.11}$$

The coefficients p_i are polynomials in I as follows:

$$p_1 = 2I(I + 1)(2I + 1)/3!,$$
 (4.12a)

$$p_2 = 2I(I + 1)(2I - 1)(2I + 1)(2I + 3)/3(5!), (4.12b)$$

and

$$p_3 = 2I(I+1)(2I-3)(2I-1)(2I+1)(2I+3)(2I+5)/3(7!).$$
(4.12c)

For our case of I = 3/2, the coefficients reduce to: $p_1 = 5$, $p_2 = 1$, and $p_3 = 0$.

For the case of $\eta\neq 0$ the observed pure quadrupole resonance frequency, $\boldsymbol{\nu}_{\bigcap}$, is given by

$$v_{Q} = \frac{6e^{2}Qq(1 + \frac{1}{3}\eta^{2})^{1/2}}{4I(2I - 1)h}.$$
 (4.13)

Therefore we may express C_3 as

$$C_3 = V_0/\rho \tag{4.14}$$

where

$$\rho = (1 + \frac{1}{3} \eta^2)^{1/2} . \tag{4.15}$$

We now use the fact that the internal field, \vec{B} , is parallel to the X-axis to reduce the expressions for the second and third moments. We find

$$S_2 = v_0^2 + 5v^2 \tag{4.16a}$$

and

$$s_3 = \frac{3v_Qv^2}{\rho} (\eta - 1)$$
 (4.16b)

Since the magnitude of the internal field is a function of temperature and still unknown, we solve equation (4.16a) for ν^2 and substitute into equation (4.16b) to get a quadratic equation for η whose solutions are given by

$$\eta = \frac{D \pm (D^2 - 4AC)^{1/2}}{2A} \tag{4.17}$$

where

$$A = \frac{g}{25} v_0^2 (S_2 - v_0^2) - S_3^2/3, \qquad (4.18a)$$

$$C = A - \frac{2}{3} S_3^2$$
, (4.18b)

and

$$D = 2A + \frac{2}{3} S_3^2 . {(4.18c)}$$

Figure 4.2 shows the energy level scheme for the Cl nucleus in zero magnetic field and in a finite magnetic field. Because we see three lines in the ordered state, each going to the zero field pure quadrupole line at the transition temperature, we may uniquely determine the energy level diagram in terms of the observed frequencies f_2 , f_3 , and f_4 . The relationships between the energy levels and the transition frequencies are given by

$$4\lambda_1 = -f_2 - 3f_3 + 2f_4, \qquad (4.19a)$$

$$4\lambda_2 = -f_2 + 3f_3 - 2f_4, \tag{4.19b}$$

$$4\lambda_3 = -f_2 + f_3 + 2f_4, \qquad (4.19c)$$

and

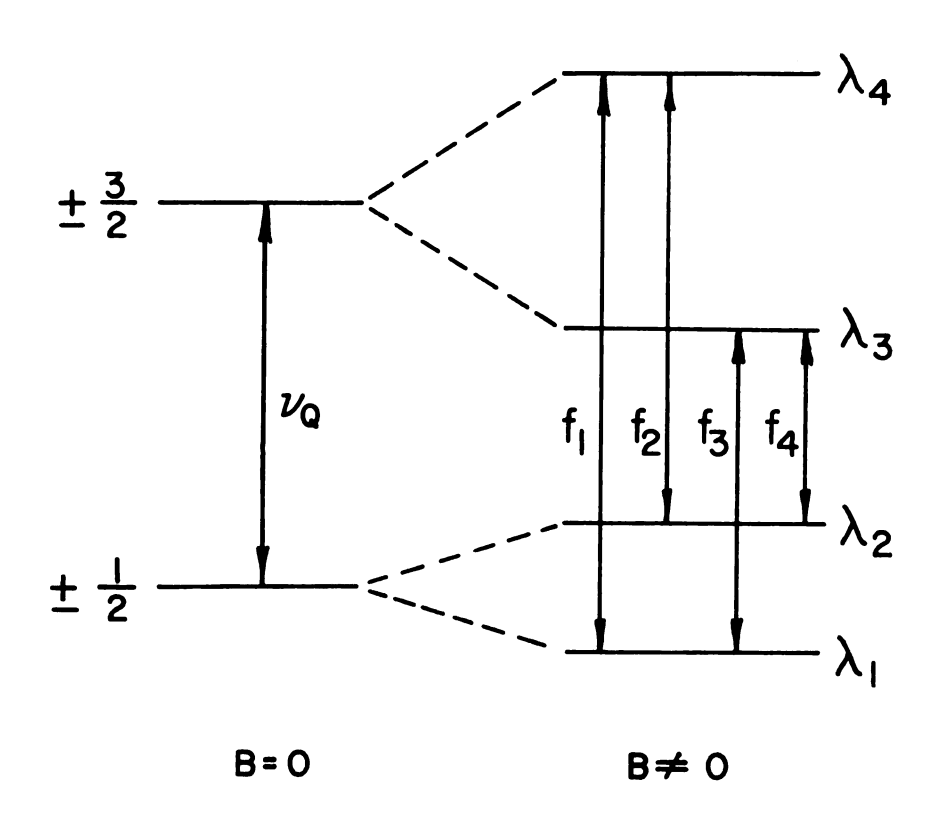


Figure 4.2. Energy Levels for a Spin 3/2 Nucleus in a Crystal

$$4\lambda_A = 3f_2 + f_3 - 2f_A.$$
 (4.19d)

We are now in a position to determine η at any temperature. All we require is a knowledge of the pure quadrupole resonance transition frequency, which we assume remains constant through the phase transition. Table B.1 of Appendix B shows the average of the five independent frequency measurements for all the observed transitions and the standard deviation of the frequency measurements. From the low temperature results we find

$$\eta = 0.4265 \pm 0.0001$$
 (4.20)

C. Determine the Magnitude of the Internal Field

We could apply the method of moments to determine the magnitude of the internal field as a function of temperature; however, we do not always have the three observed frequencies necessary to uniquely determine the energy levels. An alternate approach, which will allow us to determine the magnitude of the internal field with only a single observed frequency, is to calculate the transition frequencies in terms of the internal field magnitude and then solve for the field magnitude.

The Hamiltonian written in matrix form from equation (4.7) is

$$\begin{bmatrix} 3A - \frac{3}{2} \Omega & 0 & \sqrt{3} A\eta & 0 \\ 0 & -3A - \frac{1}{2} \Omega & 0 & \sqrt{3} A\eta \\ \sqrt{3} A\eta & 0 & -3A + \frac{1}{2} \Omega & 0 \\ 0 & \sqrt{3} A\eta & 0 & 3A + \frac{3}{2} \Omega \end{bmatrix}.$$
(4.21)

This is easily solved and gives

$$\lambda_1 = -\frac{\Omega}{2} - \frac{1}{2} \sqrt{v_Q^2 + 4(\Omega^2 - \Omega v_Q/\rho)}$$
, (4.22a)

$$\lambda_2 = -\frac{\Omega}{2} + \frac{1}{2} \sqrt{v_Q^2 + 4(\Omega^2 - \Omega v_Q/\rho)}$$
, (4.22b)

$$\lambda_{3} = \frac{\Omega}{2} - \frac{1}{2} \sqrt{\nu_{Q}^{2} + 4(\Omega^{2} + \Omega \nu_{Q}/\rho)} , \qquad (4.22c)$$

and

$$\lambda_4 = \frac{\Omega}{2} + \frac{1}{2} \sqrt{\nu_Q^2 + 4(\Omega^2 + \Omega \nu_Q/\rho)}$$
 (4.22d)

The transition frequencies are now given by

$$f_1 = \lambda_A - \lambda_1 , \qquad (4.23a)$$

$$f_2 = \lambda_4 - \lambda_2 , \qquad (4.23b)$$

$$f_3 = \lambda_3 - \lambda_1 , \qquad (4.23c)$$

and
$$f_4 = \lambda_3 - \lambda_2$$
 (4.23d)

Since there are two isotopes of chlorine which have a spin of 3/2, ³⁵Cl, 75.4% abundant, and ³⁷Cl, 24.6% abundant, we observe two pure quadrupole resonance transitions in the paramagnetic state at 5314 kHz and 4188 kHz respectively. In the ordered state we see three lines for each isotope.

The energy levels of the different isotopes will be different because of the difference in the nuclear quadrupole moments, given by

$$\frac{35_{\text{VQ}}}{37_{\text{VQ}}} = \frac{35_{\text{Q}}}{37_{\text{Q}}} = 1.26878 \tag{4.24}$$

and the differences in the nuclear gyromagnetic ratios

$$^{35}\gamma = 0.4172 \text{ kHz/gauss}$$
 (4.25a)

and

$$37_{\Upsilon} = 0.3472 \text{ kHz/gauss}$$
 (4.25b)

To take advantage of the additional data from the two isotopes in determining the magnitude of the internal field, we employ a chi squared analysis. We define χ^2 by

$$\chi^{2} = \frac{1}{N-1} \sum_{i,j} \frac{(f_{i}^{j}(T) - f_{i}^{j}(B))^{2}}{\Delta f(lw)^{2} + \Delta f_{i}^{j}(sd)^{2}}$$
(4.26)

where

j = 35 or 37, an isotope label,

i = 1, 2, ... (2I + 1), a line label,

N = the total number of observed lines at a given temperature

- Δf(lw) = the inherent uncertainty in the frequency
 measurement due to the finite line width,
 assumed independent of isotope and line
 label, and

 $\Delta f_{i}^{j}(sd)$ = the standard deviation for the five independent frequency measurements.

A simple computer program for the CDC 6500 was used to determine the value of B that minimizes χ^2 . Because the line width is very dependent on temperature and not directly measured by our spectrometer, we varied the line width in a systematic manner to force χ^2 to have a value no greater than 2.0. The uncertainty in the calculated field, B, was then determined by making a contour plot of χ^2 vs. B in the vicinity of χ^2_{\min} . From this contour the uncertainty could be assigned by noting the value of B for which χ^2 equaled $\chi^2_{\min} + 1.0$. Figure 4.3 shows the results of the internal field vs. temperature for GdCl₃. Table B.2 of Appendix B tabulates the results of the χ^2 analysis.

D. Comparison of Temperature Dependence to Theory

1) Calibration

Nuclear magnetic resonance in the absence of an applied external field measures the local field at a nuclear site.

This field is given by

$$\vec{B}_{i} = (g\mu_{B}) \sum_{j} \left\{ \frac{3(\langle \vec{s}_{j} \rangle \cdot \vec{r}_{ij}) \vec{r}_{ij}}{r_{ij}^{5}} - \frac{\langle \vec{s}_{j} \rangle}{r_{ij}^{3}} \right\}$$

$$- (\gamma_{n} \hbar)^{-1} \vec{A}_{ij} \cdot \langle \vec{s}_{j} \rangle .$$
(4.27)

The first term is the field due to the moments of the Gd ions, the second term is the transferred hyperfine field.

† is the transferred hyperfine interaction tensor between

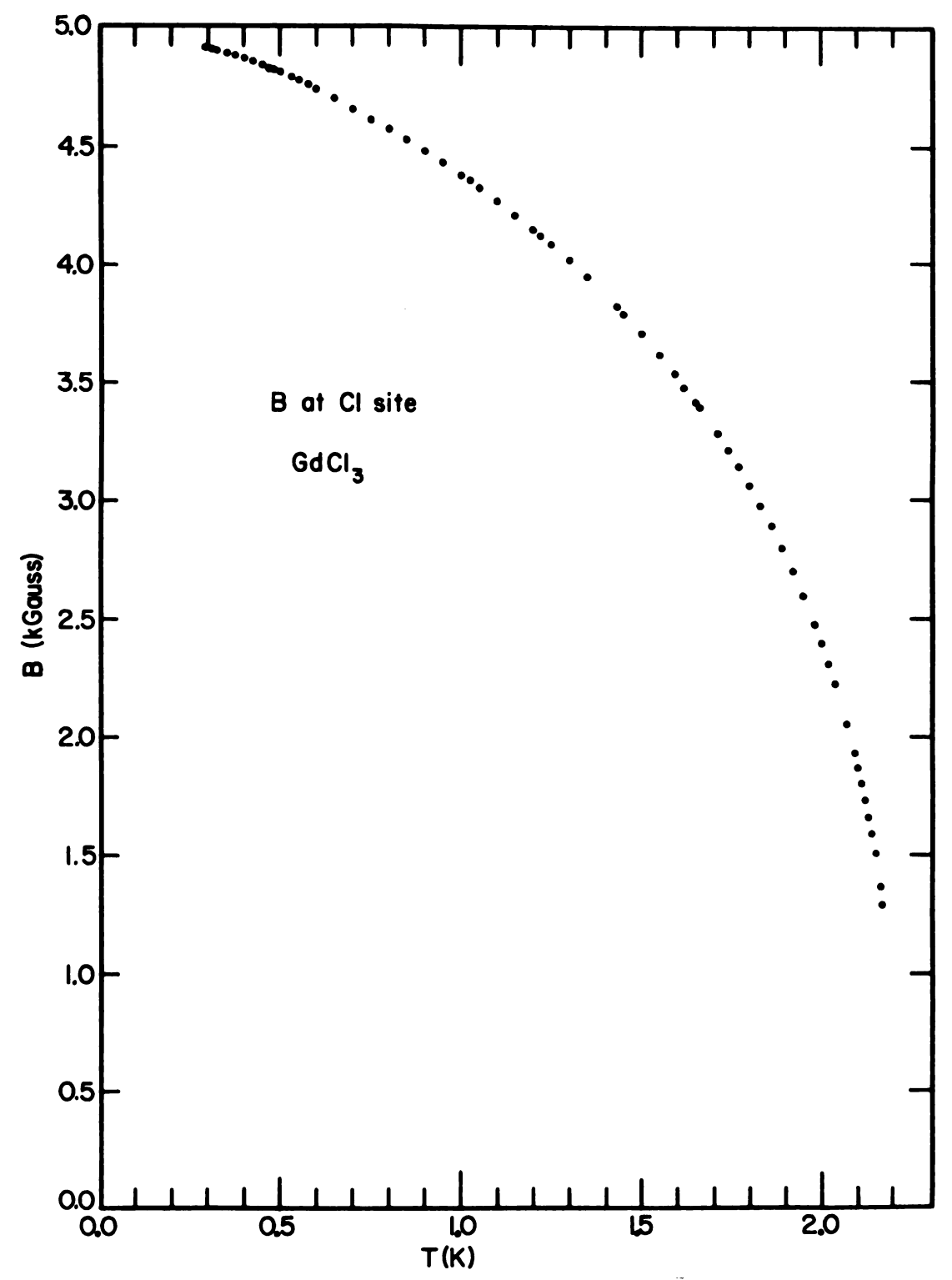


Figure 4.3. Internal Field at Chlorine Site vs. Temperature for GdCl3

the ith nucleus and the jth ion, and \vec{s}_j is the spin of the jth Gd ion. The bracket, <>, denotes the thermal average. The time necessary for thermal averaging is of the order of the period of the phonon motion. This is many orders of magnitude smaller than our sampling time, therefore we may consider $\langle \vec{s}_j \rangle$ as a temperature dependent vector.

If the lattice parameters are independent of temperature and field, i.e. no thermal contraction or magnetostriction, the dipolar contribution to \vec{B}_i is proportional to $\langle \vec{S} \rangle$. Similarly, if \vec{A} is temperature and field independent, the total \vec{B}_i is then directly proportional to $\langle \vec{S} \rangle$.

Because we have no easy and direct way of measuring the temperature and field dependence of the lattice constant and the term \overrightarrow{A} , we make the usual assumption that they are temperature and field independent.

Magnetization measurements are very difficult and often inaccurate. Wyatt (1963) has measured the magnetization vs. temperature for GdCl₃ by noting the temperature and field of the discontinuity in adiabatic isentropic magnetization measurements. Unfortunately his thermometry is only accurate to ±4 mK, and he does not discuss the accuracy of his field measurements. From his curve of specimen temperature vs. applied field during isentropic magnetization we can reasonably assume that the temperature of the kink is known to ±4 mK and the field to ±10 Oersteds.

Using this as an estimate for the accuracy of his data, we have superimposed our N.M.R. results onto his magnetization results, using the relationship

 $M(e.m.u./cm^3) = KB(gauss)$ (4.28) where $K = (0.1232 \pm 0.0027) \text{ emu/cm}^3\text{-gauss.}$ Figure 4.4 shows this comparison.

Wyatt has also measured the magnetization in applied field using a vibrating sample magnetometer. Unfortunately at an applied field, H, of about (1/2) NM_c, where N is the demagnetizing factor and $M_{_{\mathbf{S}}}$ is the spontaneous magnetization, the magnetization deviates from the expression M = H/N. If the law had held up to fields $H = NM_{e}$ then the point of departure would have been sudden and the value of the field would have been a measure of the spontaneous magnetization. He estimates the spontaneous magnetization by plotting H against the internal field, H_{i} , and extrapolates to $H_i = 0$. The results are shown in Figure 4.5 along with our results using a calibration constant, $K = (0.1137 \pm 0.0013) \text{ emu/cm}^3$ -gauss. Because of the uncertainty in the extrapolation procedure and because of the lack of agreement in the temperature dependence between our measurements we will use the isentropic magnetization measurements as a calibration.

We must keep in mind the limitations of this calibration. Whenever possible we will compare our results to the temperature dependent part of a theory, thereby not relying on the calibration. All fitting of our data to

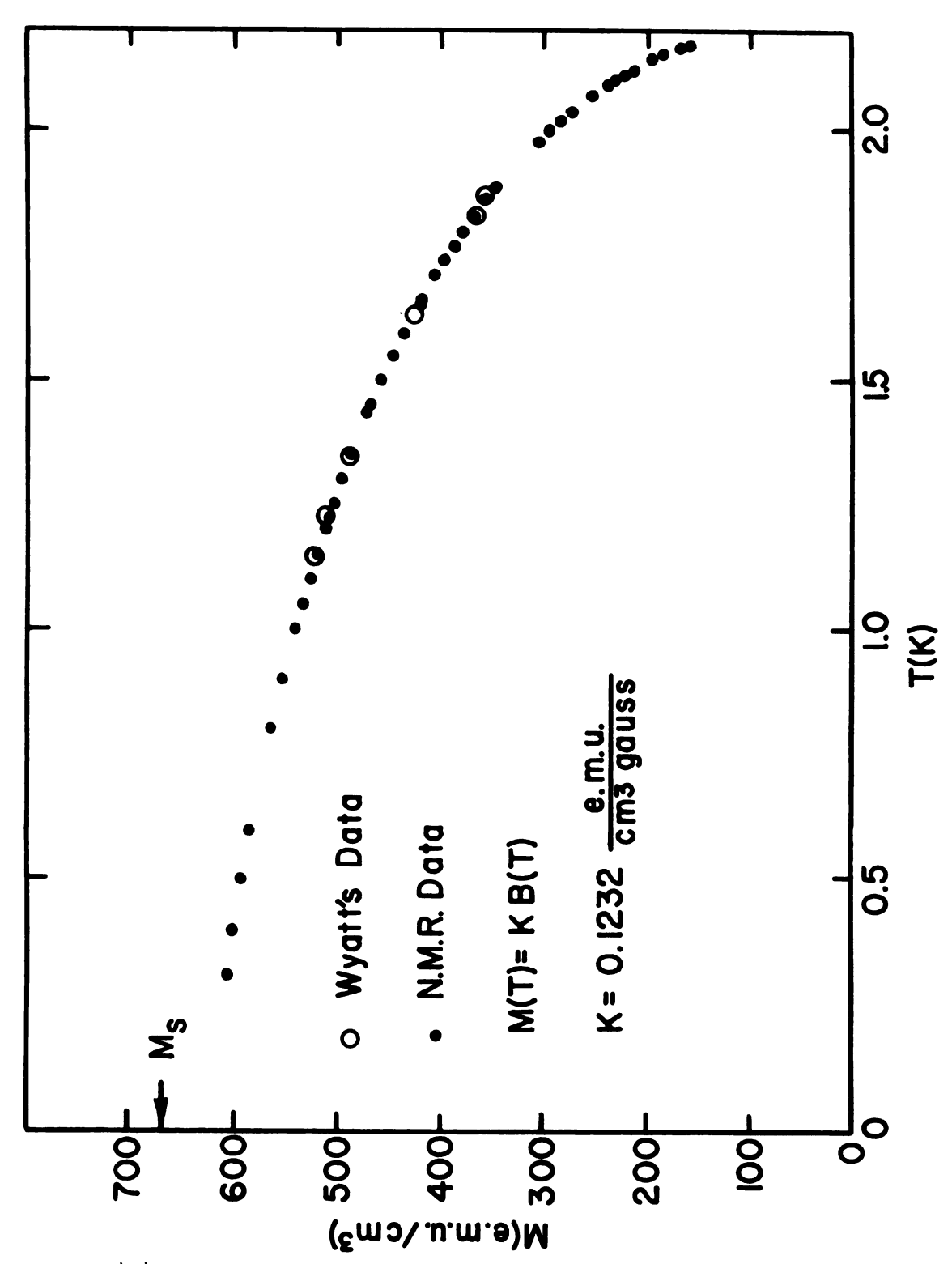


Figure 4.4. Comparison of N.M.R. and Isentropic Magnetization Data

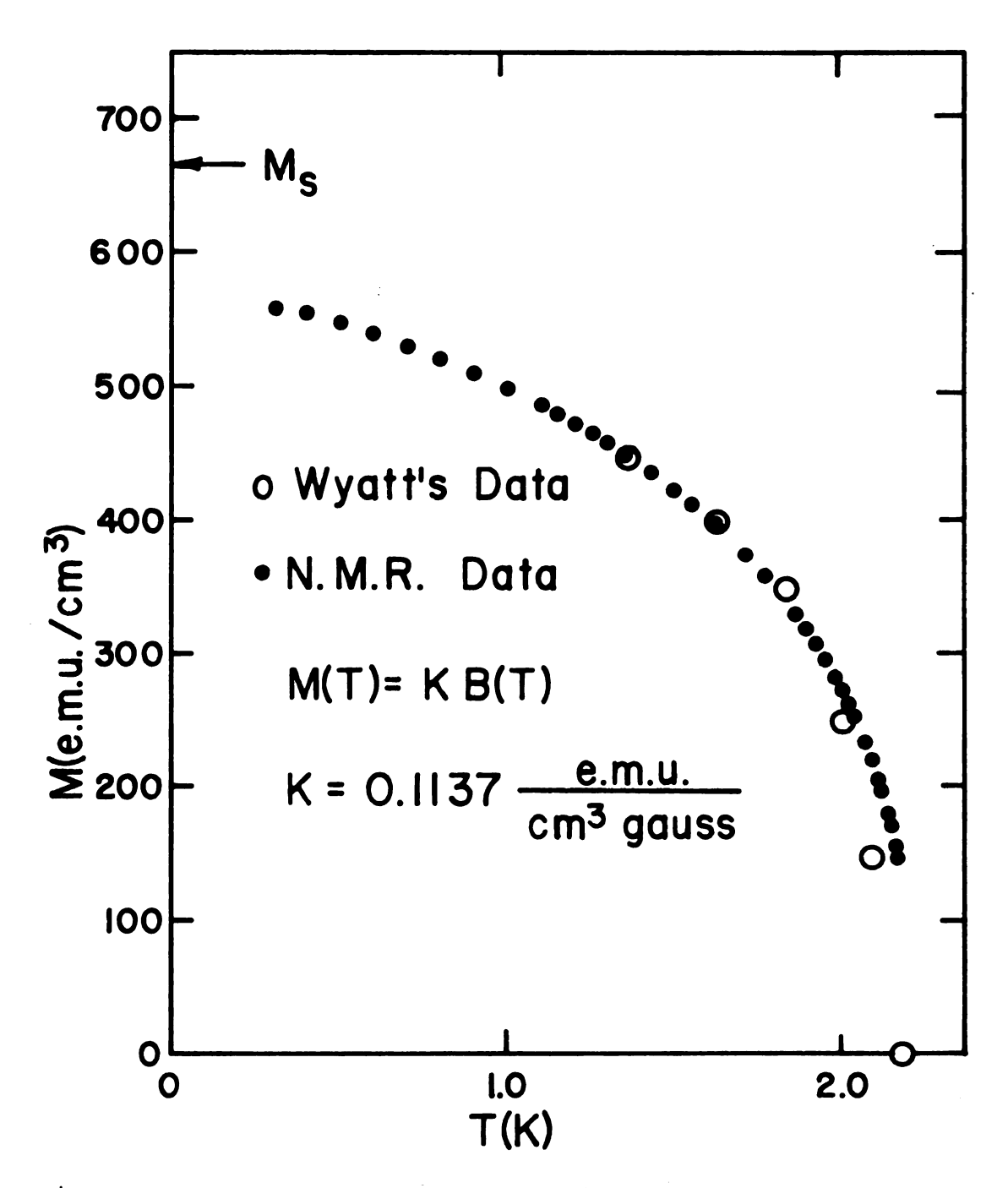


Figure 4.5. Comparison of N.M.R. and Magnetization Data

analytic expressions will be carried out using the internal field data, and all coefficients will be quoted in the appropriate units. When it is necessary to compare our results to magnetization calculations, we will include the above assumed error in the calibration.

One question which always arises when studying a ferromagnet is whether the resonances are from the center of the domains, or the domain walls. We have no conclusive evidence to answer this question. We infer that the resonance occurs in the domain rather than the domain wall. Because of the strong dipole-dipole interaction we would expect the domain resonance to be very broad, which we do not observe. Wyatt (1963) assumes the domains have a very small cross section with a wall thickness of one lattice spacing. His magnetization measurements confirm this assumption. If this is true, the precise meaning of a domain wall resonance is doubtful. Measurements in an applied field may shed some light on this question.

2) High Temperature Critical Behavior

Domb and Sykes (1962) and Fisher (1967) have pointed out that magnetic systems may be characterized by a set of "critical exponents" in the vicinity of the critical temperature. For the magnetization one writes

$$M(T) = A(T_C - T)^{\beta}$$
 (4.29)

where $\mathbf{T}_{\mathbf{C}}$ is the critical temperature and $\boldsymbol{\beta}$ the critical exponent.

Figure 4.6 shows a plot of lnB(T) vs. $ln(T_C-T)$ for T > 1.980 K. The very striking linearity indicates a behavior consistent with the critical exponent. Using a non-linear least squares fitting program we find

$$B(T) = A(T_C - T)^{\beta}$$
 (4.30)

where

$$A = (4368 \pm 31.3) \text{ gauss/K},$$
 (4.31a)

$$T_{C} = (2.214 \pm 0.0016) \text{ K}, \tag{4.31b}$$

and

$$\beta = 0.3904 \pm 0.006$$
 (4.31c)

The χ^2 for the thirteen point fit between 1.980 K and 2.170 K is 0.710. Table B.3 of Appendix B compares the measured and calculated fields.

Although we do not have any data available for $T/T_{\rm C}$ > 0.985 this behavior is consistent with the specific heat results of Landau (1971), which indicates that the critical region extends to $T/T_{\rm C}$ ~ 0.91.

The value of β is consistent with measurements on other systems. It is definitely not equal to 0.5, the value predicted by both the molecular field theory and the Green function random phase approximation calculation. The small value of χ^2 indicates that better data are needed to actually detect a deviation from critical behavior predictions. It is not impossible to improve on our data. The most immediate improvement would be to keep temperature fluctuations below 10 μK and measure the

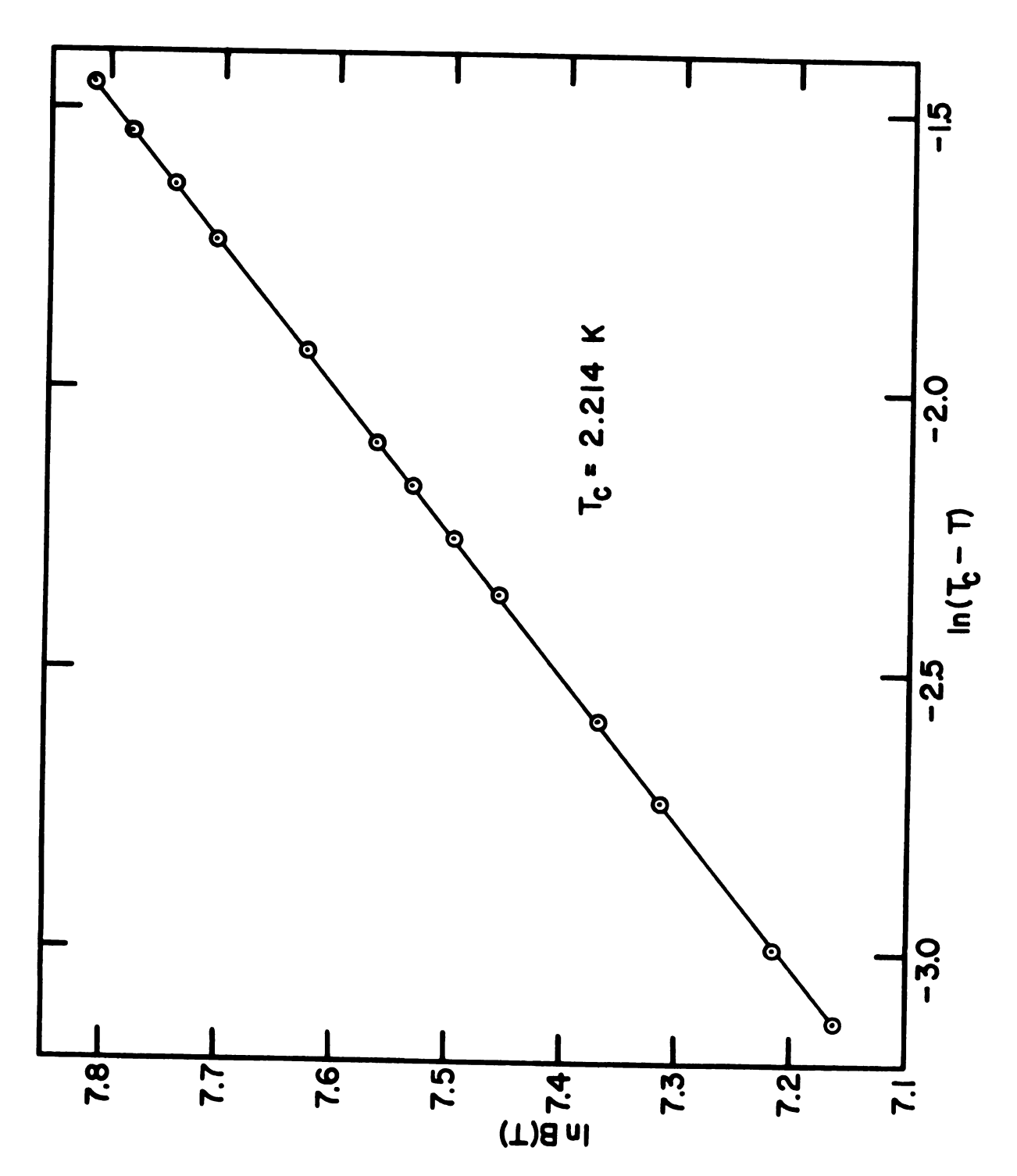


Figure 4.6. lnB(T) vs. $ln(T_c - T)$ for $T/T_c > 0.91$

transition frequencies with a frequency modulated oscillator and record the absorption line. This may also extend the data to a higher limit in $T/T_{\rm C}$, but one should not be too optimistic. As we approach the transition temperature, the line width also follows a critical exponent behavior and becomes very large. It is this inherent limitation on the measurement of B(T) vs. T with N.M.R. that cannot be eliminated.

We should also note that Landau (1971) has made high resolution specific heat measurements on large single crystals of $GdCl_3$. He finds that the asymptotic form for the specific heat is not singular. The transition is of the "diffuse" type (Pippard, 1957). He finds that the critical behavior of the specific heat ends at $T/T_c \sim 0.999$.

If microscopic imperfections are severe enough, they may limit the maximum range of the correlations; the result could be an effective subdivision of the sample into an array of microcrystals. The microcrystals will not be identical and could have slightly different ordering temperatures. In fitting his specific heat results Landau has assumed a gaussian distribution for the fraction of subsystems that order at a given T_C . He finds a half-width of 1.5 mK will reproduce his experimental results exactly. This distribution of critical temperatures will greatly affect any measurements on B(T) in the vicinity of T_C .

3) Low Temperature Behavior

As we mentioned in the previous chapter, the low temperature behavior of the magnetization provides the best comparison of theory and experiment because the theoretical treatment of the Hamiltonian is exact over a finite temperature range. In their calculations of magnetization as a function of temperature, Marquard and Stinchcombe (1967) have shown that for very low T

$$\frac{\Delta M}{M_O} \propto T^{5/2} e^{-\theta/T} \tag{4.32}$$

where

$$\Delta M \equiv (M_O - \Delta M_O) - M(T). \qquad (4.33)$$

 ${}^{M}{}_{O}$ is the saturation magnetization and ${}^{\Delta}{}^{M}{}_{O}$ is the zero point magnetization defect. The exponential term is due to the fact that there is a gap in the magnon dispersion curve at $\vec{k}=0$. The ${}^{T}{}^{5/2}$ behavior is unusual, and it is unfortunate that the temperature necessary to observe this behavior is estimated to be below 50 mK. To observe the temperature dependence of the magnetization to the accuracy necessary to establish a ${}^{T}{}^{5/2}$ behavior is almost impossible. Even with the high accuracy of the N.M.R. measurements the changes in B(T) are so small that it is not technically possible to measure and maintain the temperature of the sample to the required accuracy.

Before comparing our results to the numerical calculations of Marquard and Stinchcombe for the magnetization vs. temperature we will fit our results to an analytic

expression. Figure 4.7 shows B vs. $T^{3/2}$ for T < 1.2 K. This suggests that we may fit our results to the analytic expression

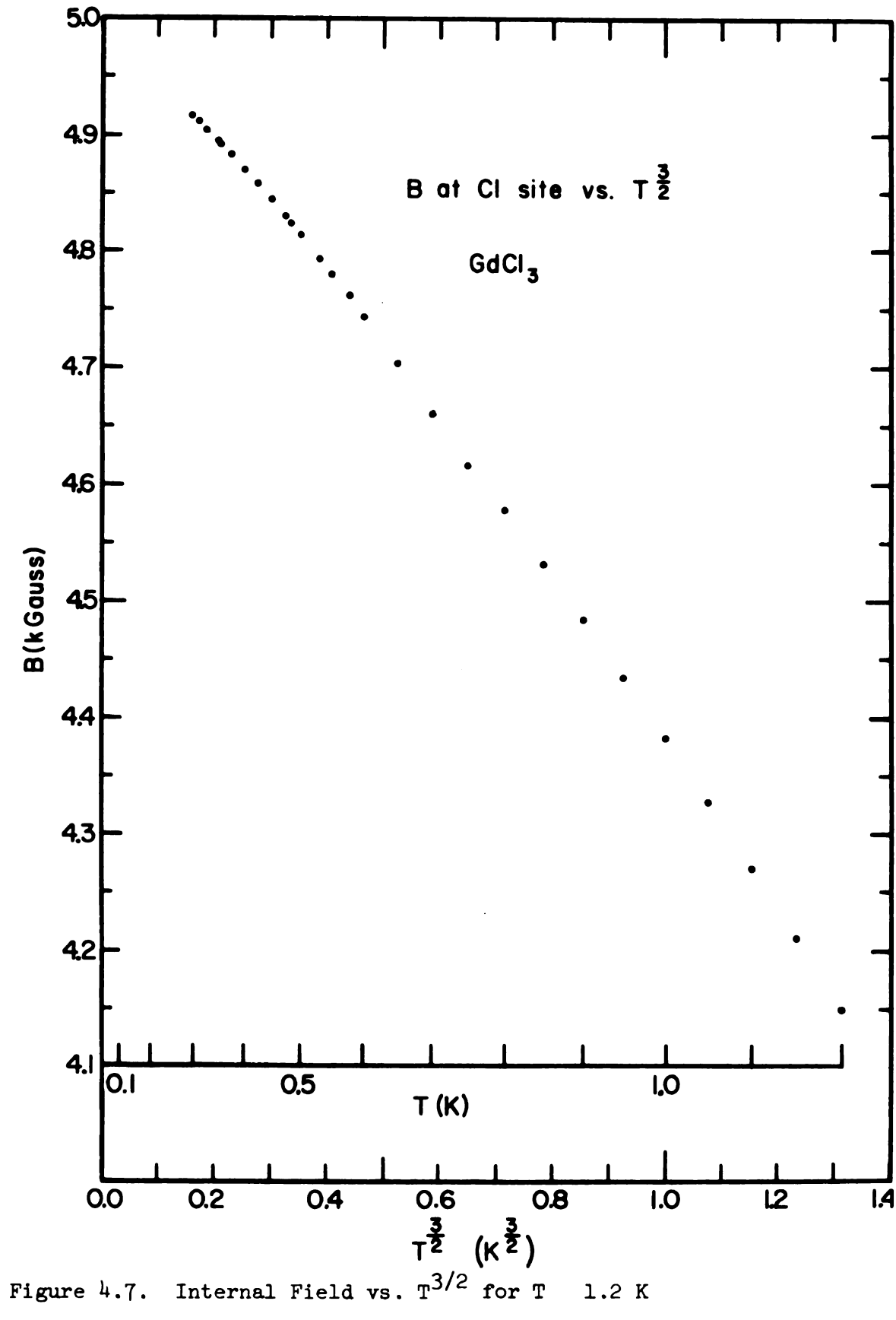
$$B(T) = B_O - A_1 T^{3/2} e^{-\theta/T}$$
 (4.34)

Since the spin wave approximation is a series expansion we have also fitted the data to

$$B(T) = B_O - (A_1 T^{3/2} + A_2 T^{5/2}) e^{-\theta/T}$$
 (4.35)

The results of these fits are shown in Table 4.1. The low value for the sum of the squares indicates that within our experimental accuracy we have a valid analytic expression for B(T). Table B.4 of Appendix B compares the measured and calculated field for both equations.

In comparing our results with the numerical calculations of Marquard and Stinchcombe (1967) we recall that our calibration of the magnetization is uncertain, therefore we must compare the temperature dependence only. From their numerical calculations we see that at T=0.300 K they have $M(T)/M_S=0.99460$, where M_S is the saturation magnetization. If we force our $B(0.3\ K)/C$ to equal 0.99460 we have C=4940.8 gauss. Using this constant we can now compare the temperature dependence of the magnetization. Figure 4.8 shows Marquard and Stinchcombe's numerical results and our data normalized to agree at 0.3 K. The uncertainty in the data is the uncertainty in B(T) deduced from the χ^2 analysis. This shows there is a definite discrepancy between the theory and the



<u>Table 4.1</u> Low Temperature Analysis

	Eqn. 4.34	Eqn. 4.35
Number of Data Points	20	20
Temperature Range	0.310 - 1.000	0.310 - 1.000
B _o (gauss)	4957.5 ± 2.4	4950.8 ± 2.9
$A_1 (gauss/K^{3/2})$	811.0 ± 9.9	963.1 ± 68.3
$A_2(gauss/K^{5/2})$	_	-90.7 ± 41.6
θ (Κ)	0.343 ± 0.015	0.430 ± 0.037
Sum of Squares	9.97	4.312

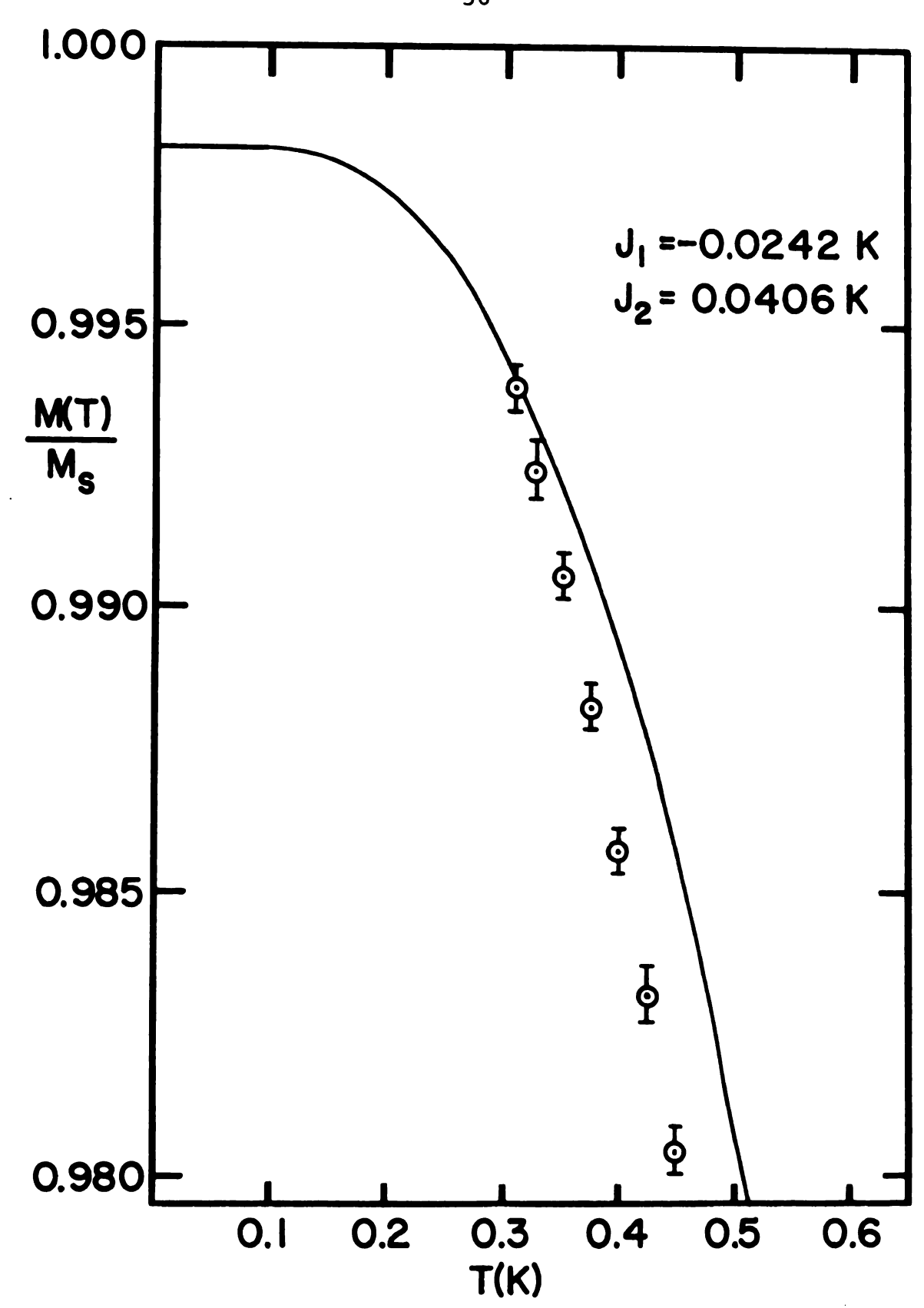


Figure 4.8. Comparison of Low Temperature Data with Spin Wave Theory

experimental results.

Marguard and Stinchcombe have also estimated the zero point magnetization defect by taking an unweighted Their result is average over the whole Brillouin zone. 0.2%. Since the non-interacting spin wave approximation is doubtful for large \vec{k} , they feel, by analogy with the antiferromagnetic ground state problem, that the "true" value may be even smaller. Using the calibration from Wyatt's data and the T = 0 value of our analytic expression, $B_0 = (4950.8 \pm 2.9)$ gauss we have that $M_{\odot} = (609.9 \pm 13.7) \text{ emu/cm}^3$. For complete alignment of the $^8\text{S}_{7/2}$ ground state we would expect 7 μ_B/ion or $M_{\Omega} = 668 \text{ emu/cm}^3$. We therefore have a zero point spin deviation of (8.7 ± 2.1) %. Although this result is very tentative, it provides strong incentive for further investigation of the zero point spin deviation.

4) Molecular Field and Green Function Comparison

From the derivation of the molecular field approximation we recall that including the dipole-dipole interaction introduces an additional term into the expression of the exchange strength. We have

$$A_{o} = J_{o} + (g\mu_{B})^{2} \sum_{j} \frac{1}{r_{ij}} (3\cos^{2}\theta_{ij} - 1)$$
 (4.36) where

$$J_{0} = z_{1}J_{nn} + z_{2}J_{nnn} , \qquad (4.37)$$

 z_1 is the number of nearest-neighbors, and z_2 the number of next-nearest-neighbors. We have calculated the dipole

sum term using the Ewald technique. For the lattice parameters $a_0 = 7.3663$ Å and $c_0 = 4.1059$ Å we have for a spherical sample

$$\sum_{j} \frac{1}{r_{ij}} (3\cos^2\theta_{ij} - 1) = 0.03089 \text{ Å}^{-3}$$
 (4.38)

Taking the value of g as 2.0, the effective exchange due to the dipoles alone, $J_{\rm dd}$, is 0.0764 K. Using the EuCl $_3$ exchange constants, $J_{\rm nn} = -(0.073 \pm 0.004)$ K and $J_{\rm nnn} = (0.091 \pm 0.004)$ K we have $A_{\rm o} = (0.476 \pm 0.032)$ K. The molecular field Curie temperature, $T_{\rm c}$, is given by

$$T_{C} = A_{O}S(S+1)/3k$$
 (4.39)

Using our value for A_{O} we have $T_{C} = (2.50 \pm 0.17)$ K.

The calculation of magnetization vs. temperature is done by solving

$$\frac{S+1}{3S} \left(\frac{T}{T_C} \right) x = B_S(x) \tag{4.40}$$

self consistently, where $B_{s}(x)$ is the Brillouin function,

$$B_s(x) = \frac{2S+1}{2S} \coth \frac{2S+1}{2S} x - \frac{1}{2S} \coth \frac{x}{2S}$$
 (4.41)

 $T/T_{\rm C}$ is the reduced temperature, often labeled $T_{\rm r}$. The reduced magnetization, $M_{\rm r}=M(T)/M(0)$, is given by $M_{\rm r}=B_{\rm S}(x)$. It is a simple matter to solve equation (4.40) for $B_{\rm S}(x)$ as a function of $T_{\rm r}$ on a computer.

When comparing magnetization vs. temperature results, all theoretical predictions look approximately the same. Because the curve of $M_r(T_r)$ is a universal curve for all results in the molecular field approximation, we will not compare the actual magnetization results, but the difference

between the reduced magnetization in question and the reduced magnetization in the molecular field approximation as a function of reduced temperature.

We first normalize our experimental measurements of temperature to T_r by dividing T by the T_c calculated in the critical point discussion. Therefore $T_r = T(K)/2.214(K)$. In normalizing our magnetization measurements we must first convert our internal field measurements to magnetization. We cannot simply normalize our B(T) by dividing B_o because this would eliminate the zero point magnetization defect. We therefore convert our B(T) to M(T) by using $K = (0.1232 \pm 0.0027)$ emu/cm³-gauss, and then calculate M_r by dividing by 668 emu/cm³. Thus we have our data in the form of M_r vs. T_r . We then use the computer to calculate $M_r(T_r)$ in the molecular field approximation and subtract this from our measured results.

Figure 4.9 is a plot of M_r (data) - M_r (molecular field) vs. T_r . The error bars on the data points are due to the uncertainty in the calibration constant, K. As we see, near T_c the magnetization rises faster than the molecular field prediction. As the temperature is lowered the experimental results fall below the molecular field prediction because the molecular field does not predict a zero point magnetization defect.

In the Becker and Plischke (1970) Green function calculation the predicted Curie temperature is (2.48 ± 0.12) K.



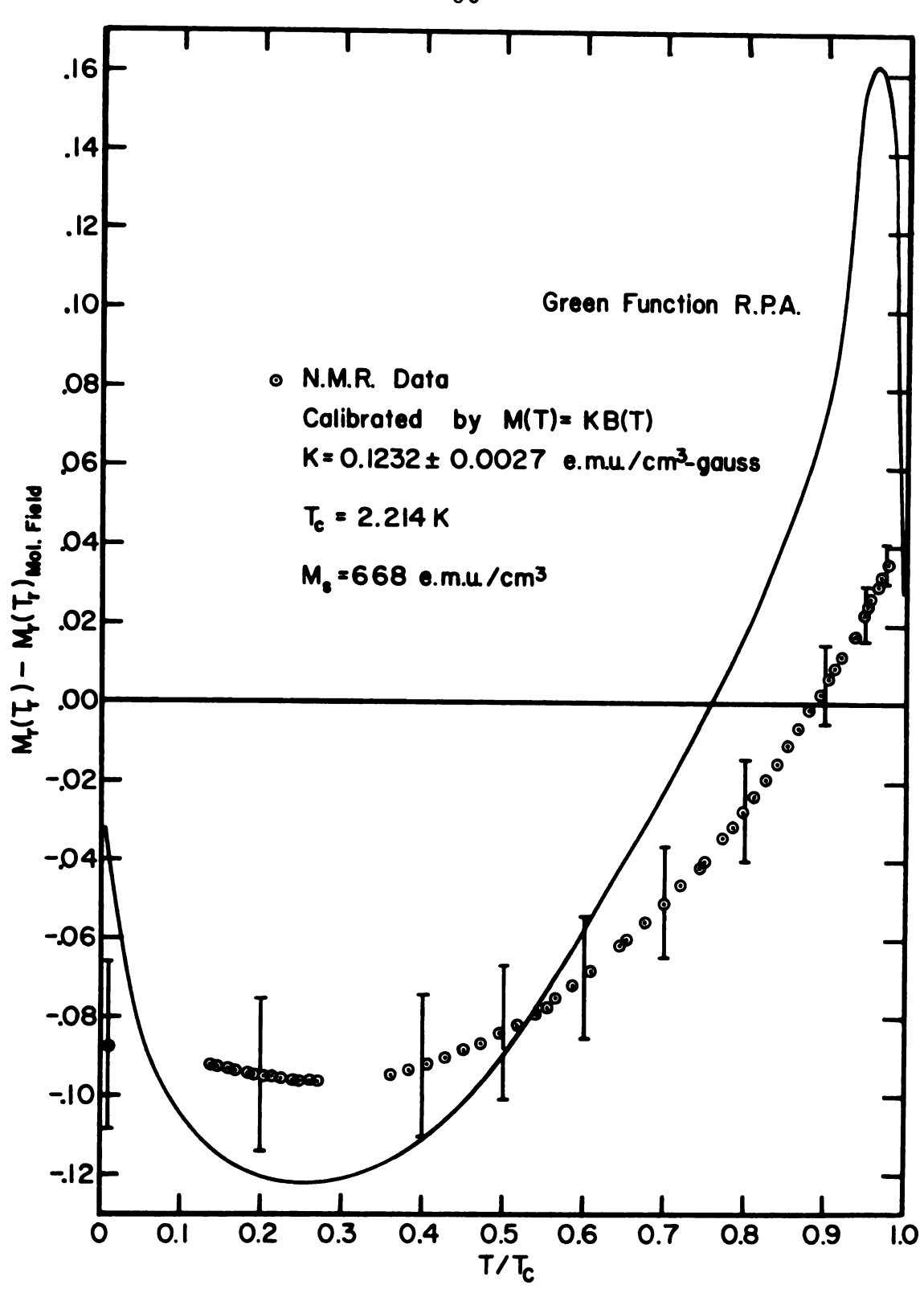


Figure 4.9. Reduced Magnetization vs. Reduced Temperature

Using their preprint we have determined $M_r(T_r)$ and subtracted the molecular field prediction. This curve is also shown in Figure 4.8. The curve has an accuracy of only 1% because of the uncertainty in measuring the distances on the preprint graph. As we see, the Green function prediction is qualitatively correct, although the correction near T_c is far too much.

E. Conclusion

The measurement of internal field vs. temperature at the Cl site is very accurate. The accuracy of the field measurements ranges from 0.4% near T_C to 0.05% at the low temperatures. The temperature measurements are within the accuracy of the present temperature scales. With this accuracy we conclude that our low temperature results do not agree with the spin wave calculation. Whether this is due to assumptions made in the calculation or an insufficient phenomenological Hamiltonian is not yet certain.

The tentative discrepancy between the zero point magnetization defect predicted by the spin wave theory and the experiment must be investigated further. We hope to measure this more accurately by doing N.M.R. in an applied field.

If the large value for the zero point magnetization defect is indeed real, we must find a mechanism to explain this. Although Gd³⁺ is an S state ion and the optical spectra show no evidence of crystal field phonon interact-

ions, it is possible there may be a strong phonon-magnon coupling. Because the exchange integral is a strong function of distance and because of the long range dipole term we may expect significant phonon-magnon coupling.

Rives and Walton (1968) have measured the field dependence of the thermal conductivity in MnCl₂·4H₂O at temperatures well below the Néel temperature. Here the Mn²⁺ ion is also an S state ion, although the dipolar contribution to the exchange interaction is negligible. In the antiferromagnetic state they find a very strong dependence of the thermal conductivity on applied field, resulting in a kink at the spin flop transition. Similar experiments can and should be done on GdCl₃.

These two experiments will hopefully provide the theorist with enough new information to again tackle the theoretical problem of the magnetic behavior of ${\rm GdCl}_3$.

V. PrCl3 THEORY AND BACKGROUND

The Pr³⁺ ion and PrCl₃ in particular have proven to be very interesting. The concentrated salt has two regions of cooperative behavior. The first is a linear chain magnetic behavior centered around 0.85 K, and the second is a phase transition to a three-dimensional ordered state at 0.4 K. We will be primarily concerned with the latter phase transition.

A. Pr³⁺ Ion Properties

The absorption spectrum of the Pr $^{3+}$ ion shows the ground level to be $^{3}\text{H}_{4}$ (Judd, 1957). The point symmetry in LaCl $_{3}$ is C $_{3h}$, which gives a non-Kramers degenerate ground state, $\cos\left(\theta\right)\left|4,\pm4\right>+\sin\left(\theta\right)\left|4,\pm2\right>$, with the notation $\left|\text{J},\text{M}_{\text{J}}\right>$. The first excited state is $\left|4,3\right>$ and is 33.1 cm $^{-1}$ above the ground state.

Hutchinson Jr. and Wong (1958) have measured the paramagnetic resonance absorption of \Pr^{3+} in LaCl_3 . Their results are summarized by the spin Hamiltonian

$$H = g_{\parallel} \mu_{B} H^{z} S^{z} + g_{\perp} \mu_{B} (H^{x} S^{x} + H^{y} S^{y}) +$$

$$hcAS^{z} I^{z} + \Delta_{x} S^{x} + \Delta_{y} S^{y}. \qquad (5.1)$$

The first two terms are the Zeeman interaction terms between the electron spins and the applied field. The third term is the transferred hyperfine interaction between the 141 Pr nucleus, I = 5/2, and the electron spins. The ground state

of the C_{3h} crystal field should not give rise to paramagnetic resonance since g=0 and the transition from one state of the doublet to the other does not contain either a $\Delta M_J=0$ or a $\Delta M_J=\pm 1$ transition. They have included the fourth term, $\Delta_X S^X + \Delta_Y S^Y$ with $\Delta = (\Delta_X^2 + \Delta_Y^2)^{1/2}$ to account for crystal strains and distortions, and thermal fluctuations. Their results are $g=1.035\pm0.005$, $g=0.1\pm0.15$, $\Delta = (5.02\pm0.03) \times 10^{-2}$ cm⁻¹, and $\Delta = 0.02$ cm⁻¹. Later Culvahouse, Pfortmiller, and Schinke (1968) have shown that the microwave electric field is responsible for the magnetic field dependent absorption of Pr^{3+} ions. They replace the Δ term with a term of the form $\gamma(E^XS^X + E^YS^Y)$ where $\gamma = 6.0 \times 10^{-4}$ (cm⁻¹/statvolt. cm⁻¹).

B. Pr³⁺ and Pair Resonance

The Hamiltonian for two interacting ions, each with an effective spin of one-half, may be written in the form (Culvahouse, Schinke, and Pfortmiller, 1969)

$$H = \mu_{B}(\vec{H} \cdot \vec{g}_{1} \cdot \vec{s}_{1} + \vec{H} \cdot \vec{g}_{2} \cdot \vec{s}_{2}) + \sum_{mm'} A_{mm'}(1) T_{1m}(I_{1}) T_{1m'}(S_{1}) + A_{mm'}(2) T_{1m}(I_{2}) T_{1m'}(S_{2}) + J_{mm'}(1,2) T_{1m}(S_{1}) T_{1m'}(S_{2}).$$
(5.2)

The first two terms are the same as the single ion terms discussed above. The last term is the interaction term between the electron spins. The existence of an inversion center between the spins and the fact that the axis joining

the nearest-neighbor spins has a rotation symmetry of three or higher reduces the Hamiltonian to the form

$$H = g_{\parallel} \mu_{B} H^{z} (S_{1}^{z} + S_{2}^{z}) + g_{\perp} \mu_{B} [H^{x} (S_{1}^{x} + S_{2}^{x}) + H^{y} (S_{1}^{y} + S_{2}^{y})] + A (I_{1}^{z} S_{1}^{z} + I_{2}^{z} S_{2}^{z}) + B (I_{1}^{x} S_{1}^{x} + I_{2}^{x} S_{2}^{x} + I_{1}^{y} S_{1}^{y} + I_{2}^{y} S_{2}^{y}) + K_{0} \vec{S}_{1} \cdot \vec{S}_{2} + K^{z} S_{1}^{z} S_{1}^{z} .$$
 (5.3)

The interaction term may also be written

$$J_{00}S_1^{z}S_2^{z} - J_{1-1}(S_1^{x}S_2^{x} + S_1^{y}S_2^{y})$$
 (5.4a)

where

$$K_0 = -J_{1-1}$$
 and $K^2 = J_{00} + J_{1-1}$. (5.4b)

Pfortmiller (1970) has measured the pair spectra of the nearest-neighbor pairs of Pr^{3+} in $La_2(C_2H_5SO_4)_6\cdot 9H_2O$, LaES, and in LaCl₃. His results are shown in Table 5.1.

In estimating the actual interaction mechanism for the LaCl_3 host lattice, Pfortmiller finds: 1) the error in $\operatorname{J}_{\operatorname{OO}}$ is too large to actually confirm a non-dipolar contribution to $\operatorname{J}_{\operatorname{OO}}$, 2) exchange is a negligible source for J_{1-1} , based on arguments regarding the size of the exchange, and 3) an enhancement factor of 10 is necessary to account for J_{1-1} in terms of an electric quadrupole-quadrupole interaction alone. Finally he concludes, "Although large interactions exist between the Pr^{3+} n.n. pairs, the dominant mechanism, if indeed only one can be singled out, is not evident."

Axial Pairs Spin-Spin Interaction Parameters for \Pr^3 Table 5.1.

-
, E
of
units
energy
have
parameters
interaction
A11

,		Experimental Parameters	mental eters		Non-Dipolar Contributions	polar utions				
Crystal Lattice	exp Ko	K _Z	Joo	exp J1-1	J ₀₀	Jn.d. exp	exp 8z	Aexp	exp 8z	A exp
LaES	297°0 +	-0.474	-0.0073	-0.467	-0.0004	-0.467	1.665	-0.467 1.665 .0815	0.007	0.0001
	+.001	+.001	±.0003	+.001	±.0003	+.001	+.002	1 .0005	+.002	±.0001
LaC13	+1.983	-1.905	+0.077	-1.983	+0.084	-1.983	0.827	6070.	0.204	0.0094
	+.10	+.002	+.10	+.10	+. 10	+. 10	+.003	1 .0005	- .003	+.0001

The signs of the interaction parameters have not been determined experimentally, but reflect the sign of the calculated EQQ interaction parameter for J_{1-1} .

Note added in proof: the sign of \mathbf{J}_{1-1} listed in the table was experimentally verified.

definitely be attributed to the off-axis next-nearestneighbor pairs, although this does not preclude the existence of strong next-nearest-neighbor pair interactions.

C. Bulk Properties

The pair spectra results indicate an interaction between the Pr³⁺ ions along the chain. Colwell, Mangum and Utton (1969) have measured the specific heat of PrCl₃ from 0.2 K to 4.0 K. They find a broad peak in the specific heat centered at 0.85 K which is consistent with a linear chain interaction. They also find a sharp peak at 0.4 K indicating the onset of long range ordering. Because the pair spectra results do not give any information on the interaction between the chains, and because the pure quadrupole resonance line splits at 0.4 K, the three-dimensional critical temperature, we undertook an N.M.R. study in the three-dimensional ordered state to determine the type and symmetry of the low temperature phase. Figure 5.1 shows the zero field quadrupole frequency of ³⁵Cl as a function of temperature (Colwell, Mangum and Utton, 1969).

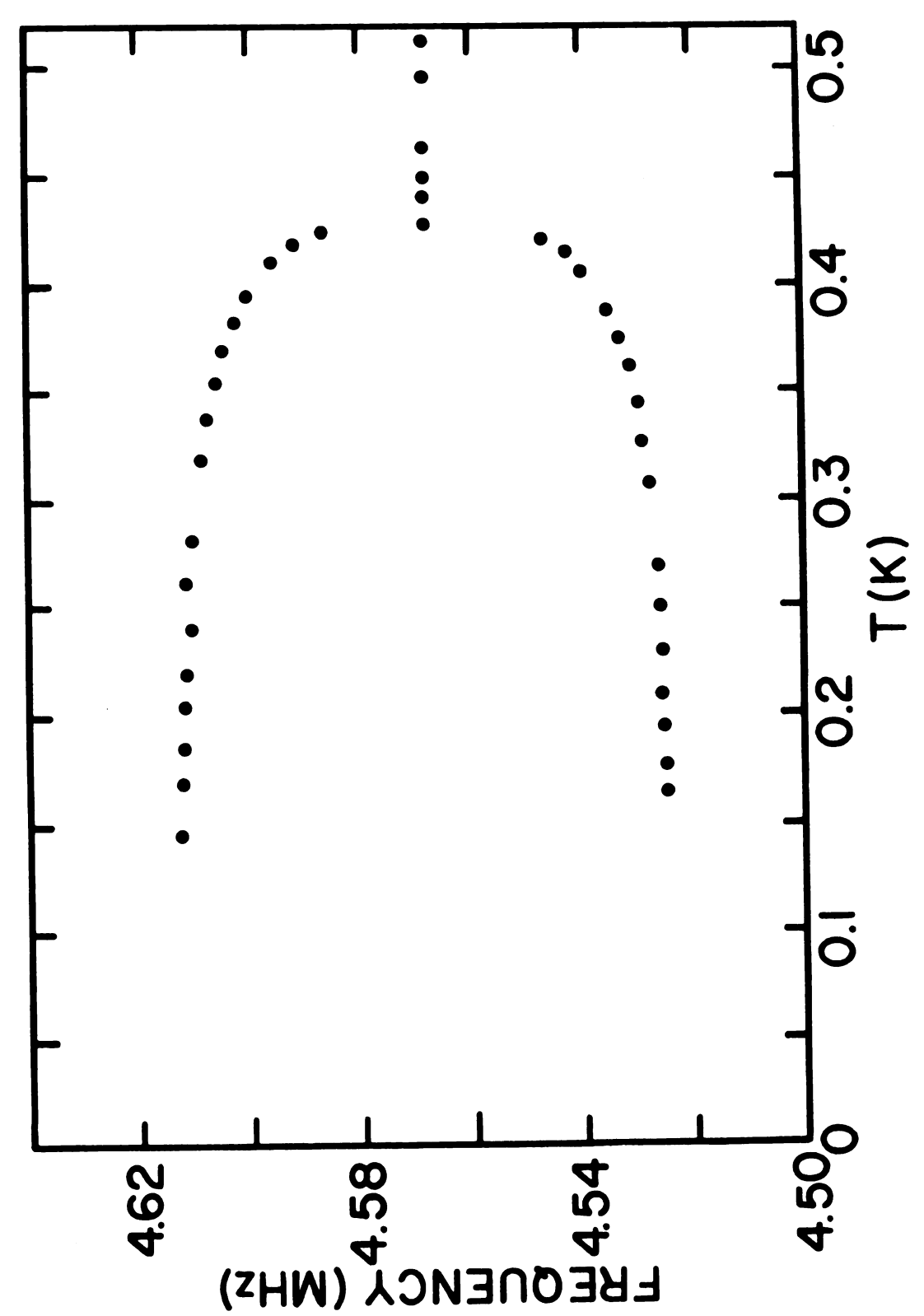


Figure 5.1. Zero Field Splitting of Pure Quadrupole Line, PrCl₃

VI. C1 N.M.R. RESULTS FOR $PrCl_3$

A. Paramagnetic Phase

Before we study the ordered phase of PrCl $_3$ we determine the asymmetry parameter, η , in the paramagnetic phase. The pure quadrupole resonance frequencies in PrCl $_3$ are $^{35}v_Q=4566.6$ kHz and $^{37}v_Q=3599.3$ kHz. Figure 6.1 shows the 35 Cl transition frequencies as a function of applied field for the field parallel to C $_3$, the X-axis of the electric field gradient tensor. With this data we apply the method of moments discussed in chapter IV and determine η . We find $\eta=0.4937$. This is significantly different from the value found by Hughes, Montgomery, Moulton, and Carlson (1964) and may be attributed to the insensitivity of the rotation diagram to η , which was the method they used to find η .

Figure 6.2 shows the 35 Cl transition frequencies as a function of orientation in a constant applied field. The field is rotated in the plane perpendicular to the C₃ axis, and has a value of 500 Oersteds. Because of the 3-fold symmetry, applying a field at an angle θ to the Z-axis of one chlorine site is equivalent to applying the same field at an angle $\theta' = \theta \pm 120^{\circ}$ to the other two sites. We therefore expect three identical resonance patterns shifted by 120°. From the symmetry of the interaction Hamiltonian we also expect the resonance pattern to have a periodicity of 180°. Both of these effects are observed. The subscript

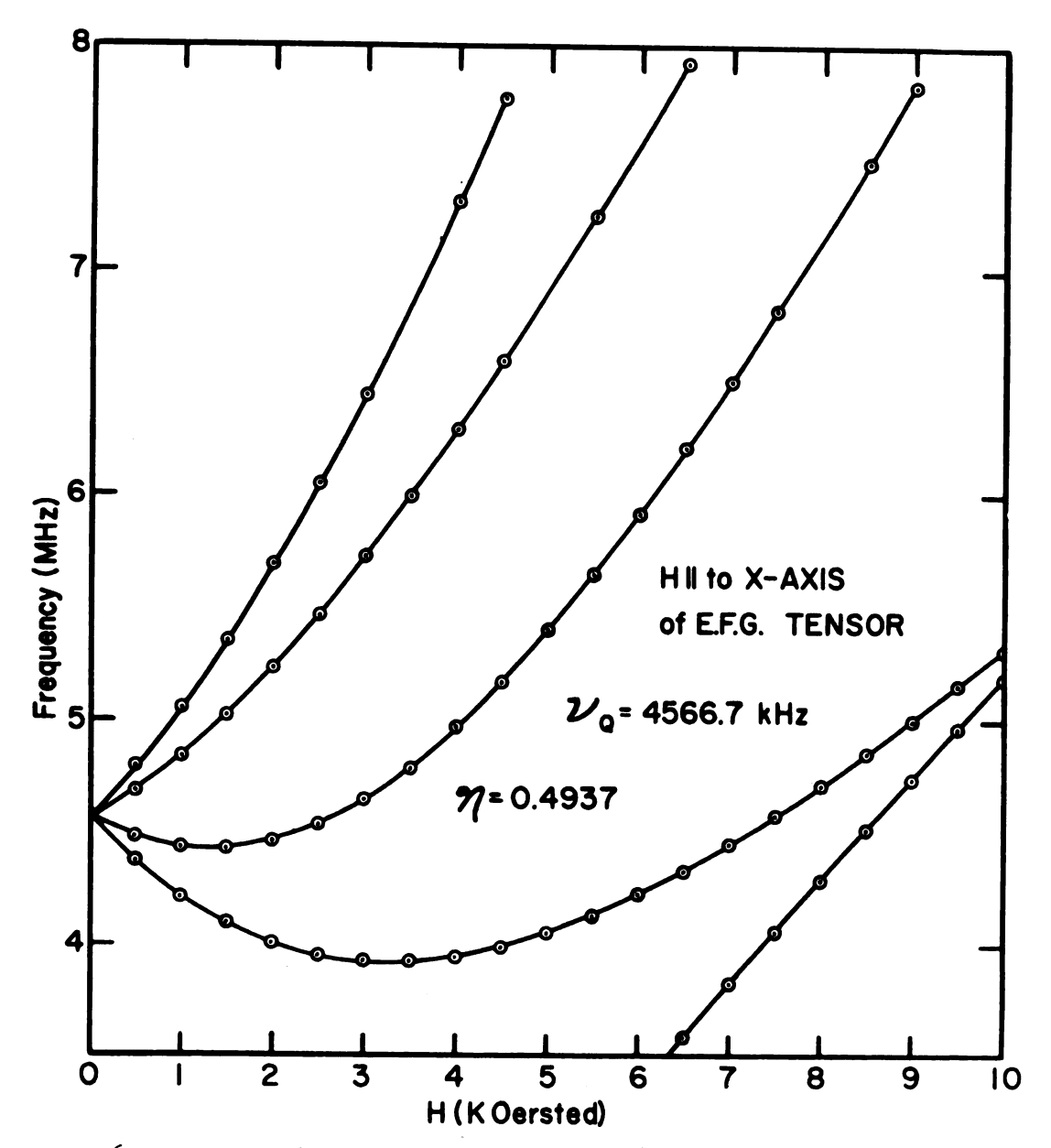


Figure 6.1. Transition Frequencies vs. Field, High Temperature Phase

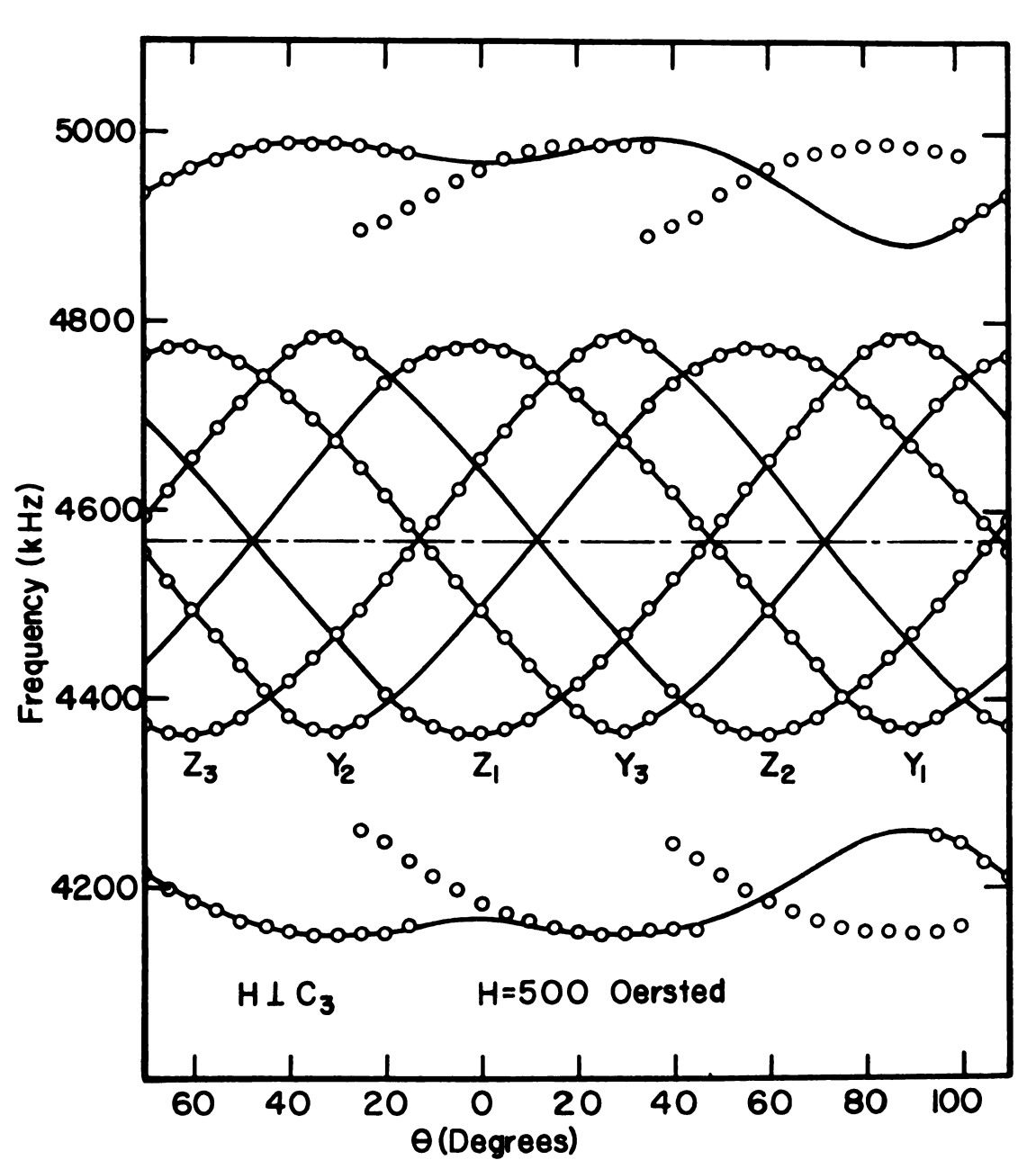


Figure 6.2. Rotation Diagram, H \perp C₃, High Temperature Phase

on the axis labels are arbitrary and refer to the different sites.

B. Low Temperature Phase, T < 0.4 K

Figure 6.3 shows the same rotation diagram in the ordered state. The zero field splitting is about 60 kHz. Note that this resonance pattern also has a period of 180° and that the 3-fold symmetry is still present. Also, the principal axes of the electric field gradient tensor have not shifted.

Figure 6.4 shows the field dependence of the transition frequencies for the applied field parallel to the Z-axis of site (1). This orientation is 30° from the Y-axis of both sites (2) and (3). At this location the transition frequencies for site (3) are identical to those of site (2). Of the twelve observed transition frequencies we are therefore able to associate eight of them with site (2) and four of them with site (1). Because the eight transition frequencies of site (2) form two sets of four, each converging to one of the zero field transition frequencies as Happl. approaches zero, we conclude that the zero field splitting below 0.4 K is NOT due to a spontaneous internal magnetic field at the chlorine site. If the splitting is due to an internal field we would see at most two lines converging to the zero field resonance frequencies. The four line convergence indicates that the degeneracy of the quadrupole Hamiltonian present in the paramagnetic state is not removed by the phase

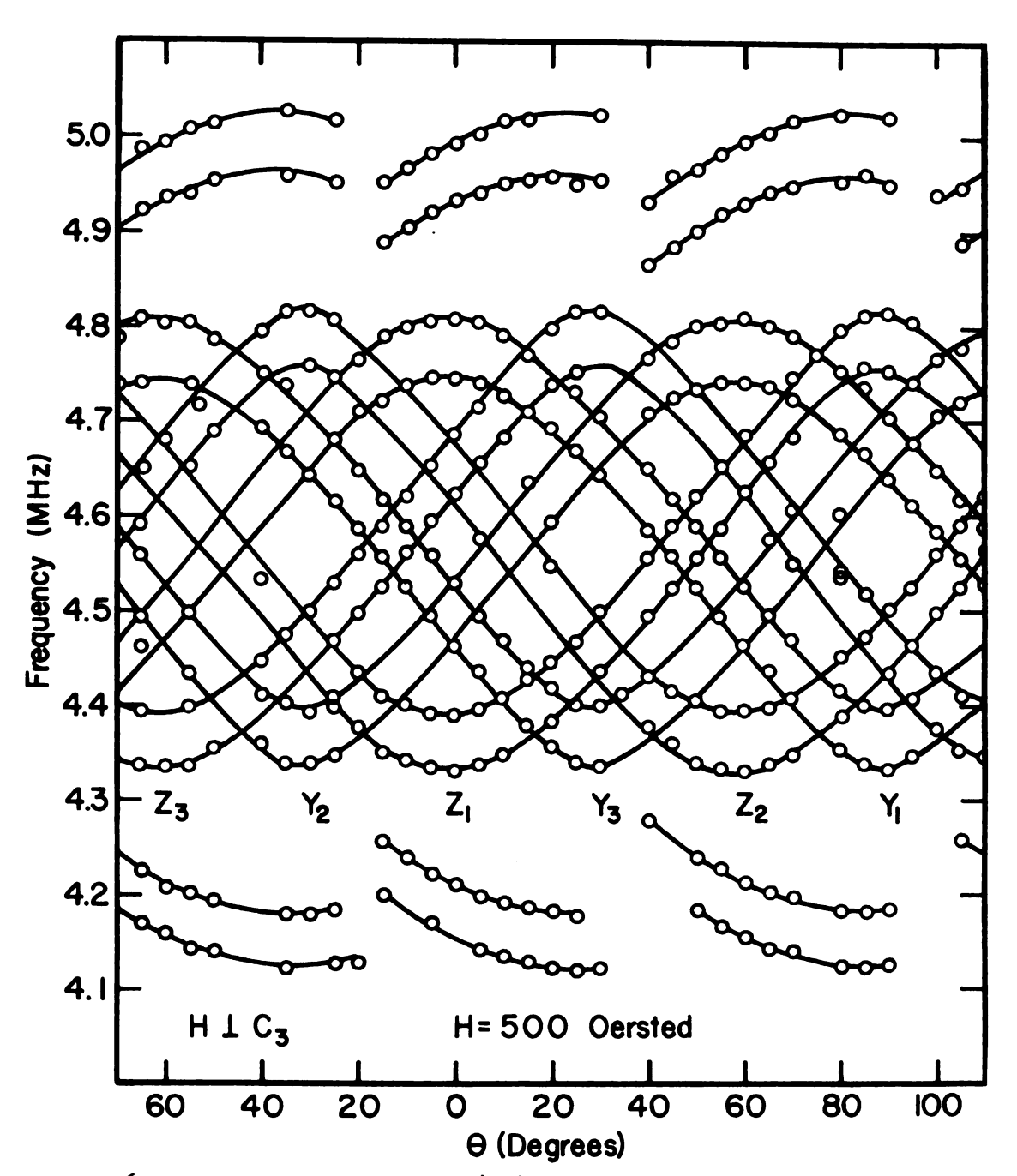


Figure 6.3. Rotation Diagram, H \perp C₃, Low Temperature Phase



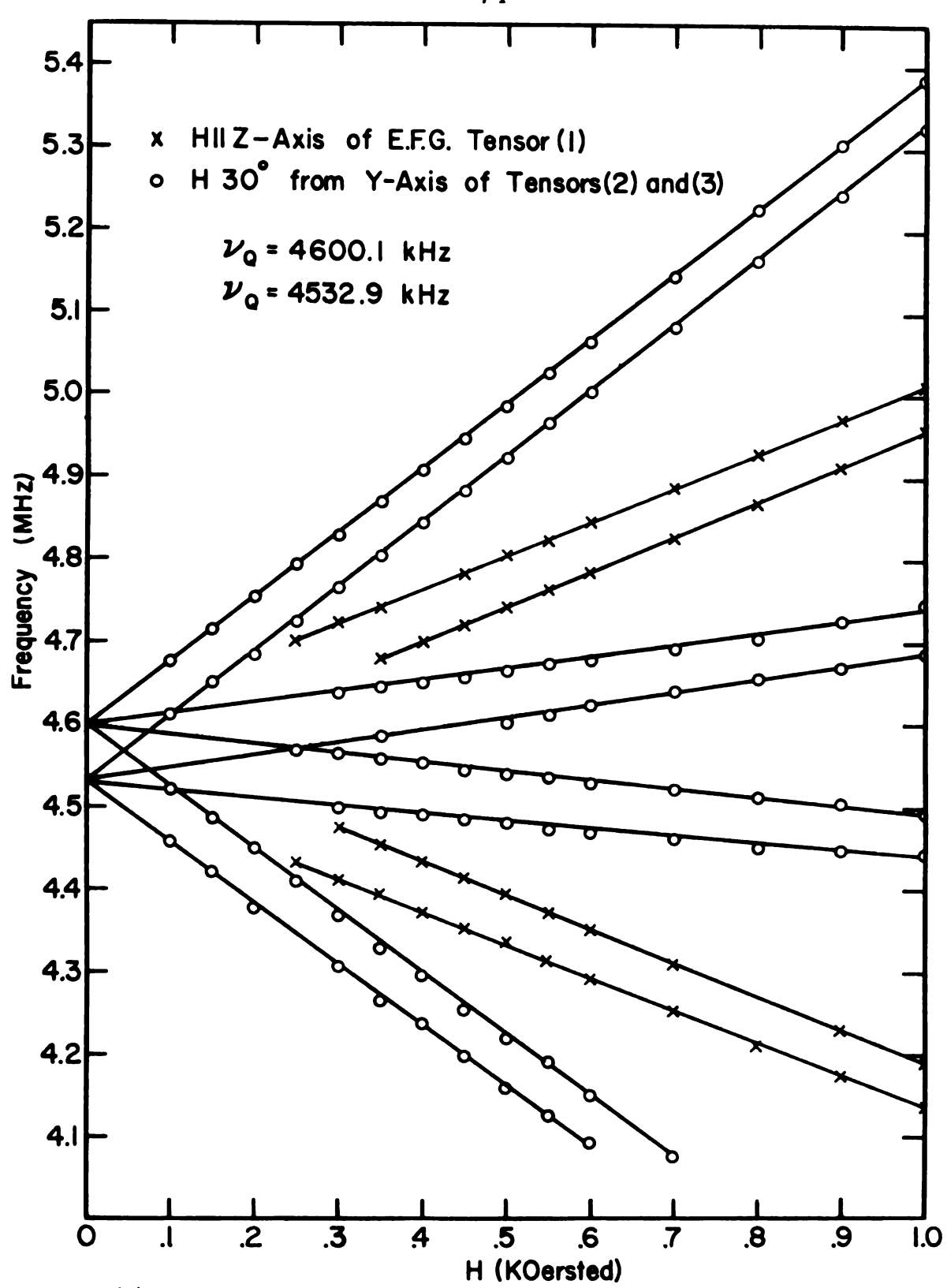


Figure 6.4. Transition Frequencies vs. Field, Low Temperature Phase

transition, therefore there is no internal magnetic field.

The zero field splitting is due to an effective lowering of the crystal symmetry, thereby creating two non-equivalent chlorine sites.

This conclusion is further substantiated by a calculation of the observed spectrum. The Hamiltonian of equation (4.7) can be diagonalized exactly by a computer for an arbitrary orientation and magnitude of \vec{B} . We have calculated the spectrum for a rotation identical to that of Figure 6.3. The pure quadrupole resonance frequency was assumed to be the zero field frequencies measured in the ordered state. The asymmetry parameter is the same as that measured in the high temperature phase, T > 0.4 K, and the magnitude of the internal field is just the applied field of 500 Oersteds. The calculated spectrum and observed spectrum agree to within the uncertainties in the measured frequencies. The measured and calculated frequencies are shown in Table C.1 of Appendix C.

To determine if the application of a magnetic field has any effect on the ordered phase, we applied an external magnetic field of up to 10 Kgauss along the Y-axis. The results are shown in Figure 6.5. It appears that even a 10 Kgauss field does not alter the zero field splitting. We have also been unable to detect any changes in the transition temperature with the application of a magnetic field.

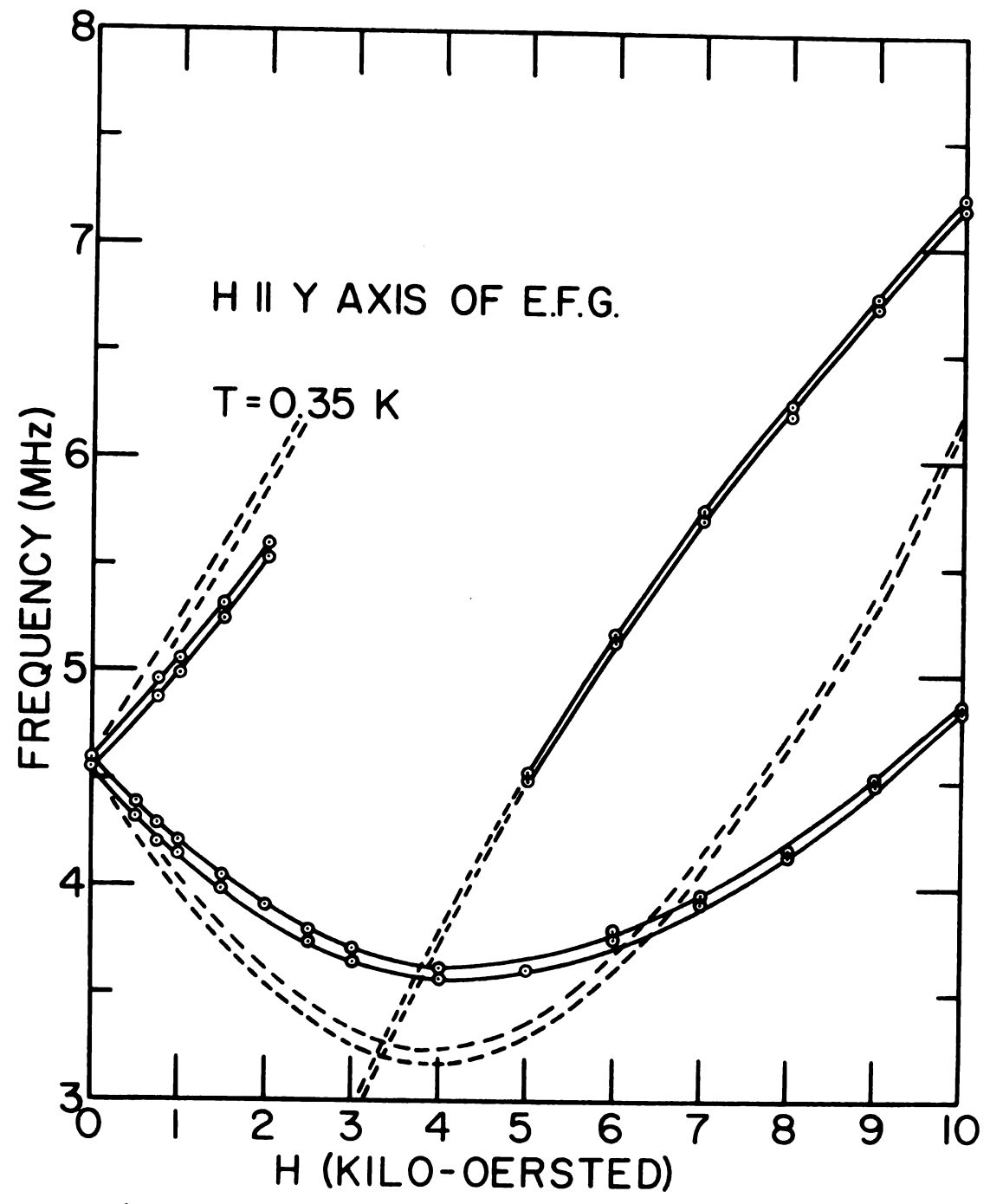


Figure 6.5. High Field Behavior of Transition Frequencies, Low Temperature Phase

To determine the symmetry of the ordered phase we note that the 3-fold symmetry present in the high temperature phase is retained in the low temperature phase. The space group of the high temperature phase is $P6_3/m$. This belongs to the class 6/m or C_{6h} in Schoenflies notation. The phase transition lowers the symmetry, therefore the class of the low temperature phase must be either 6/m or one of its subclasses: $\overline{6}$, 6, $\overline{3}$, 3, 2/m, m, 2, $\overline{1}$, or 1. The subclasses 2/m, 2, $\overline{1}$, and 1 do not retain the 3-fold symmetry and may be eliminated as possible candidates. The possible space groups for each of the other four classes are listed in Table 6.1 along with the reason for their being allowed or not allowed.

The allowed space group P6 removes the symmetry element of inversion and allows one set of three chlorines on a mirror plane to move out and the other to move in. The space group P3 also removes the mirror plane, therefore allowing the Pr to move out of the plane of the chlorines.

Although we have not definitely established the existence of a real crystallographic phase transition, the actual ordering mechanism should also remove these same symmetry elements.

When the zero field lines are recorded with a cw marginal oscillator and second derivative detection using magnetic modulation we see the lines shown in Figure 6.6. The upper line is from the high temperature phase and is

<u>Table 6.1</u>. Analysis of Possible Space Groups for $PrCl_3$

Class	Space Group	Reason
6/m	P6 ₃ /m	Improper number of Cl positions
6/m	P6/m	Both Preither in a plane or on the same symmetry line.
6	р С	Allowed
6	P6 ₃	Improper number of Cl positions
6	P6 ₄	Improper number of Cl positions
6	P6 ₂	Improper number of Cl positions
6	P6 ₅	Improper number of Cl positions
6	P6 ₁	Improper number of Cl positions
6	Р6	Both Pr in the same plane
3	R3	Improper number of Cl positions
3	P 3	Improper number of Cl positions
3	R3	Improper number of Cl positions
3	P3 ₂	Improper number of Cl positions
3	P3 ₁	Improper number of Cl positions
3	Р3	Allowed

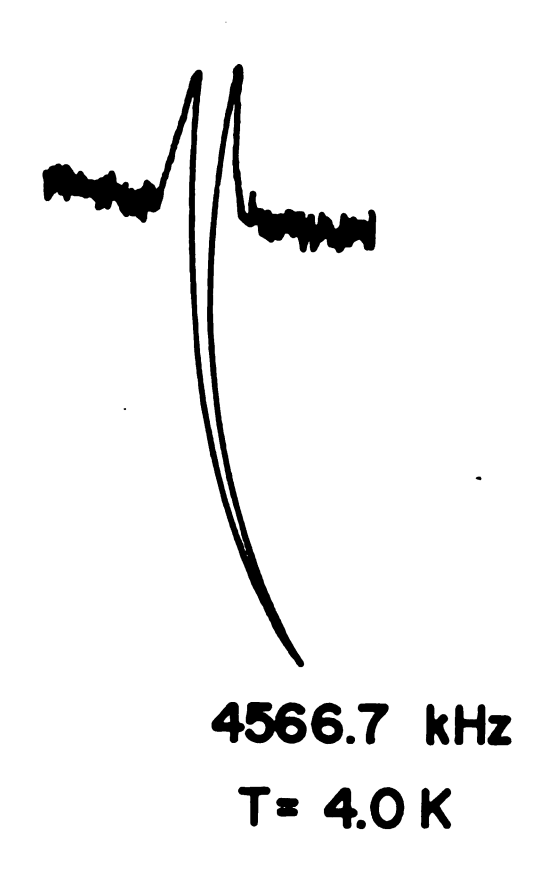




Figure 6.6 Second Derivative of Absorption Curve, PrCl₃.

symmetric down to the critical temperature. In the low temperature phase the lines are asymmetric and change shape as a function of temperature. This asymmetry is also observed when frequency modulation is used. Since the low temperature phase is of lower symmetry we have postulated that the observed line is not necessarily due to a single site.

If we assume that the absorption curve is a gaussian of the form

$$A(f) = \frac{1}{\sqrt{2\pi}} \frac{1}{\sigma} e^{-\frac{(f-f^{\circ})^{2}}{2\sigma^{2}}}$$
 (6.1)

where f is the frequency of the detecting oscillator, f° is the resonance frequency of the line, and σ is the line width, we find that the observed line shape is given by

A"(f) =
$$\frac{1}{\sqrt{\pi}}$$
 {4(f-f°)² - 2} e^{-(f-f°)²} (6.2) where we assume $\sigma = \frac{1}{\sqrt{2}}$.

We then assume that the observed line in the low temperature phase is given by

$$A''(f) = \sum_{i=1}^{N} \frac{1}{\sqrt{\pi}} \left\{ 4(f-f_i^\circ)^2 - 2 \right\} e^{-(f-f_i^\circ)^2}$$
 (6.3)

where N is the number of nearly equivalent sites. We can reproduce the observed asymmetry if we let N = 3, and let $f_3 = f_2 = 0$ and $f_1 = 1/\sqrt{2}$, or the line width. This calculation is shown in Figure 6.7. From this we may conclude that the 3-fold symmetry is slightly removed. An attempt to

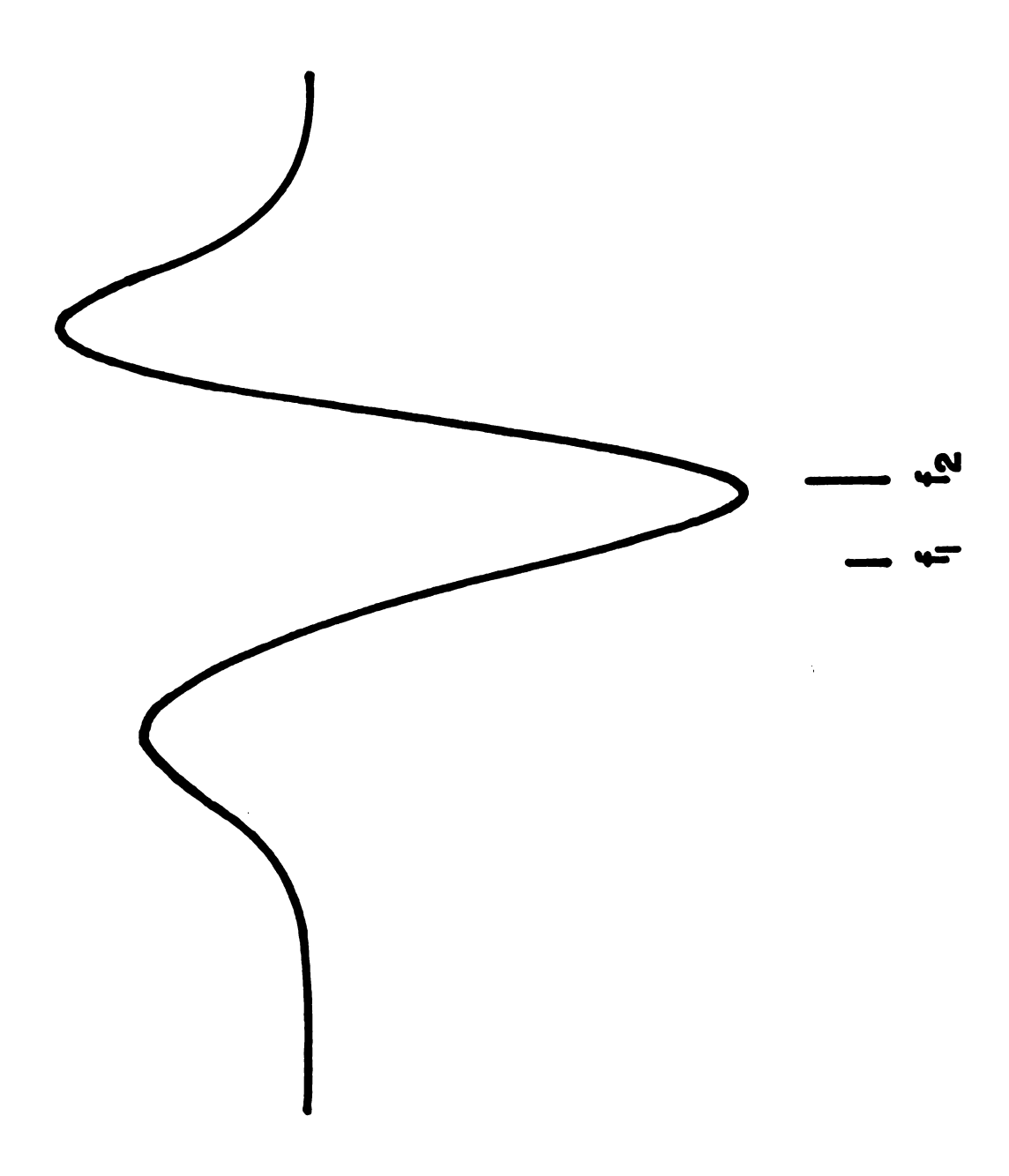


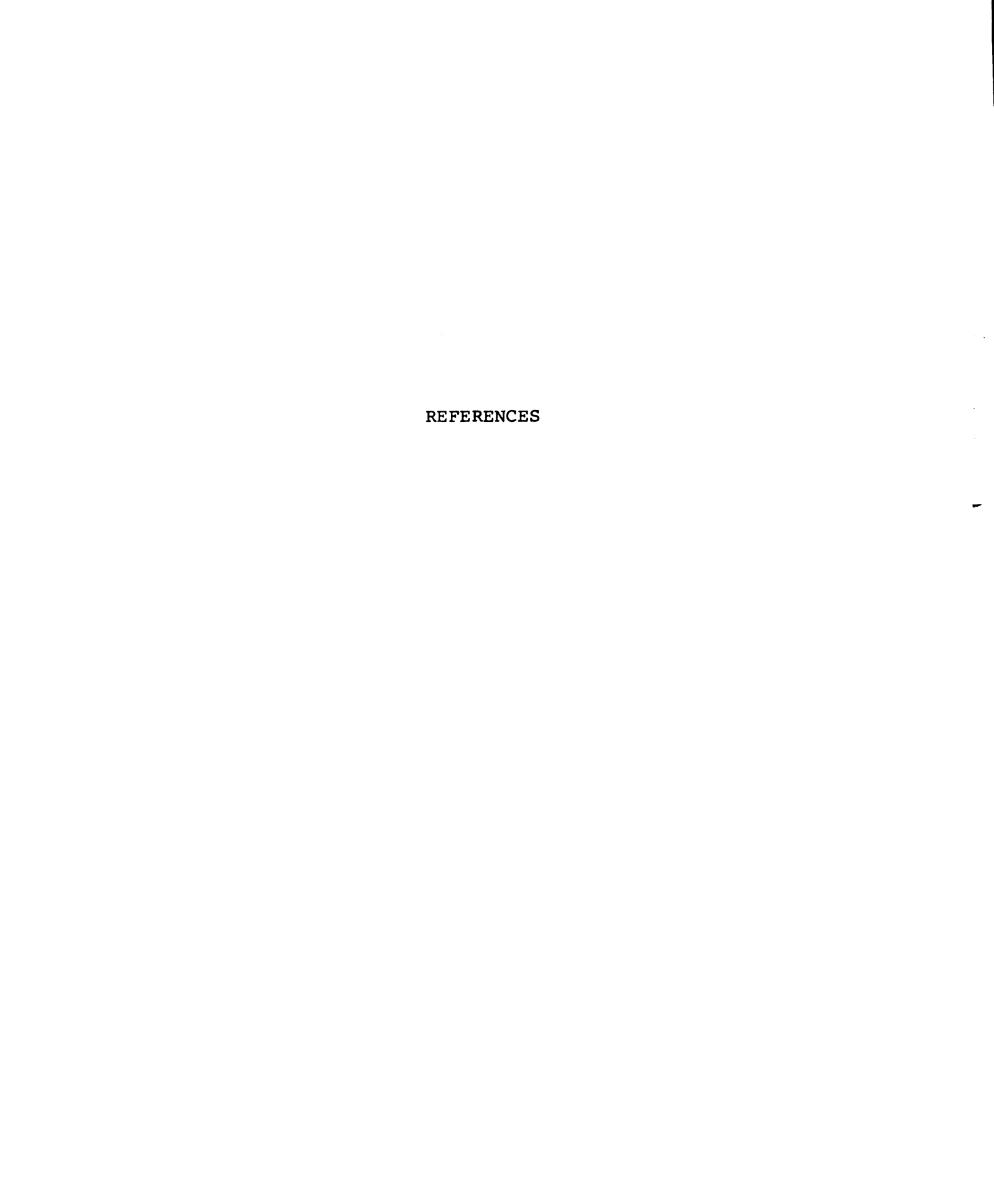
Figure 6.7 Calculated Second Derivative of Absorption Curve.

measure the deviation from 3-fold symmetry using the rotation spectrum was unsuccessful.

C. Conclusions

From the N.M.R. results, we conclude that the low temperature phase transition in PrCl, is not to an antiferromagnetic phase as previously assumed, but instead is to an ordered state which effectively lowers the crystal symmetry. The actual mechanism responsible for the ordering can not be determined by N.M.R. Because the ground state of the Pr³⁺ ion is a non-Kramers doublet we may assume that a strong coupling to the lattice vibrations is present. the exchange constants are of the proper magnitude this will allow a Jahn-Teller type distortion (Allen, 1968). Evidence for a strong spin-phonon coupling is present from the unique Cl spin-spin and spin-lattice relaxation times (Mangum and Thorton, 1969), and from the phonon bottleneck predicted by the electron spin lattice relaxation measurements (Bohan and Stapelton, 1969). Cohen and Moos (1967) have also observed very sharp lines in the vibronic spectra which are not understood.

A complete description of the phase transition will probably include the phonons, but before this is possible, we must determine the exact nature of the low temperature phase.



REFERENCES

- Abel, W. R., Anderson, A. C., and Wheatley, J. C., 1964, Rev. Sci. Inst., 35, 444.
- Allen Jr., S. J., 1968, Phys. Rev., 166, 530.
- Anderson, P. W., 1963a, Solid State Physics, 14, 99, edited by F. Seitz and D. Turnball, Academic Press, New York.
- Anderson, P. W., 1963b, in Magnetism, Vol. I, edited by
 G. T. Rado and H. Suhl, Academic Press, New York.
- Becker, E. and Plischke, M., 1970, Phys. Rev. B., 1, 314.
- Birgeneau, R. J., 1967, thesis, <u>Magnetic Interactions in</u>

 Rare Earth Insulators, Yale University.
- Birgeneau, R. J., Hutchings, M. T., and Rogers, R. N., 1968, Phys. Rev., 175, 1116.
- Brigeneau, R. J., Hutchings, M. T., and Wolf, W. P., 1967, J. Appl. Phys. 38, 957.
- Bloch, F., 1930, Z. Physik, 61, 206.
- Bloch, F., 1932, Z. Physik, 74, 295.
- Bohan, T. L., and Stapelton, H. J., 1969, Phys. Rev., <u>182</u> 385.
- Brichwedde, F. G., 1970, "1958 He Scale of Temperatures",
 Natl. Bur. Standards, Monograph 10.
- Brown, L. C. and Parker, P. M., 1955, Phys. Rev., 100, 1764.
- Clover, R. B. and Wolf, W. P., 1968, Solid State Communications, 6, 331.
- Cohen, E. and Moos, H. W., 1967, Phys. Rev., 161, 258.

- Colwell, J. H., Mangum, B. W., and Utton, D. B., 1969, Phys. Rev., 181, 842.
- Culvahouse, J. W., Pfortmiller, L., and Schinke, D. P., 1968, J. Applied Phys., 39, 690.
- Culvahouse, J. W., Schinke, D. P., and Pfortmiller, L. G., 1969, Phys. Rev., 177, 454.
- Dirac, P. A. M., 1929, Proc. Roy. Soc., Al23, 714.
- Domb, C. and Sykes, M. F., 1962, Phys. Rev., 128, 168.
- Fisher, M. E., 1967, Reports on Progress in Physics, 30, 615, edited by A. C. Stickland, Inst. of Phys. and the Phys. Soc. London.
- Freddi, A. and Modena, I., 1968, Cryogenics, 8, 18.
- Heisenberg, W., 1926, Z. Physik, 38, 411.
- Holstein, T. and Primakoff, H., 1940, Phys. Rev., 58, 1098.
- Hughes, W. E., Montgomery, C. G., Moulton, W. G., and Carlson, E. H., 1964, J. Chem. Phys., 41, 3470.
- Hutchings, M. T., 1964, Solid State Physics, 16, 227, edited by F. Seitz and D. Turnball, Academic Press, New York.
- Hutchings, M. T., Birgeneau, R. J., and Wolf, W. P., 1968, Phys. Rev., <u>168</u>, 1026.
- Hutchinson Jr., C. A., Judd, B. R., and Pope, D. F. D., 1957, Proc. Phys. Soc. (London), <u>B70</u>, 514.
- Hutchinson Jr., C. A. and Wong, E., 1958, J. Chem. Phys., 29, 754.
- Judd, B. R., 1957, Proc. Roy. Soc. London, A241, 414.
- Judd, B. R., 1963, Operator Techniques in Atomic Spectroscopy, McGraw-Hill, New York.

- Landau, D. P., 1971, J. Physique, 32, 1012.
- Mack, C., 1966, Essentials of Statistics for Scientists

 and Technologists, Pelenum Publishing Co., New
 York.
- Mangum, B. W. and Thorton, D. D., 1969, Phys. Rev. Letters, 22, 1105.
- Marquard, C. D., 1967, Proc. Phys. Soc., 92, 650.
- Marquard, C. D. and Stinchcomb, R. B., 1967, Proc. Phys. Soc., 92, 665.
- Mayer, J. E. and Mayer, M. G., 1940, Statistical Mechanics,

 John Wiley & Sons, New York.
- Morita, T. and Tanaka, T., 1966, Phys. Rev., 145, 288.
- Morosin, B., 1968, J. Chem. Phys., 49, 3007.
- Parks, S. I., 1967, thesis, N.M.R. in Paramagnetic NdBr₃

 and UI₃ and in Antiferromagnetic UI₃, Florida

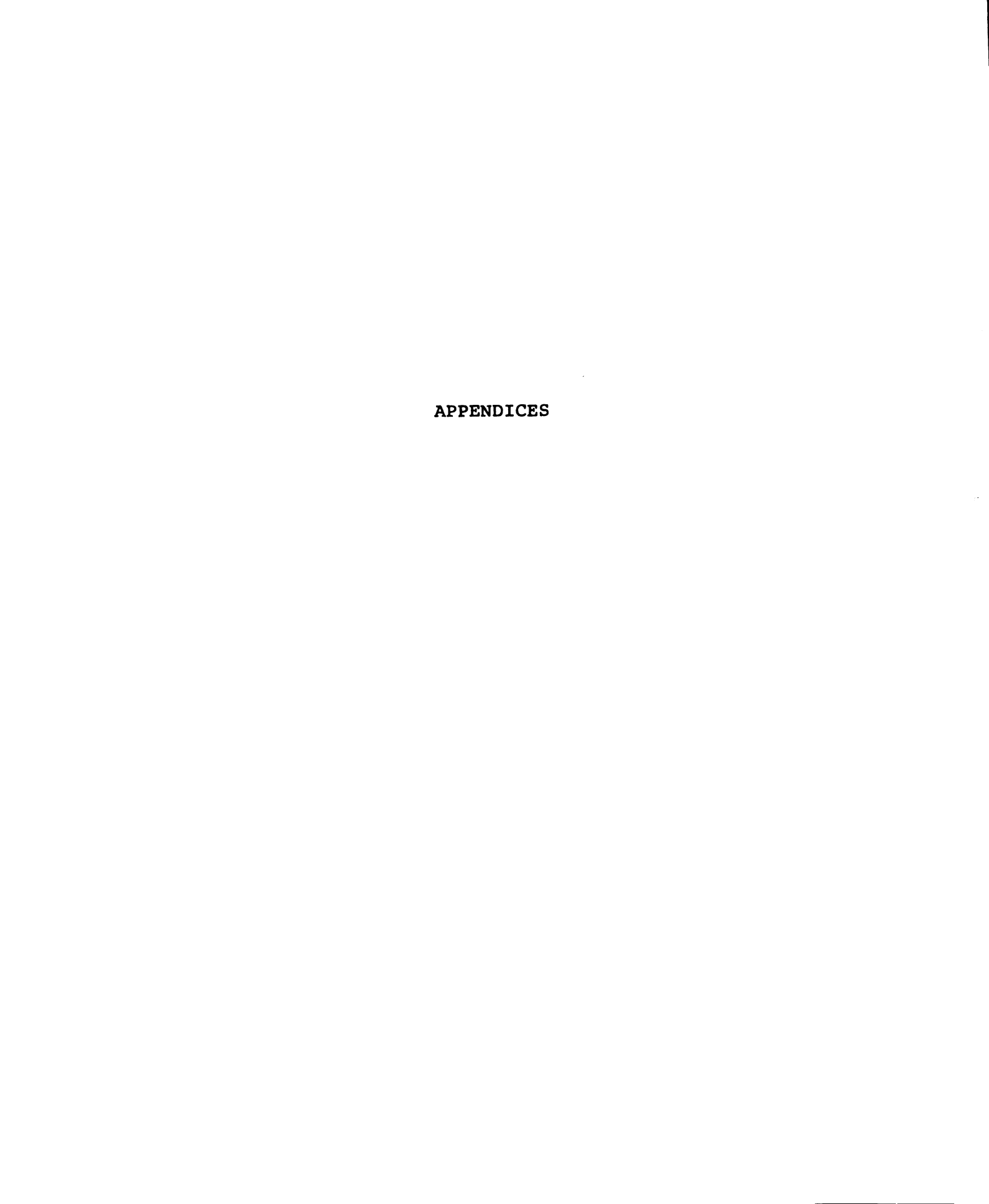
 State University.
- Pfortmiller, L. G., 1970, thesis, <u>EPR Studies of</u>

 <u>Pradeodymium in Trigonal Crystals</u>, University of Kansas.
- Piksis, A. H., Dieke, G. H., and Crosswhite, H. M., 1967, J. Chem. Phys., 47, 5083.
- Pippard, B., 1957, Classical Thermodynamics, Cambridge Press, London.
- Rives, J. E. and Walton, D., 1968, Phys. Letters, 27A, 609.
- Sherman, R. H., Sydoriak, S. G., and Roberts, T. R., 1962,

 Report No. LAMS-2701, (unpublished).

- Smart, J. S., 1966, Effective Field Theories of Magnetism,
 W. B. Saunders Co., Philadepphia and London.
- Stevens, K. W. H., 1963, in <u>Magnetism</u>, Vol. I, edited by G. T. Rado and H. Suhl, Academic Press, New York.
- Streib, B. Callen, H. B., and Horwitz, G., 1963, Phys. Rev. 130, 1798.
- Sydoriak, S. G. and Roberts, T. R., 1957, Phys. Rev., <u>106</u>, 175.
- Walton, D., 1966, Rev. Sci. Inst., 37, 734.
- White, G. H., 1968, Experimental Techniques in Low-Temperature Physics, Second Edition, Oxford Press.
- Williamson, J. H., 1968, Can. J. Phys., 46, 1845.
- Wolf, W. P., 1971, J. Physique, 32, 26.
- Wolf, W. P., Leask, M. J. M., Mangum, B., and Wyatt, A. F. G., 1961, J. Phys. Soc. Japan, 17, Suppl. B-I, 487.
- Wyatt, A. F. G., 1963, thesis, <u>Some Properties of Magnetic</u>

 <u>Ions in Solids</u>, Oxford University.
- Zachariasen, W. H., 1948, Acta Cryst., 1, 265.
- Zubarev, D. N., 1960, Usp. Fiz. Nauk., 71, 71. (English
 Translation: Soviet Phys.--Uspekhi, 3, 320).



APPENDIX A

CALIBRATION OF THE ³He SOLITRON GERMANIUM RESISTOR

The susceptibility coil calibration data are given in Table A. l. These data are fit to the equation $D = A(T^{*-1}) + B.$ Using a normal least squares analysis the result is

$$D = -(50824 \pm 81)T^{*-1} + (69692 \pm 101)$$
 (A.1)

Because the normal least squares analysis weights all points equally, which is not our case as indicated by the variation in ΔT^{*-1} of Table A.1, we also fit the data using a least squares program of Williamson (1968) which weights the datum points with the inverse square of the standard deviation of each point, and allows for standard deviations in both the T^{*-1} and D values of the datum. The result of this fit is

$$D = -(50527 \pm 76)T^{*-1} + (69382 \pm 75)$$
 (A.2)

The low temperatures calculated using these two results agree to within the uncertainty in the calculated temperatures. We will use the latter result because our data do not fit the criteria for the normal least squares analysis.

Table A. 3 shows the raw data for R vs. D for T < 0.6 K and the calculated temperatures based on the Williamson analysis. The uncertainty in the temperature is due to the uncertainties in the coefficients A and B. Table A.4 shows the

Table A.1. Susceptibility Coil Calibration Data

T(K)	$\frac{1}{T} \star \left(\frac{1}{K}\right)$	Δ ¹ / _T * _{X 10} -4a	Dial Reading ^b	∆ Dial Reading
1.200	0.8302	3.0	27404	20
1.121	0.8882	3.5	24530	10
1.052	0.9459	4.5	21582	10
0.990	1.0045	5.0	18600	10
0.936	1.0617	5.9	15693	10
0.887	1.1196	7.0	12935	10
0.842	1.1785	9.7	09898	10
0.802	1.2364	12.8	06889	20
0.766	1.2934	14.1	03976	15
0.701	1.4108	24.3	-01936	10
0.673	1.4681	31.9	-04900	10
0.647	1.5256	34.0	-07836	05
0.623	1.5828	45.1	-10808	05
0.600	1.6417	56.1	-13873	10

^a The uncertainty in T^{*-1} arises from the uncertainty in T which is approximately constant for all temperatures.

b This is the dial reading on a Cryogenics mutual inductance bridge and is directly proportional to the susceptibility.

calibration data for R vs. T for the temperature range 0.3 K to 1.2 K. Below 0.6 K the temperature is taken from Table A.3, above 0.6 K the temperature is determined by measuring the vapor pressure of the ³He bath. These data were fit to the equation

$$\ln(R) = a_0 + a_1 \ln(T) + a_2/T.$$
 (A.3)

Because the germanium resistor is so heavily doped we do not expect it to follow a single equation over a large temperature range. For this reason we have divided up the temperature range from 0.3 K to 1.2 K into four sections and fitted each section separately. The standard method of least squares (Mack, 1966) was used to determine the coefficients, a_0 , a_1 , and a_2 . The results of this fit are given in Table A.2. The last column in Table A.4 shows $(R_{\text{calc.}} - R_{\text{meas.}})/(dR/dT)$ to show the effective temperature deviation between the calculated and measured values.

Table A.2. Coefficients for ³He Solitron Ge Resistor

Temp. Range (K)	a _O	a ₁	a ₂
1.200 to 0.700 0.699 to 0.550	5.769325 6.378414	-0.875580 -1.859392	1.142215 0.470550
0.549 to 0.415	6.139522	-1.639297	0.675030
0.414 to 0.300	6.076923	-1.717617	0.664094

Table A.3. Raw Data for Ge Resistor Calibration

Dial Reading	T(K)	△ T(mK)	R(ohms)
-15097 -16362 -18232 -19856 -21407 -23180 -24851 -26700 -28500 -30500 -32390 -34437 -36613 -38900 -41555 -44000 -46917 -50180 -52374 -54517 -58285 -60812 -64326 -71293 -74810 -79549 -84410 -88900 -93180	0.589 0.580 0.567 0.556 0.556 0.517 0.536 0.526 0.515 0.505 0.495 0.485 0.475 0.465 0.465 0.455 0.443 0.433 0.421 0.409 0.401 0.394 0.381 0.373 0.363 0.373 0.363 0.343 0.322 0.311 0.301 0.292	1.5 1.4 1.4 1.3 1.3 1.2 1.2 1.1 1.1 1.1 1.0 1.0 0.9 0.9 0.9 0.9 0.8 0.8 0.7 0.7 0.7 0.7	3500 X 1 3650 X 1 3880 X 1 4090 X 1 4300 X 1 4550 X 1 4800 X 1 5100 X 1 5100 X 1 5750 X 1 6100 X 1 6500 X 1 6500 X 1 7457 X 1 8100 X 1 8700 X 1 1030 X 10 1100 X 10 1160 X 10 1200 X 10 12100 X 10 2400 X 10 2400 X 10 2750 X 10 3100 X 10 3507 X 10

Table A.4. R. vs. T Calibration Data and Deviation

Т (К)	△ T (mK)	R (ohms)	(R _c -R _m)/(dR/dT) (mK)
1.172	1.0	738.4	0.20
			-0.29
1.150	1.0	765.3	0.05
1.106	1.0	823.4	-0.24
1.100	1.0	832.5	0.11
1.050	1.0	911.1	0.12
1.047	1.0	916.1	0.04
1.000	1.0	1004.6	0.40
0.995	1.0	1014.4	0.19
0.903	1.0	1240.6	-0.10
0.900	1.0	1244.9	-1.6 3
0.850	1.0	1413.5	-0.61
0.827	1.0	1507.0	0.40
0.800	1.0	1623.2	-0.11
0.762	1.0	1818.0	- 0.26
0.7 50	1.0	1891.5	0.30
0.707	1.0	2180.6	- 0.32
0.700	1.0	2240.6	0.19
0.675	1.0	2453.8	- 0.25
0.658	1.0	2615.6	- 0.65
0.650	1.0	2712.7	0.60
0.625	1.0	3002.0	0.44
0.616	1.0	3110.4	- 0.16
0.589	1.5	3500.0	- 0.23
0.580	1.4	3650.0	-0.02
0.567	1.4	3880.0	0.06
0.556	1.4	4090.0	0.03
0.547	1.3	4300.0	0.73
0.536	1.3	4550.0	0.31
0.526	1.3	4800.0	0.06
0.515	1.2	5100.0	-0.19
0.505	1.2	5400.0	-0.34
0.495	1.2	5750.0	0.16
0.485	1.1	6100.0	-0.24
0.475	1.1	6500.0	- 0.22
0.465	1.1	6950.0	0.01
0.455	1.1	7457.0	0.43
0.443	1.0	8100.0	0.23
0.433	1.0	8700.0	0.06
0.421	1.0	9500.0	-0.27
0.409	0.9	10300.0	0.45
0.401	0.9	11000.0	0.37
0.394	0.9	11600.0	-0.40
0.381	0.9	13000.0	-0.52
0.373	0.8	14000.0	-0.47
0.363	0.8	15500.0	0.17

Table A.4. (cont'd.)

Т	△ T	R	(R _C -R _m)/(dR/dT)
(к)	(mK)	(ohms)	(mK)
0.343	0.8	19000.0	0.12
0.334	0.7	21000.0	0.32
0.322	0.7	24000.0	0.01
0.311	0.7	27500.0	0.29
0.301	0.7	31000.0	-0.29
0.292	0.7	35070.0	-0.04

APPENDIX B

GdCl3 TABLES OF DATA AND COMPARISONS

Table B.1 shows the transition frequencies of ³⁵Cl and ³⁷Cl as a function of temperature in the ordered state.

The zero field paramagnetic state transition frequencies are 5314 kHz for ³⁵Cl and 4188 kHz for ³⁷Cl. The recorded frequencies are the average of five independent readings and the standard deviation, SD, is the statistical standard deviation for the five readings. J is the isotope label and I the line label discussed in the text. The uncertainty in the temperature is the same as the uncertainty in the vapor pressure tables, ± 2mK. The table is in three sections, one for each different data taking run.

Table B.2 shows the results of the chi squared analysis used to determine the magnitude of the internal field.

Table B.3 shows the comparison between the measured internal field and the analytic expression for the critical behavior.

Table B.4 shows the same comparison for the spin wave region.

94

Table B.1 Section 1 Cl Transition Frequencies in GdCl3, 4He Data

TEMP	J	1	FREQ.	S.D.
2.170				
	35	2	5708.81	•58
	35	3	5120.00	.41
	35 37	4	4876.37	1.37
	37 37	2 3	4521.57 4032.79	•44 •20
	31	3	4032619	•20
2.164				
	35	2 3	5735.58	•50
	35 35		5115.83	.07
	35 37	4	4859.37 4545.87	1.19 .87
	37 37	2 3	4029.43	.30
	31	J	4027813	•00
2.149		_		
	35 35	2	5791.63	•63
	35 35	3 4	5108.43 4822.07	•21 •43
	35 37	2	4590.04	1.14
	37	3	4025.46	•46
	0,	•	, , , , , , , , , , , , , , , , , , ,	
2.139				
	35	2	5824.74	•48
	35 35	3	5106.01	.31
	35 37	4	4803.96	•51 1•60
	37 37	2 3	4622.03 4023.26	•44
	37 37	4	3770.94	.70
	0.	·	3110621	• • •
2.120				
	35	4	4770.45	•31
	37	4	3743.97	.87
2.110				
	35	3	5106.14	7.30
	35	4	4755.94	•24
	37	4	3732.77	•55

Table B.1 Section 1 (cont'd.)

TEMP	J	I	FREQ.	S.D.
2.100				
	35	2	5937,53	*•85
	35	3	5102.83	1.51
	35	4	4742.56	.41
	37	4	3722.28	•43
2.091				
	35	2	5967.81	•50
	35	3	5105.14	•20
	35	4	4731.66	•15
	37	3	4025.45	1.44
	37	4	3713.69	•35
2.069				
	35	2	6021.19	•48
	35	3	5108.80	.12
	35	4	4708.90	•26
	37	2	4788.06	3.24
	37	3	4032.38	•33
	37	4	3696.62	•69
2.037				
	35	2	6097.52	.18
	35	3	5117.80	•15
	35	4	4680.30	•19
	37	2	4852.06	•67
	37	3	4041.11	•24
	37	4	3674.63	.63
2.019				
-	35	2	6136.14	.19
	35	3	5125.44	•25
	35	4	4667.28	.02
	37	2	4884.25	•64
	37	3	4046.93	•43
	37	4	3664.74	•42

Table B.1 Section 1 (cont'd.)

TEMP	J	I	FREQ.	S.D.
2.000	35 35 35 37 37	2 ·3 ·4 2 3 4	6177.27 5130.16 4654.43 4920.35 4054.02 3655.33	•14 •11 •09 •24 •18 •29
1.980	35 35 35 37 37	2 3 4 2 3 4	6214.34 5137.65 4643.86 4952.56 4061.25 3646.49	.41 .20 .32 .35 .36
1.949	35 35 35 37 37	2 3 4 2 3 4	6274.37 5150.35 4628.33 5002.42 4073.51 3636.03	.17 .08 .25 .20 .18
1.920	35 35 35 37 37	2 3 4 2 3 4	6323.92 5162.42 4616.49 5045.42 4085.88 3626.73	.12 .09 .35 .45 .19
1.890	35 35 35 37 37	2 3 4 2 3 4	6373.93 5175.80 4605.54 5088.00 4098.70 3619.07	.28 .16 .11 .40 .14

Table B.1 Section 1 (cont'd.)

TEMP	J	I	FREQ.	S.D.
1.860	35 35	2 3	6420.04 5188.85	•53 •09
	35 37 37 37	4 2 3 4	4597.46 5127.30 4110.97 3613.73	.19 .06 .11
1.830	35	2	4445 27	20
	35 35 35 37 37	2 3 4 2 3	6465.27 5202.75 4590.20 5165.76 4124.10	.20 .13 .40 .23
1.799	37 35	2	3608.33 6509.08	•26
	35 35 37 37	3 4 3 4	5216.83 4583.40 4137.77 3604.08	.20 .21 .25 .37
1.769	35	2	6549.63	•39
	35 35 37 37	3 4 3 4	5230.73 4578.00 4150.55 3600.92	.05 .07 .09
1.741	35	2	6585.58	•29
	35 35 37 37	3 4 3 4	5243.51 4573.95 4162.66 3598.45	.10 .11 .13

Table B.1 Section 1 (cont'd.)

TEMP	J	I	FREQ.	S.D.
1.712				
	35	2	6623.19	.24
	35	· 3	5257.48	.12
	35	4	4569.99	.07
	37	2	5300.02	.19
	37	3	4175.62	.11
	37	4	3596.13	•50
1.661				
	35	2	6683.39	.21
	35	3	5280.71	.06
	35	4	4565.01	.13
	37	2	5351.50	•34
	37	3	4197.12	•03
	37	4	3593.56	.18
1.650				
	35	2	6694.67	.19
	35	3	5285.10	.08
	35	4	4564.03	•04
	37	2	5360.99	•32
	37	3	4201.31	•13
	37	4	3593.38	.30
1.618				
	35	2	6728.36	•32
	35	3	5298.77	.07
	35	4	4561.67	•03
	37	2	5389.72	.17
	37	3	4213.83	• 06
	37	4	3592.17	•22
1.594			•	
	35	2	6761.12	.61
	35	2 3	5312.84	.10
	35	4	4559.89	• 05
	37	2 3	5417.87	•22
	37		4226.86	•30
	37	4	3591.52	.30

Table B.1 Section 1 (cont'd.)

TEMP	J	I	FREQ.	S.D.
1.550				
	35	2	6805.68	•20
	35	3	5331.88	.19
	35	4	4558.00	.09
	37	2	5455.80	•43
	37	3	4244.24	•34
	37	4	3591.02	•56
1.500				
	35	2	6855.16	.17
	35	3	5354.04	.12
	35	4	4556.52	.03
	37	2	5497.99	•24
	37	3	4264.38	•20
	37	4	3591.33	•38
1.450				
	35	2	6902.29	.17
	35	3	5375.83	.12
	35	4	4555.76	•06
•	37	2	5537.98	•31
	37	3	4284.15	•07
	37	4	3592.19	•55
1.431				
	35	2	6919.53	•29
	35	3	5383.91	.11
	35	4	4555.57	.04
	37	2	5552.33	•42
	37	3	4291.59	•13
	37	4	3592.32	•24
1.350				
	35	2	6989.14	.21
	35	2 3	5417.01	•05
	35	4	4555.75	.03
	37	2	5611.45	•33
	37		4321.75	•15
	37	4	3594.38	.19

Table B.1 Section 1 (cont'd.)

TEMP	J	I	FREQ.	S.D.
1.299				
	35 35	·3	7029.47	•51
	35 35	3 4	5436.96 4556.60	•05 •08
	37	2	5645.94	.15
	37	3	4340.03	•28
	37	4	3596.05	.18
1.251				
	35	2	7067.78	•27
	35	3	5456.52	•08
	35	4	4557.70	•06
	37 37	2 3	5678.41 4357.57	•09 •07
	37	4	3598.04	.23
1.200 a				
	35	2	7105.74	.21
	35	3	5475.79	.06
	35	4	4559.07	•02
	37	2	5710.45	•38
	37 37	3 4	4374.84 3600.15	•15 •23
	3,	•	3000413	•23
1.025 a				
= , .	35	3	5541.18	•22
	35	2	7227.62	.39
	37	2	5814.22	.18
	37 37	3 4	4433.67	•05
	31	4	3609.07	.14

A Not used because the uncertainty in the temperature measurement is too large.

101

Table B.1 Section 2 3He Data of Feb 26, 1971

TEMP	J	I	FREQ.	S.D.
•599	35	2	7458.51	•31
	35	3	5673.84	•27
	35	4	4587.21	•25
•577	35	2	7468.63	•84
	35	3	5680.46	•45
	35	4	4588.72	•45
•530	35	2	7488.42	•34
	35	3	5691.71	•29
	35	4	4590.37	•64
•483	35	2	7507.51	•75
	35	3	5702.93	•43
	35	4	4592.49	•26
•450	35	2	7519.05	•59
	35	3	5711.11	•30
	35	4	4593.95	•41
•401	35 35 35	2 3 4	7534.75 5720.68 4596.30	•26 •51 •22

<u>Table B.1</u>. Section 3 He Data of March 24, 25, and 26, 1971

TEMP	J	1	FREQ.	S.D.
1.222	35	2	7088.08	.26
	35	3	5466.97	.17
	35	4	4558.80	.69
1.200	35	2	7103.62	•25
	35	3	5475.26	•09
	35	4	4557.39	•38
1.150	35	2	7140.45	.20
	35	3	5494.56	.11
	35	4	4559.10	.50
1.100	35	2	7175.26	.13
	35	3	5512.88	.23
	35	4	4561.75	.50
1.050	35	2	7208.37	•19
	35	3	5531.00	•09
	35	4	4564.69	•50
1.000	35	2	7241.11	.23
	35	3	5548.96	.11
	35	4	4565.93	.40
•950	35	2	7272.01	.10
	35	3	5566.03	.07
	35	4	4567.88	.16
•900	35	2	7301.64	•09
	35	3	5582.90	•06
	35	4	4570.70	•50

Table B.1 Section 3 (cont'd.)

TEMP	J	I	FREQ.	S.D.
.850	35	2	7329.89	•12
	35	3	5599.16	•17
	35	4	4573.43	•50
.800	35	2	7357.90	•24
	35	3	5614.85	•15
	35	4	4576.40	•50
•750 ^b	35	2	7380.89	•15
	35	3	5628.17	•11
	35	4	4578.36	•50
.700 ^b	35 35 35	2 3 4	7407.10 5643.89 4581.06	•12 •07 •50
•650 ^b	35	2	7433.57	•20
	35	3	5659.61	•08
	35	4	4583.20	•50
•550	35	2	7479.04	•12
	35	3	5686.83	•11
	37	2	6027.83	•17
•500	35	2	7499.70	•17
	35	3	5699.20	•41
	37	2	6045.24	•29
•474	35	2	7509.74	•17
	35	3	5705.25	•12
	37	2	6053.61	•20

Table B.1 Section 3 (cont'd.)

TEMP	J	I	FREQ.	S.D.
•425	35 35 37	2 3 2	7526.88 5715.72 6068.65	.19 .12 .59
•400	35	2	7534.41	•15
	35	3	5720.51	•16
	37	2	6074.80	•29
•375	35	2	7542.10	•19
	35	3	5725.30	•14
	37	2	6081.30	•22
•350	35	2	7549.15	•14
	35	3	5729.55	•14
	37	2	6087.34	•09
•325	35	2	7554.64	•19
	35	3	5733.05	•12
	37	2	6092.26	•12
.310	35 35 37	2 3 2	7559.08 5736.00 6095.98	.06 .03 .22
•293 ^c	35 35 37	2 3 2	7563.10 5738.23 6098.79	.04 .17 .31

Thermal equilibrium difficult to obtain, these points not used.

C Not used because its the lowest temperature point.

				
T(K) (Kelvins)	B (gauss)	∆ B ^a (gauss)	χ²	∆ f(1·w) (kHz)
2.170 2.164 2.149 2.139 2.100 2.100 2.091 2.069 2.037 2.000 1.980 1.949 1.799 1.7661 1.650 1.650 1.650 1.650 1.431 1.350 1.222 ^d 1.222 ^d 1.200 1.150 1.100 1.050 1.000 0.950 0.950 0.900 0.950 0.900 0.900 0.900 0.950 0.9000 0.900 0	1290.3 1362.0 1589.8 17359.8 1872.0 1932.0 2054.0 2055.0 2056.0 2	0.55550055005500500505055055005555000555500555005555	AV. 0.90 1.04 1.09 1.27 1.06 0.72 1.14 0.80 AV. 1.28 AV. AV. AV. AV. AV. AV. O.93 1.30 AV. 0.82 AV. AV. O.92 0.60 0.92 0.60 0.92 0.79 1.10 0.55 0.79 0.69 1.20 1.10 0.55 0.79 0.69 1.20 1.10 0.55 0.79 0.69 0.504 1.215 1.534 AV.	1.0 0.7 1.0 1.0 1.0 0.7 1.0 1.0 0.5 0.5 0.5 0.5 0.5 0.5 0.5 0

Table B.2. (cont'd.)

T(K) (Kelvins)	B (gauss)	∆Ba (gauss)	x ²	∆ f(1·w) (kHz)
0.650e 0.599 0.577 0.550 0.530 0.500 0.483 0.474 0.450 0.425 0.401 0.400 0.375 0.350 0.325 0.310	4704.1 4744.6 4762.0 4780.1 4793.4 4813.7 4823.9 4830.0 4844.4 4858.1 4869.7 4869.7 4883.1 4894.6 4903.8 4911.0	1.0 1.5 2.0 1.0 2.0 1.5 1.5 0.5 2.5 2.0 2.0 2.0	AV. AV. 1.32 1.30 0.94 1.17 0.92 1.061 0.24° 1.46 0.94 1.33 1.31 1.47 1.81	 0.0 1.0 0.0 1.0 0.0 1.0 0.0 0.0 1.0 1.0

^a \triangle B is estimated to within 0.5 gauss.

b Only values for $\Delta f(1 \cdot w)$ of 0.0, 1.0, 0.7, and 0.5 were used. When the results for 0.0 and 1.0 differed by less than 0.5 gauss even though χ^2 ranged from well below 1.0 to well above 1.0, an average between the two values was taken.

^c Increasing $\Delta f(1 \cdot w)$ will only make χ^2 smaller; this indicates a large spurious standard deviation error.

 $^{^{\}rm d}$ All temperatures 1.22 K and below used the $^{\rm 3}{\rm He}$ system.

^e This value was not used in the analysis; thermal equilibrium was difficult to achieve and the temperature was difficult to measure.

Table B.3. Comparison of B(T) with Analytic Expression for $T \sim T_c$.

Temperature (Kelvins)	B(T) (gauss)	▲B(T) (gauss)	B _m - B _c (gauss)
2.170	1290.3	2.5	-2.330
2.164	1362.0	4.5	3.520
2.149	1505.0	3.5	0.550
2.139	1589.2	4.5	-1.440
2.120	1735.8	4.5	-1.070
2.110	1805.3	4.5	-1.340
2.100	1872.4	5.0	-0.051
2.091	1932.0	4.5	3.270
2.069	2054.0	2.5	- 2.510
2.037	2224.0	2.0	1.400
2.019	2308.0	4.0	-0.370
2.000	2396.4	2.0	2.780
1.980	2475.9	2.5	-2.610

The analytic expression is $B(T) = A(T_c - T)^{\beta}$ where $A = (4368.4 \pm 31.3)$ gauss/K^{\beta}, $T_c = (2.214 \pm 0.0016)$ K, and $\pm (0.3904 \pm 0.006)$. The chi squared value is 0.710.

T(K)	B(T)	△B(T)	B _m - B _c	B _m - B _C
(Kelvins)	(gauss)	(gauss)	Set A	Set B
0.310 0.325 0.350 0.375 0.400 0.401 0.425 0.450 0.474 0.483 0.500 0.530 0.550 0.577 0.599 0.800 ^a 0.850 0.950	4911.0 4903.8 4874.6 4883.1 4870.5 4869.7 4858.1 4844.4 4830.0 4823.9 4813.7 4793.4 4780.1 4762.0 4744.6 4578.4 4532.0 4484.7 4434.8 4382.9	2.0 2.5 2.0 2.0 0.5 2.5 0.5 1.5 2.0 1.0 2.0 1.5 1.0	-0.24 -1.43 0.09 0.18 -0.01 -0.29 0.81 1.09 0.81 0.17 0.54 -0.33 -0.15 0.60 -0.90 -1.21 -1.06 -0.27 0.58 0.83	0.53 -0.91 0.27 0.10 -0.26 -0.55 0.45 0.69 0.42 -0.20 0.21 -0.54 -0.25 0.66 -0.69 -0.14 -0.15 0.63 0.37 -0.42

Set A fitted to: $B(T) = 4957.5 - 811.0 T^{3/2} exp(-0.343/T)$

Set B fitted to: $B(T) = 4950.8 - (963.1 T^{3/2} - 90.7 T^{5/2}) \exp(-0.430/T)$

APPENDIX C

PrCl₃ DATA

Table C.1 shows the measured frequencies as a function of angle for an external field of 500 Oersteds applied in the plane perpendicular to the C_3 axis in the ordered state. The angles are in the laboratory reference system. The site label is arbitrary. LN is the line number which defines the transition, 1 being the highest in frequency and 4 lowest. The H and L refer to the High and Low zero field lines respectively. Because the lines are weak and were only measured once, the accuracy of the frequency measurement is estimated at \pm 5 kHz. The calculated frequency assumes H = 500 Oersteds, η = 0.4937, $v_Q(H)$ = 4598.6 kHz, and $v_Q(L)$ = 4535.5 kHz. The location of the Z-principal axis in the laboratory reference frame is assumed to be: Z_1 = 350°, Z_2 = 290°, and Z_3 = 50°.

Table C.1. Cl Transition Frequencies in PrCl₃

Angle (deg)	Site	LN	LOC	Freq. (kHz)	Calc. (kHz)
25%	1	i	(-1	4961.90	4960.35
2માય•	ı	4	1	+1m3.70	4140.43
≥a	7	~	н	4737.70	4796.01
A40.	Ċ	~	1.	473H.20	4732.43
٠١ ١٠	,	.3	ч	4347.50	4414.52
2H1/1.		3	1	4356.30	4341.44
> H 11 .	3	~	ч	4615.00	4609.77
A160 .	1		l	45/6.50	454h.15
>15 1.	3	٤	1	4530.20	4536.35
2.40.	i	ì	• •	4993.80	4988 - 41
٠٠٠ م	1	1	1.	4934.50	4425•41
٠٠ يواج	i	4	14	4210.60	4223.26
نه ۱۰ و م	<i>:</i> '		14	490()•H()	440%.53
ن در چه فر	c ³	1	1.	4747.50	4745.55
290.	7	, š	ч	43××,9(i	4391.43
241.	7	.1	1	4337.00	4328.35
• الوام	3	C	H	4641.20	4673.58
2911.	i	2	I.	4627.70	4610.58
٠ ١ ٢٠٠	3	1	н	4522.70	4538.10
291.	3	5	L	4467.70	4475.10
3000	1	1	H	5012.50	50u7.44
30 .	1	i	1	4953.40	4944.47
30 .	1	4	Н	4140.41)	4201.30
5 (1 i) .	P	.3	t.	4353.60	4341.44
300	1	_	1.	4667.40	4672.11
40 -	3	•	н	4464.00	447H•n5
396.	•	1	t.,	4407.40	4415.67
31 = •	ď	•	ч	4753.20	4762.33
51 ° .	~	<i>(</i> *	1_	4672.KI)	4699.26
li).	?	.5	H	4455.10	4434.53
31 4.	3	0	н	4794.30	4788.91
3100	3	4	14	4411.30	4426.20
320.	4	-	14	4/01.90	4714.92
120.	م	C.	1	4642.40	4651.87
121.	بر	.4	14	4448.40	4488.99
320.	2	.3	1	4442.10	4425.94
3/1.	1	e.	14	4814.70	441n.39
3/1.	1	0	t.	4757.20	4753.42
321.	3	, 4	H	4343.20	4349.14
120 .	1	,3	1	4337.40	433h.22

Table C.1. (cont'd.)

Angle (deg)	Site	LN	LOC	Freq. (kHz)	Calc. (kHz)
111.	ı		н	4705.50	4762.33
3.5%	1	(ı	4710.70	4644.26
331.	i	.•	ы	4435.40	4434.54
3 5 1 .	-	/	14	4047.511	4059.33
3.3	2	c	1	45×5•×()	4596.29
5.5%	2	3	+4	4559.60	4547.11
330.	6	,3	1.	4444•4()	44H4•()H
\$40.	l	_	н	4798.60	4796.01
341.	1	d	I	473H.H()	4732.93
34 1.	1	,5	H	4401.10	44114.50
3400	1	1	1.	4 344 • 4 ()	4341.44
141.	ć	•	+4	4621.20	4609.71
341.	م	-	l_	4550.70	4546.75
341.	d	.1	н	4549.40	4549.36
1411.	یے	4	I_	4524.411	4536.35
341.	₹	i	ч	4966.30	4960.35
\$4.1 _a	3	1	1	4405.00	4897.35
351.	1	-	-4	4806 <u>.</u> 60	4808.63
345 F.	ì	•	l.	4744.90	4745.55
すつり ・	ì	.3	Н	4388.40	4341.43
355 th 🕳	1	1	ţ	4331.00	4324.35
359.	c'	~	Н	4685°50	4673.54
151.	(<i>(</i> :	ı	4623.10	4610.54
15 1.	<i>c</i> '	3	ч	4524.40	4534.10
3500	~	3	1	4452.20	4475.10
371.	\$	i	١.	4917.00	4925.41
ا المعلم	3	→	14	4213.50	4223.26
35%	•	4	1.	4154.70	4160.27
3m≒.	1	-	14	4741.70	4796.01
in i.	1	-	L	4727.60	4732.93
ind.	l	3	l,	434H.60	4341.44
354.	7	c	1.	4683 _• 00	4572.11
36 / •	ے	.3	ч	4468.40	4478.65
1011.	1	ŧ	F1	5016.90	50v7.84
364.	3	1	ł,	4450.90	4944 . KZ
3m1).	4	4	Ч	4142.70	4201.30

Table C.1. (cont'd.)

Angle (deg)	Site	LN	LOC	Freq. (kHz)	Calc. (kHz)
10.	1	Ċ	н	4738.60	4752 . 33
1: •	ı	(1.	4693.70	4694.26
J 🗥 😱	1	3	11	4446.30	4439.54
1 10.	1	3	1	4384 _• 00	4376.47
1:.	?	ć	н	4797.10	4788.91
1 .	?	3	н	4417.00	4426.20
10.	7	3	1.	4355.46	4363.23
10.	3	1	1.	4959.00	4954.80
i 1.	. 3	4	ч	4184.70	4188.50
111.	i	c	н	4705.40	4714.42
211.	i	~	1_	4645.00	4651.87
C-1 •	1	.5	н	4496.71)	4488.99
200	l	ځ.	L.	4436.30	4425.94
200	7	-	Н	4416.50	4816.39
20.	7	3	н	4401.10	4399.19
٠ (١ -	<i>(</i> :	3	l.	4334.90	4336.22
20.	3	1	H	5023.60	5018.99
~ i •	.5	1	l_	4454.50	4955.43
5.1.	1	<i>C</i>	н	4644.70	4659.33
31.	1	2	1_	45X5·5()	4546.29
3.1 •	ì	.5	Н	4577.40	454/.11
3 P.	1	\$	1_	4494.40	4484.04
511.	7	1	ı	4866.80	48n4.31
30 €	2	4	4	4274.50	4247.41
\$ i · •	.3	<i>C</i> '	14	4764.50	4762.31
311.	4	C	t., .	4708.80	4699.26
411	1	6	н	462 1. 80	46114.71
4) •	ì	~	1.	4557.70	4540.15
40.	1	.٠	ч	4592 . 00	4594.36
4).	1	3	1_	4527.20	453n.35
40.	2	1	н	4967.00	4960.35
47.	?	1	1_	4902.70	4847.35
*+ () •	?	4	н	4241.10	4253.40
4.1	.5	ď	н	4801.80	479n.01
4	5	<i>(</i>	ł.	4733.20	4732.43
4 1.	•	.5	ч	4415.90	44(14.57
41.	3	3	l.	4341.00	4341.44

Table C.1. (cont'd.)

Ang (de		Site	LN	LOC	Freq. (kHz)	Calc. (kHz)
	1.		.,	1.1	06N= 00	4673.5 ^R
	5 11.	1	<i>c'</i>	H	4680.40	4610.53
	5 ¹¹ •	l	~	Ļ	4625.UU	
	~ `` •	i	5	F4	4525 . 90	4538•10 4475•10
	· ·	i.	3	1.	4464.10	
	J 11 •	7	i		4929.70	4925.41
) /·	ć,	•	· ·	4214.20	4223.26
	711.		₩ *	I.	4157.60	4160.27
) •	.3		ы <u>.</u>	4807.50	4808.63
	٠ ١٠٠	.1	-	t	4/41.20	4745.55
	າ : •	1	4	14	4345.40	4391.43
•	71.	1	,4	l.	4331.00	4328.35
•	hu.	1	-	14	474H.00	4735.10
•	n:.	ì	0	1_	4684.60	4672.11
•	rs-1 .	1	4	14	4108.50	447H.65
(?	ι	1-4	5018.00	5007.84
	na .	<i>c</i> *	1	1	4444.50	4944.42
	nd.	7	4	ч	4148.40	4201.30
)U.	3	~	н	4742.10	4796.01
		.3	•	1	4723.90	4732.93
	n).	3	.3	1.	4 144,41)	4341.44
	/	1	(н	4747.40	4788.91
	71	ì		H	4417.00	4426.20
	/ i) .	ì	.*	ί,	4354.40	4363.23
	7.1	رم ب	1	i. L	4954.50	4954.80
	7 ·) •	<u>ر</u> ح	4	년 년	4185.30	4188 • n0
	10.		4	1.	4125.50	4125.56
	/	۷.		т. Н	4753.10	4762.33
	· ·	3	<i>C</i>		4688.30	4699.26
			C A	L		4439.53
	/ / ·	÷	1	Н	4452.50	
	7''•	3	3	I _	4388.70	4376.47
	ط) .	1	C	н	4815.50	4816.19
,	⊣ ∵•	ì	6	t.	4754.80	4753.42
,		i	3	ч	434/.00	4399.19
i	ч., •	1	3	ł	4313.50	4336.22
•	≒ + 1 •	,	i	t	4944.40	4955.73
	4.0 ·	0	4	! (4185.60	4124.93
,	et () •	م	4	•,	4127.40	4121.87
,	∹ ,+.	3	<i>(</i>	ч	47114.41)	4714.92
,	4 1	•	1	I	4534.50	4651.47
;	() .	5	+	н	4501.40	4488.49
	5 i 🕝	.\$	•	1.	443/.10	4425.44

Table C.1. (cont'd)

Angle (deg)	Site	LN	LOC	Freq. (kHz)	Calc. (kHz)
97.	l	-	14	4764.40	4788.91
Na co	1	7	1,	4704.00	4725.91
٧,,	ī	1	H	4437.40	4426.211
4,	i	. 1	1	4375.40	4363.23
41.	<u>,</u>	4	14	4649.30	4659.33
911.	٤	ć	t.	4543.40	4546.24
- ≠11 •	3	.4	H	4500.10	4547.11
1411	3	•	1.	4497.50	4484.08
12 12 15 m	i	1	Н	4987.20	4975.34
200.	1	i	t.	4921.10	4912.34
245°	1	→	H	4225.40	4237.45
247.	<i>C</i>	•	н	4805.70	4805.39
dan.	?	ď	1	4740.00	4742.31
2H5.	~	ょ	н	4374.60	4394.79
ZHO.	2	4	L	4335.70	4331.71
245°	.3	c'	н	4651.70	4641.73
となっ 。	3	c	1.	45X4.50	4578 . 72
ジェン・	3	3	l.	4494.10	4505.70
247.	1	1	н	5006.50	4999.29
24m.	1	j	t.	494().4()	4936.28
247.	1	4	н	4202.60	4211.16
247.	م	6	н	4402.10	4805.39
245.	?	ح	I,	4738.20	4742.31
747.	3	c	1.	4652.40	4641.88
245.	.3	3	H	4446.30	4501.92
245.	3	3	l.	4433.40	4444.93
31).	1	1	i 1	5026.10	5019.44
315.	i	ı	ŧ.	495H.00	4456.39
315.	1	4	Н	4142.20	4185.70
31 > •	م	1	н	4736.50	4739.94
315.	بح	2	I.	4667.10	4676.8H
31%.		4	н	4473.70	4462.81
315.	\$	~	н	4813.90	4808.43
315.	3	.5	ч	4402.10	4407.04
315.	3	.3	•	4337.20	4344.07

Table C.1. (cont'd)

Angle (deg)	Site	LN	LOC	Freq. (kHz)	Calc. (kHz)
325.	1	j	1.	4950.30	4953.74
125.	1	4	.; Н	41dh.b0	4186.01
323.	ì	4	l.	4124.30	4122.45
125.	ئے	خ	Н	4640.20	4687.88
325.	2	2	L	4614.90	4624.44
177.	ر د	3	H	4526.40	4517.25
327.	ć	3	1_	446H.80	4454.21
360.	3	ž	ਜ	4806.80	4808.43
167 ·	3	5	1	4746.10	4745.45
327.	3	3	4	4398.30	4407.04
325.	3	3	L	4346.70	4344.07
315.	ì	۲	н	4784.90	4781.32
335.	1	7	l_	4721.60	4718.25
335.	1	3	14	4410.00	4419.71
335.	1	3	t.	4351.20	4356.70
335.	2	2	н	4617.10	4624.64
335.	2	?	1.	4555.80	4560.01
335.	2	.4	Н	4588.10	4578.09
335.	7	3	L	4525.50	4515.06
335.	3	j	н	4452.10	4943.46
335.	3	4	ч	4257.30	4270.5×
145.	i	7	н	4806.00	4805.39
34 7.	1	?	ŧ	4745.00	4742.31
147.	1	3	н	4392.00	4394.79
34 7.	1	3	I.	4334.90	4331.71
147.	E	>	н	4651.40	4641.73
5411.	7	r	Ι,	4594.60	4578.72
.14) .	~	3	н	4554.10	4564.71
345.	Ċ.	3	1.	4445.00	4505.70
345.	3	i	Н	4983.20	4975.34
347.	.3	ì	ı	4920.30	4412.34
347.	5	4	H	4223.90	4237.45
3'7 7 .	i	~	н	4802.70	4805.39
\$50 · 0 •	1	c '	ŧ.	4734.30	4742.31
355.	1	3	н	4396.30	4394.79
3700	1	•	ŧ	4318.20	4331.71
17 ·•	7	1	ч	4714.4()	4704.37
3,200	c'	1	L.	4655 • 6 (I	4641.HH
350 0	ć,	.1	н	4495.60	4507.92
157.	7	5	1_	4435.20	4444.93
150.	.3	1	1.	4941.40	4936.21
۴ د دوډ	.3	4	14	4200.HO	4211.16
3250	. 3	4	(414 1.00	4144.15

Table C.1. (cont'd)

Angle (deg)	Site	LN	LOC	Freq. (kHz)	Calc. (kHz)
~.	3	1	14	5018.80	5014.01
n •	.3	i	L	4954.10	4450.98
···· •	ز	4	Н	4189.30	4193.78
10.	1	ć '	ы	4731.50	4739.94
1 > •	i	C	L	4607.40	4676.83
15.	ì	3	н	4404.30	4462.87
i · · ·	ϵ'	2	44	4814.90	4808.43
1 .	6	>	I,	4752.40	4745.45
15.	7	•	1.	4334.00	4344.07
15.	4	4	4	4180.20	4185.70
i 🕤 🔹	•	4	1,	4171.10	4122.65
37.	l	•	બ	4617.80	4624.64
1) •	i	C	1_	4554.30	4566.67
15.	1	.3	F4	45×14.50	4578.09
40.	i	,	t,	4526.00	4515.07
₹50.	Ċ	1	н	4959.50	4443.96
3m.	.3	(Н	47n3.HU	4781.32
37.	.3	~	l_	4723.60	471H.25
. 5 ℃ •	1	3	ч	4414.50	4419.77
3	3	.3	t.	4354.80	4356.70
41.	ì	e	н	4652.20	4641.73
45.	i	1	1	45HH.71	4578.72
+ > •	i	.5	++	4555•60	4568.71
٠+ ٦ •	1	3	ŀ	4445.40	4505.70
+ 5 •	7	1	1	4914.50	4912.34
47.	1	4	ч	4264.50	4237.45
+1	C'	4	ŧ	41n8.d0	41/4.45
+ · · ·	`3	ř	ь.	4213.20	4805.39
47.	3	\mathcal{C}	ı	4744.60	4742.31
45.	3	•	11	4341.40	4 144 . 74
'+ ``•	1	.5	ŧ	4334.30	4331.71
1318	i	c	i- i	4657.40	4704.H1
) · •	1	5	Ħ	4444.70	4507.92
') ` · •	1	,1	1_	44.34.711	4444.41
` ` ``•	6	i	ŧ	4442.70	4436.28
つ) 。	7	4	14	4203.20	4211.16
") * > •	/	4	1,	4144.41)	4148.15
″າ າ .	3	C	н	4400.10	4405.39
'n . •	3	•	t.	4731.20	4742.31
٠٠ د در	\$	•	Н	4 199.30	4344.74
``	1	3	1	4339.10	4331.71

Table C.1. (cont'd.)

Angle (deg)	Site	LN	LOC	Freq. (kHz)	Calc. (kHz)
7.	1	·	н	4812.30	4908 . 43
75.	ì	۲	t.	4757.00	4745.45
15.	1	4	1	4340.10	4344.07
75.	4	7	ч	4730.20	4739.94
15.	4	7	ŧ.	4566.40	4676.88
75.	\$	4	н	44/1.n()	4462.81
н э.	i	ņ	н	4407.00	490H•43
H > •	ì		1	4742.20	4745.47
85.	1	.5	ы	4410.10	4407.04
×5.	i	•	1_	4344.60	4344.07
d).	i	c	Н	46/5.40	46H7.HH
ದ∿•	. \$	C	١	4612.40	4624.84
M > •	•	3	н	4527.70	4517.25
M 7 •	•	.3	l	4457.20	4454.21
9.1.	1	1	1.	4러전서·6()	4880.97
9 7.	i	کے	+4	4720.40	4763.54
95.	i	.₹	1.	4416.00	4388.02
95.	3	ć	н	4618.00	4629.69
9.,.	3	4	F .	4554.61)	4566.67
45.	1	.3	14	4589.50	4578.04
9,.	•	.1	l_	4527.20	4515.06
100.	1	4	н	4244.60	4253.40
104 .	1	Ć.	н	4624.30	4609.77
10+	•	يے	l.	45n4.80	4546.75
100.	1	3	H	4585.40	4544.37
1000	•	.5	ŧ.	4525.40	453n.35

MICHIGAN STATE UNIV. LIBRARIES
31293101088056